BEST PRACTICES TO ADDRESS ISSUES OF EXCESS AGGREGATE DUST IN NEBRASKA

FINAL REPORT

Jiong Hu (PI), Yong-Rak Kim (Co-PI)

Research Team: Temirlan Barissov, Shayan Gholami, Julia Grasley

Department of Civil and Environmental Engineering
University of Nebraska-Lincoln, 1400 R St, Lincoln, NE 68588

Zachry Department of Civil & Environmental Engineering
Texas A&M University, 400 Bizzell St, College Station, TX 77843

Sponsored By

Nebraska Department of Transportation and U.S. Department of Transportation Federal Highway Administration

December 31, 2020

NEBRASKA
Good Life. Great Journey.
DEPARTMENT OF TRANSPORTATION

UNIVERSITY OF Nebraska Lincoln

TEXAS A&M UNIVERSITY

TECHNICAL REPORT DOCUMENTATION PAGE

1. Report No. M114	2. Government Accession No.	3. Recipient's Catalog No.
4. Title and Subtitle Best Practices to Address Issues of Excess Aggregate Dust in Nebraska		5. Report Date December 2020
		6. Performing Organization Code
7. Author(s) Jiong Hu, Yong-Rak Kim, Temirlan Barissov, Shaya Gholami, Julia Grasley		8. Performing Organization Report No. If applicable, enter any/all unique numbers assigned to the performing organization.
9. Performing Organization Name and Address Department of Civil and Environmental Engineering University of Nebraska-Lincoln, 1400 R St, Lincoln, NE 68588 Zachry Department of Civil & Environmental Engineering Texas A&M University, 400 Bizzell St, College Station, TX 77843		10. Work Unit No.
		11. Contract SPR-P1(20) M114
12. Sponsoring Agency Name and Address Nebraska Department of Transportation Research Section 1400 Hwy 2 Lincoln, NE 68502		13. Type of Report and Period Covered Final Report July 2019-December 2020
		14. Sponsoring Agency Code
15. Supplementary Notes		

16. Abstract

The negative impacts of an excessive amount of dust on concrete performance have been known and reported in different states. The extent and impact of dust on concrete performance, which depends not only on quantity but also on the nature of dust could be complicated. For example, clay coatings showed a more harmful impact on concrete performance compared with carbonates (limestone dust) or stone dust. While clays that weakly adhere to aggregate will be dispersed in the mixing water and could lead to the workability or air entrainment issues, clays that are strongly bonded to the aggregate surface will remain at the aggregate surface after the mixing process and may disrupt the aggregate-paste bond and results in strength and durability issues. The upper-limits of aggregate dust (fines) content currently included in most state agencies' specifications are not necessarily sufficient to prevent aggregate issues. This study includes five different types of aggregates, limestone, gravel, dolomite, granite, and quartz, collected from Nebraska, South Dakota, and Wyoming. A comprehensive evaluation of the aggregate dusts was performed using sieve analysis, washing test, sand equivalent test, methylene blue test, and X-ray powder diffraction. Besides the evaluation of fresh, hardened, and durability properties of concrete, advanced tests were used to characterize aggregate-paste bonding inside concrete prepared with different aggregate types and cleanliness. While aggregate collected in this study all appear to meet the current NDOT criteria of coarse aggregate fine content and fine aggregate sand equivalent value, additional test such as methylene blue value could provide more insights into the type of dust on the aggregate surface, especially the coarse aggregate. Modified Methylene blue value (MMBV) could potentially be used to control the coarse aggregate dust. However, future investigation is needed to establish a correlation between MMBV and field concrete performance that can be eventually used to set up criteria for quality control.

17. Key Words Aggregate dust, microfine, fine content, type, methylene blue, interface	18. Distribution Statement No restrictions. This document is available through the National Technical Information Service. 5285 Port Royal Road Springfield, VA 22161

19. Security Classification (of this report) Unclassified	20. Security Classification (of this page) Unclassified	21. No. of Pages 122	22. Price

Form DOT F 1700.7 (8-72) Reproduction of completed page authorized

DISCLAIMER

The contents of this report reflect the views of the authors, who are responsible for the facts and the accuracy of the information presented herein. The contents do not necessarily reflect the official views or policies neither of the Nebraska Department of Transportations nor the University of Nebraska-Lincoln. This report does not constitute a standard, specification, or regulation. Trade or manufacturers' names, which may appear in this report, are cited only because they are considered essential to the objectives of the report.

The United States (U.S.) government and the State of Nebraska do not endorse products or manufacturers. This material is based upon work supported by the Federal Highway Administration under SPR-P1(20) M114. Any opinions, findings and conclusions or recommendations expressed in this publication are those of the author(s) and do not necessarily reflect the views of the Federal Highway Administration."

ACKNOWLEDGEMENTS

The authors would like to thank the Nebraska Department of Transportation (NDOT) for funding the research project. In particular, the authors thank NDOT Technical Advisory Committee members for their technical support and valuable inputs and assists throughout the project. The authors would also like to thank Lyman-Richey Corp., and Ash Grove Cement Company for the kind donation of materials for this research. Finally, the authors would like to thank Miras Mamirov, Flavia Ribeiro Furtado De Mendonca, Andrew Ruder, and Jose Olvera Cortes, and for their valuable assistance throughout the project.

TABLE OF CONTENTS

LIST OF FIGURES

LIST OF TABLES

CHAPTER 1. INTRODUCTION

1.1 Background

Concrete is one of the most widely used construction materials, which is generally composed of cement, water, aggregates, and various admixtures. While the main strength and durability characteristics of the concrete depending on the physical and chemical properties of cement and cementitious materials (SCMs), and the chemical reactions between them and water, aggregates generally are not chemically reactive and acting only as filler materials. Although the influence of mineralogy, mechanical properties, and gradation of the aggregates are commonly studied, some aggregates may contain excess dusts, also referred to as microfines or coatings, which could have a major impact on the concrete performance.

Excess aggregate dust, also known as "dirty" aggregate, can cause issues in concrete at different stages. Even though the negative impacts of an excessive amount of dust on concrete performance have been known and reported in different states, the impact of the types and amounts of clays on concrete performance is still not fully understood. While the potential negative impact is well-recognized, it is also known that the mineralogy of the dust is critical. For example, clay coatings showed a more harmful impact on concrete performance compared with other dusts such as carbonates (limestone dust) or stone dust. Clays that weakly adhere to aggregate will be dispersed in the mixing water and, therefore, will be integrated into the cement paste, which could lead to the workability issue. Specific clays mixed with a particular type of air-entraining admixtures (AEA) can largely neutralize the function of the AEA and make it difficult to achieve required freeze/thaw resistance. On the other hand, clays that are strongly bonded to the aggregate surface will remain mostly located at the aggregate surface after the mixing process and, therefore, may disrupt the aggregate-paste bond (usually referred to as interfacial transition zone (ITZ)) and results in strength and durability issues. Examples of the extent of aggregate dust-related issues include dust coating observed during paving operations, air entrainment issues, and negative impact on mechanical properties and durability of concrete.

The extent and impact of dust in concrete depend not only on quantity but also on the nature of dust. Due to the different mineralogical characteristics, clays with higher cation exchange capacity (CEC), such as montmorillonite, tend to cause more issues because of the higher absorption and swelling rate. With the excessive amount of dust often found in western Nebraska aggregate, the Nebraska Department of Transportation (NDOT) requires that aggregates shall be washed to clean any coatings when aggregates are from dry pit locations. While NDOT had adopted a proactive practice of requiring a Sand Equivalent value not less than 90 in accordance with AASTHO T176 with aggregates from dry pits, and a maximum fine (No. 200 minus) content of aggregate lower than 3%, it is still not clear if the current practice is sufficient to accurately quantify aggregate dusts based on clay types, and what the acceptable dust content should be. Parameters such as the Methylene Blue Value (MBV) might provide a better evaluation of the quality of clay, and potentially help to better understand the impact of aggregate dust on concrete performance than the current specification methods. In order to effectively prevent the aggregate dust issue, a more fundamental understanding of the nature of the impact of dust is necessary.

Besides traditional tests for fresh, hardened, and durability properties, advanced techniques such as scanning electron microscope and energy dispersive X-ray spectroscopy (SEM/EDX), micro-CT, and nanoindentation will be used to help to better understand the characteristics and mineralogy of aggregate dust as well as its effects, such as the impact on ITZ debonding and deterioration in concrete.

1.2. Objectives

The overall goal of this research is to determine the best practice to address potential issues of excess aggregate dust in Nebraska concrete. To achieve the goal, three specific objectives of this study are to:

(1)Select and conduct various laboratory tests to characterize different types of aggregate dusts;

(2)Access the negative impact of excess dust on NDOT concrete properties and performance; and

(3)Identify the best practice to further improve current NDOT methods to control the negative effects of excess dust in concrete mixtures.

1.3. Report Organization

This project report is divided into five chapters. Following the introduction, the report provides a detailed background regarding excess aggregate dust in concrete in Chapter 2 provides a summary of the literature search. Chapter 3 presents the overview of materials and experimental program used in the study, including different test methods to evaluate aggregate dusts, as well as concrete mixing procedures and testing methods. Next, Chapter 4 provides detailed results and analyses from the experimental study, which include aggregate dust characterization, aggregate-paste interface analysis from different advanced techniques, and performance of concrete made with different aggregates. Finally, Chapter 5 concludes the report by summarizing the findings from this study.

CHAPTER 2. BACKGROUND

2.1. Introduction

This chapter provides a summary of the effects of excess aggregate dusts on concrete properties and performance and practices of federal and state agencies department of transportation (DOT) to address the issue. Agency specifications in the regions/states with similar climates as Nebraska will also be reviewed. The literature review was focus on 1). Impact of aggregate dust (content and type) on concrete performance; 2). Current monitoring methods employed to detect the type and content of excess dust; and 3). Thresholds of dust (fines) content used in other DOTs.

2.2. Microfines Classification and Properties

Microfines are generally defined as impurity or surface coating particles present in aggregate matrix and finer than 75 -μm (passing through No. 200 sieve). Based on their properties, origin, and nature, coating particles can be classified as follows: stone dust, clay particles, bituminous oil, alkali, organic matter, calcareous, sugar coatings, and others (Goldbeck, 1932). However, it is generally accepted to classify microfines as clay particles, stone dust, and calcium carbonates, the types commonly present in the aggregate matrix and attributed to causing issues of Athe concrete performance (Gullerud, 2002; Desire and Leopold, 2013; Munoz et al., 2007; Cramer et al., 2010).

It is believed that stone dust particles are the most common microfine type present in the aggregate matrix, the formation of which is associated with the production procedure of aggregate of a controlled gradation by crushing quarried stone, or with the natural weathering of parent rock (Stewart et al., 2007). Calcium carbonates are found in limestone or dolostone quarries. The presence of clay coatings is generally explained by the precipitation and deposition of particles from groundwater or Earth's crust, especially common in natural sand quarries (Schmitt, 1990).

Apparently, the effect of microfines presence will mostly depend on whether the particles be still attached to aggregate surfaces or detached and introduced to the cement paste after mixing (Munoz et al., 2007; Desire & Leopold, 2013). This depends on the chemical and physical properties, and that is why an accurate sampling, distinguishing, and studying of fines properties is required to predict further influence on the concrete performance.

Stone dust particles and calcium carbonates are commonly believed to have lower water absorption capacity and be weakly attached to the aggregate surface, and could be easily detached by the normal washing process. Clay particles are commonly finer than other microfines (<2μm), have a larger specific area, and a net negative surface charge. Some types of clays tend to strongly adhere to the aggregate surfaces by stronger electrostatic forces, and thus clays should be further classified to kaolin, illite, and montmorillonites, the three most common types of clay minerals present in earth's crust, which have different crystalline structure (Schmitt, 1990; Gullerud, 2002; Munoz et al., 2010; Fernandez et al., 2011). As clay particles carry a net negative charge, they are able to retain cations on their surface, and this measure is called cation exchange capacity (CEC) (Sumner & Miller, 1996). Clays with higher CEC tend to adhere more firmly to the aggregate surfaces and have a swelling crystalline structure, which attributes to higher water adsorption capacity (Munoz et al., 2007). A summary of key characteristics of aggregate microfines, including

chemical composition, absorption capacity, adherence to aggregate surface, and swelling and CEC can be found below in Table 1.

Table 1. Summary of key characteristics of aggregate microfines.

Type		Typical Sources	Chemical Composition	Absorption Capacity	Adherence to Agg. Surface	Swelling and CEC
Stone dust		Crushing, screening and weathering of most stone, sand and gravel aggregates[4]	Composition similar to processed aggregate[1]	Low[1]	Weak[1]	N/A
Calcium carbonates		Precipitation from groundwater in sand and gravel deposits or formation in some quarried deposits like limestone and dolomite[1,4]	$CaCO_3$	Medium[1]	Weak to medium[1]	N/A
Clays	Kaolinite	Overburden layers or seams in stone quarries, sand or gravel deposits. Inadequate storage on the Earth surface[4]	$Al_2Si_2O_5(OH)_4$[3]	Low[2,3]	Weak[2]	Non-swelling[3] Low CEC (1.7-2.4 meq/100g)[2]
	Illite		$(Si_4)(Al, Mg, Fe)_{2.3}O_{10}(OH)_2 \bullet (K,H_20)$[3]	Medium[2,3]	Weak to medium[2]	Non-swelling[2] Medium (15 meq/100g)[2]
	Montmorillonite		$(Na,Ca)_{0.33}(Al_{1.67}Mg_{0.33})Si_2O_{10}(OH)_2 \bullet (H_2O)$[3]	High[2,3]	Strong[2]	Crystalline-swelling[2] High (74-79 meq/100g)[2]

[1]Schmitt 1990
[2]Munoz et al. 2010
[3]Fernandez et. al. 2011
[4]Goldbeck 1932

2.3. Influence of Microfines on concrete characteristics

The influence of microfines on concrete characteristics depends on the microfines' physiochemical properties and the state of presence: dispersed in the mix or still adhere to the aggregate surface even after mixing with cement paste (Goldbeck, 1932; Schmitt, 1990).

2.3.1. Effect of Microfines on Fresh Concrete Properties

Fresh concrete properties are mostly affected by loose or detached fines that were introduced into the paste during the mixing procedure, which is more common for dust and carbonate coatings (Gullerud, 2002). They could affect the workability, withhold the air entrainment process, or influence the early hydration process by introducing additional chemical reactions.

The results of the previous research works noted the increase of the water demand and, consequently, the decrease in the workability if the presence of dust and clay particles was not accounted for. This was commonly attributed to the increased surface area of fine particles (Celik

and Marar, 1996). Moreover, the shape and texture characteristics of these particles showed a significant influence on the extent to which they will decrease the workability. The presence of the calcium carbonate microfines may even result in the improvement of workability (Antoni et al., 2015). Round shaped carbonate particles tend to have relatively low water demand than angular dust particles (Bigas & Gallias, 2001). Besides, the study of Chan et al. (2013) presented evidence that the crushed stone dust particles have a negative effect not only on workability but also on workability retention. Clay particles with swelling crystalline structure and larger surface area, such as montmorillonites, show larger water demand than dust particles and other clays as kaolinite and illite (Gullerud, 2002; Munoz et al., 2007).

According to Munoz et al. (2010), excess stone dust and calcium carbonates have little effect on the air content, whereas excessive clay particles are causing a major decrease in air content even with a major application of air entrainment agents (AEAs). This was explained by the high water adsorption capacity of clay particles so that in the mixes where the mixing water amount was not adjusted for microfines presence, there is no enough water for proper AEAs work or possible interaction between AEA and clay particles, which disrupts the stable formation of air bubbles. The experimental study of Munoz et al. (2007) showed the slight effect of stone dust particles on the AEA demand, whereas the amount of AEA required for desired air content in mixes with the presence of clays was significantly higher. The study of Gullerud (2002) also showed a little effect of stone dust and carbonates on the air content, while the presence of clay particles had a significant negative impact. On the other hand, the study of Celik and Marar (1996) showed a decrease in the air content of the batches prepared with an increased amount of stone dust. The decrease in the air void number was attributed to the filler effect of microfines.

While stone dust particles have no significant effect on the hydration process, carbonates and clays initiate different chemical reactions (Schmitt, 1990; Pera et al., 1999; Noble, 1970; Pike, 1992). The study of Pera et al. (1999) showed the accelerated hydration of tricalcium silicate (C_3S, the main constituent of Portland cement contributing to the early strength development) as a result of the presence of calcium carbonates. However, the interaction between clay and cement particles is different. Noble (1970) suggests that during the process of hydration and production of CH, part of calcium ions and calcium hydroxide (CH) are being absorbed in the clay structure and surfaces by cation exchange mechanisms, followed by possible encapsulation of cement grains and CH crystallites by clay particles and hydration products. Thus, clay particles form an impermeable layer around the cement grains, which results in a decreased hydration rate (Pike, 1992). The results of the experimental study of Munoz et al. 2007 proved this concept, showing the decreased rate of early hydration reactions, lower concentration of CH, and a higher concentration of unhydrated cement particles in the mix with sodium montmorillonites, clay particles with high cation exchange capacity. However, the same study showed the opposite effect of calcium montmorillonite and kaolin presence when the early hydration rate was increased.

The quantitative summary of how different types of microfines affected the fresh properties of concrete is presented in Table 2. It can be noticed that the negative impact increased not only with the increase in the amount of microfines (P200 value), but also with the increase of the Methylene Blue Value (MBV).

Table 2. Summary of effect of microfines on fresh properties based on previous studies.

Coating type	P200 (%) and MBV (mg/g)	Workability (% change compared to control mix)	Air Content (% change compared to control mix)
Calcium carbonate[1]	P200 - 0.3% MBV – 0.78 mg/g	No effect	6% decrease
Calcium carbonate and clay[1]	P200 – 1.3% MBV – 6.0 mg/g	42% decrease	No effect
Stone dust[1]	P200 – 1.9% MBV – 3.7 mg/g	60% decrease	9% decrease
Stone dust and clay[2]	P200 – 0.76% MBV – 0.8 mg/g	8% decrease	No effect
Stone dust and clay[2] (montmorillonite)	P200 – 1.47% MBV – 6.67 mg/g	42% decrease	14% decrease
Stone dust and clay[1] (mainly montmorillonite)	P200 – 1.3% MBV – 11.4 mg/g	40% decrease	13% increase
Clay[2] (Illite)	P200 – 0.4% MBV – 6.67 mg/g	8% decrease	5% decrease
Clay[2] (Kaolinite)	P200 – 0.68% MBV – 6.76 mg/g	33% decrease	5% decrease 12% increase (with 4.4% extra water)
Clay[2] (Na-montmorillonite)	P200 – 1.45% MBV – 15.8 mg/g	100% decrease (no slump)	31% decrease 5% drop (with 20% extra water)
Clay[2] (Ca-montmorillonite)	P200 – 0.79% MBV–106.7 mg/g	75% decrease	57% decrease 21% increase (w/ 40% extra water)

[1]Gullerud 2002

[2]Munoz et al. 2007

2.3.2. Effect of Microfines on Mechanical Properties of Hardened Concrete

As the presence of the microfines may increase the water demand and if the absorption of microfines will be ignored, it can lead to the decreased effective water-to-binder ratio and the increased compressive strength (Goldbeck, 1932). The study of 18 different stone dust additions to the concrete mix by Ahn and Fowler (2001) showed an increase in the compressive and tensile strength of the concrete specimens when the water-to-binder ratio was not adjusted. However, the introduction of additional mixing water amounts to satisfy additional water requirement result in a gross water-to-binder ratio increase and a decrease in compressive strength. Batches that were mixed with an addition of extra water to provide better workability, demonstrated a decrease in strength (Munoz et al., 2010).

Another possible negative impact of microfines presence on concrete strength characteristics is associated with weaker aggregate-cement paste bond formation, which is mostly related to the presence of firmly attached clay particles (Goldbeck, 1932; Schmitt, 1990). Tasong et al. (1998) described the following three main mechanisms of the bond development between aggregate and cement paste: a mechanical interlock between the rough aggregate surface and hydration products; a growth of an epitaxial layer of hydration products on aggregate surfaces; and a bond between aggregate and hydrating cement grains as a result of chemical reactions. Thus, the presence of the

microfines may disrupt the proper aggregate-to-cement paste bond development even by influencing one of these mechanisms.

Stone dust particles are generally dispersed or detached during the concrete mixing procedure, thereby having little effect on the interfacial transition zone. However, if they still adhere to the aggregate surface, theoretically, they may disrupt a proper interlock or penetration of cement hydration products into the aggregate surface pores (Gullerud, 2002). No significant effect of dust microfines on the concrete strength was shown if the specimens were properly cured (Gullerud, 2002; Cramer et al., 2010; Munoz et al., 2010). The presence of carbonates resulted in an increase of the compressive and more significantly of the tensile strength due to additional pozzolanic reaction, and the formation of calcium hydro-carbonaluminates described earlier (Pera et al., 1999; Gullerud, 2002, Munoz et al., 2010).

Clay particles firmly attached to the aggregate surface may disrupt proper bond development and result in a more porous and weak interfacial transition zone by forming a thick water layer around the aggregate surface due to their high water absorption and crystalline swelling (Gullerud, 2002). Thus, the presence of the clays that strongly adhere to aggregate surfaces (typically montmorillonites with high cation exchange capacity) and high absorption capacity results in a more significant strength decrease than other clays (kaolin and illite) (Munoz et al., 2007).

However, the contribution of the interfacial transition zone to the overall strength of the concrete is not as high as it seems to be. In their study, Darwin (1999) states that the properties of the aggregate and cement paste materials are more important than the bond strength between them, which can account only for 15% of the overall strength.

The quantitative summary of how different types of microfines affected the mechanical properties of concrete is presented in Table 4. Results showed that the presence of the carbonates had a positive impact on tensile strength development only, while the presence of dust was not significant in coatings where the amount of harmful clays was low. Clay type dusts tend to lead to a more negative impact on the strength of concrete, with the highest negative impact from montmorillonites (clays with high MBV). It is worth noticing that the addition of an extra amount of mixing water in the mixes with montmorillonites had a positive effect on the strength of the concrete. This can be explained by possible improved packing of more workable concrete mixture and due to the fact that a significant amount of unhydrated cement particles was found in the cement paste with a high amount of montmorillonites and not adjusted water amount (Munoz et al., 2007).

Table 3. Summary of effect of microfines on mechanical properties based on previous studies.

Coating type	P200 (%) MBV (mg/g)	Change in compressive strength (%)	Change in tensile strength (%)
Calcium carbonate[1]	P200 - 0.3% MBV – 0.78 mg/g	No significant effect	19% increase
Calcium carbonate and clay[1]	P200 – 1.3% MBV – 6.0 mg/g	No significant effect	10% increase
Stone dust[1]	P200 – 1.9% MBV – 3.7 mg/g	No significant effect	No significant effect
Stone dust and Clay[2]	P200 – 0.76% MBV – 0.8 mg/g	9% decrease	No significant effect
Stone dust and clay[2] (montmorillonite)	P200 – 1.47% MBV – 6.67 mg/g	9% decrease	No significant effect
Stone dust and clay[1] (mainly montmorillonite)	P200 – 1.3% MBV – 11.4 mg/g	5% decrease	11% increase
Clay[2] (Illite)	P200 – 0.4% MBV – 6.67 mg/g	16% decrease	16% decrease
Clay[2] (Kaolin)	P200 – 0.68% MBV – 6.76 mg/g	13% decrease 40% decrease[3]	5% decrease 35% decrease[3]
Clay[2] (Na-montmorillonite)	P200 – 1.45% MBV – 15.8 mg/g	88% decrease 54% decrease[3]	79% decrease 36% decrease[3]
Clay[2] (Ca-montmorillonite)	P200 – 0.79% MBV–106.7 mg/g	75% decrease 47% decrease[3]	65% decrease 41% decrease[3]

[1]Gullerud 2002

[2]Munoz et al. 2007

[3]For batches where additional mixing water was added to maintain workability

2.3.3. Effect of Microfines on Durability Characteristics

As was described earlier, aggregate coatings that remain adhered to the aggregate surface may modify the interfacial transition zone, making the bond between aggregate and cement paste more porous, which can significantly influence the durability characteristics of the concrete (Munoz et al. 2010). The formation of percolated ITZ paths (Figure 1) may further increase the mass transport properties of the concrete, thereby enhancing the permeability and the access of water and other harmful solutions into the concrete matrix (Winslow et al. 1993; Caliskan et al. 2002).

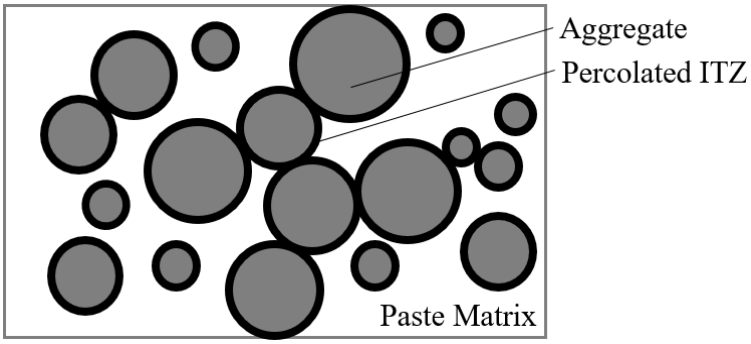

Figure 1. Schematic of interfacial zone percolation (Adapted from Winslow et al. 1994).

An increase in the permeability may also be associated with the increase in the water-to-binder ratio, when additional mixing water was introduced to the fresh concrete matrix in order to maintain the desired workability level, which was decreased due to the extra water requirement of the microfines present in the mix (Munoz et al., 2007).

Previous studies show that the largest effect on concrete shrinkage was associated with the presence of clay particles. The magnitude of shrinkage strongly correlates with the water adsorption capacity of microfines, as the presence of montmorillonites resulted in the biggest shrinkage increase (Munoz et al., 2007). Having less adsorption capacity, stone dust, and carbonates resulted in less and almost no effect on the concrete shrinkage, respectively (Gullerud, 2002; Munoz et al., 2010).

The quantitative summary of how different types of microfines affected the drying shrinkage is presented in Table 4. Similar to the impact on concrete strength, the addition of an extra amount of mixing water in the bathes with montmorillonites had a positive effect on the shrinkage of the concrete.

Table 4. Summary of effect of microfines on shrinkage of concrete based on previous studies.

Coating type	Change in drying shrinkage (%)
Calcium carbonate[1]	No significant effect
Calcium carbonate and clay[1]	No significant effect
Stone dust[1]	26% increase
Stone dust and Clay[2]	No significant effect
Stone dust and clay[2] (montmorillonite)	No significant effect
Stone dust and clay[1] (mainly montmorillonite)	41% increase
Clay[2] (Illite)	No significant effect
Clay[2] (Kaolin)	21% increase /16% increase[3]
Clay[2] (Na-montmorillonite)	54% increase /52% increase[3]
Clay[2] (Ca-montmorillonite)	161% increase /62% increase[3]

[1]Gullerud 2002

[2]Munoz et al. 2007

[3]For batches where additional mixing water was added to maintain workability

2.4. Current Practice and Microfines Monitoring Tests

The grading and quality of fine and coarse aggregates are commonly specified by ASTM C33 (Standard Specification for Concrete Aggregates), where microfines are referred to as material passing No.200 sieve (finer than 75-μm) and mainly composed of stone dust, derived as a result of crushing procedure to obtain manufactured aggregate, and in some cases deleterious constituents: clay lumps, coal, and organic particles. While it is specified that the presence of organic impurities should be determined and limited by ASTM C40 (Standard Test Method for Organic Impurities in Fine Aggregates for Concrete), and of coal particles by 1.0% of the total mass of the sample, there is no specification to distinguish between clay particles and stone dust, limiting the overall presence of microfines to be less than 3.0%, except for manufactured or recycled aggregate samples free of clay, where the limit can be raised to 5.0-7.0% depending on concrete abrasion conditions (Figure 2).

The presence of stone dust and deleterious particles in the coarse aggregate matrix is also stated by ASTM C33, but specified based on the weathering conditions of the region (Figure 2) and type of construction.

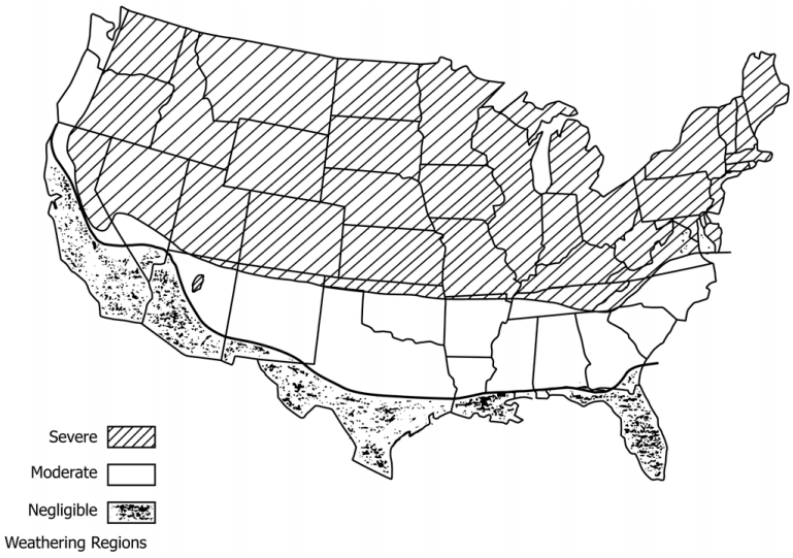

Figure 2. Location of Weathering Regions (adapted from ASTM C33/C33M-18).

Nebraska and other Midwest states are associated with its cold climate where concrete is generally subjected to repeated freezing and thawing, and the application of aggressive deicing chemicals, and thus are categorized as the regions with severe weathering conditions (S). For these locations, the maximum allowable percent of microfines present in the coarse aggregates' matrix is established to be 1.0%, except for aggregates free of clay or when used in combination with fairly clean fine aggregates, containing fewer microfines than a specified limit.

Table 5. Limits for impurities in fine and coarse aggregates according to ASTM C33.

Aggregate	Item		Mass Percent (%)
Fine Aggregates	Organic impurities [A]		-
	Coal and lignite impurities		0.5-1.0[B]
	Fines passing No.200	With possible clay presence	3.0
		Free of clay or shale	5.0-7.0[C]
Coarse Aggregates	Coal and lignite impurities		0.5-1.0[D]
	Fines passing No.200	With possible clay presence	1.0[E]
		Free of clay or shale	1.5

[A] Specified by ASTM C40

[B] If concrete surface appearance is important, the limit is 0.5%, otherwise – 1.0%

[C] If concrete is subjected to abrasion, the limit is 5.0%, otherwise – 7.0%

[D] For interior or not exposed to weather concrete is 1.0%, otherwise – 0.5%

[E] To be increased if fine aggregate contains an acceptable amount of microfines to:

$L = 1 + [(P) / (100 - P)] \times (T - A)$

P – amount of fine aggregates as a percent of total aggregates

T – established limit for microfines in the fine aggregates

A – actual amount of microfines in the fine aggregates

In addition to general ASTM C33 requirements, all aggregates producers are obliged to follow the requirements of the local Department of Transportations (DOT), which can modify the above-listed microfines limits taking into consideration features and conditions of local aggregate quarries. The summary DOT requirements of all Midwest and neighboring states is presented in Table 6. Based on the summary, the average allowable amount of materials finer than No. 200 for fine aggregate is approximately 2.94% (standard deviation of 0.90%), which is similar to the current NDOT requirement of 3%. However, the average amount of materials finer than No. 200 for coarse aggregate was found to be at 1.60% (standard deviation of 0.69%) and 1.70% (standard deviation of 0.82%), which is significantly lower than the current NDOT requirement of 3%.

Table 6. Maximum allowable amount of microfines and other deleterious substances established by Midwest and neighboring state DOTs.

DOT	Fines Aggregate requirements		Coarse Aggregate requirements	
	Microfines P200 (%)	Other Deleterious substances	Microfines P200 (%)	Other Deleterious substances
FHWA	3.0%[1]	CL+F ≤ 3.0% C ≤ 1.0.% OI[3]	1.0%[4]	CL+F ≤ 2.0% CH ≤ 3.0% Total ≤ 3.0%
Nebraska	3.0% NDOT 27[2]	CL ≤ 0.5% LW ≤ 3.5% (Vol)	3.0% NDOT 27[2]	CL ≤ 0.5% SH ≤ 1.0% SF ≤ 3.5% LW ≤ 3.5% (Vol.) Total ≤ 3.5%
California	3.0-4.0%[2,5]	-	3.0-4.0%[2,5]	-
Colorado	3.0% Proc 3[1]	CL+F ≤ 3.0% C ≤ 1.0.% OI[3]	1.0%[1]	CL+F ≤ 2.0% CH ≤ 3.0% Total ≤ 3.0%
Idaho	4.0%[2,6]	OI[3] CL ≤ 1.0% C ≤ 1.0% Others ≤ 5.0%	1.0%[1]	CL ≤ 0.5% CL+F ≤ 2.0% C ≤ 1.0% TE ≤ 15%
Illinois	3.0% ITP 11[1]	OI[3] SH ≤ 1.0% CL ≤ 1.0% C+SH ≤ 1.0% Total: 3.0%	1.0% ITP 11[1]	SH ≤ 1.0% CL ≤ 0.25% C < 0.25% SF ≤ 4.0% Others ≤ 4.0% Total ≤ 5.0%
Indiana	3.0%[1]	OI[3]	1.5%[1]	CL+F ≤ 1.0% C+SF ≤ 4.0% CH ≤ 3.0%
Iowa	1.5%[2]	C+SH ≤ 2.0%	1.5%[2]	CL+F ≤ 0.5% C+SH ≤ 0.5% OI ≤ 0.01%
Kansas	2.0% KT-3[1]	OI[3] CL+F ≤ 1.0%	2.5% KT-3[1]	SH ≤ 0.5% CL ≤ 1.0% C ≤ 0.5%

Michigan	3.0%[7] MTM 108[1]	OI[3]	For natural and glacial: 1.0% For crushed stone: 2.0% For crushed PCC: 3.0% MTM 108[1]	SF ≤ 2.0% (3.0%*) CH ≤ 2.5% (7.0%*) Total ≤ 4.0* (9.0%* 2.0**) * for crushed PCC **for natural CA
Minnesota	2.5%[2]	SH+SF ≤ 2.5% C ≤ 0.3% OI[3]	For Gravel: 1.0%[2] For Crushed stone: 1.5%[2]	SP ≤ 1.0-1.5% SF ≤ 2.5% CL ≤ 0.3% Total ≤ 3.5%
Missouri	2.0%[2,8]	CL+SH ≤ 0.25% C ≤ 0.50% Others: 0.10%	2.5%[2,9]	SP ≤ 1.0-1.5% SF ≤ 2.5% CL ≤ 0.3% Total: 3.5%
Montana	3.0%[2]	CL+F ≤ 3.0% OI[3]	1.0%[2,4]	LW ≤ 3.0% CL+F ≤ 3.0% Total: 5.0% TE ≤ 15.0%
Nevada	5.0% Nev. T206[1]	CL ≤ 1.0% OI[3]	1.0% Nev. T206[1]	CL ≤ 1.0%
North Dakota	3.0%[2]	OI[3]	1.0%[2]	SH ≤ 0.7% SP ≤ 4.0% C ≤ 0.5% TE ≤ 15%
Ohio	5.0%[1]	Organic Impurities[3] Shale particles: S1029	3.8% / 2.2%[1,10]	SF ≤ 3.0% (2.0%*) C ≤ 1.0% (0.25%*) CL ≤ 0.25% (0.25%*) SH ≤ 1.0% (0.5%*) LC ≤ 1.0% (0.5%*) AL ≤ 1.0% (0.5%*) CH ≤ 1.0% (0.5%) * for super-structures
Oklahoma	3.0%[1]	CL+F ≤ 3.0% C ≤ 1.0.% OI[3]	2.0%[1,11]	CL+F ≤ 2.0% CH ≤ 3.0% Total ≤ 3.0%
South Dakota	1.5%[5] SD206[1]	CL ≤ 0.5% C ≤ 0.3% LW ≤ 1.0% AL+MC+SF ≤ 1.0% OI[3]	1.5%[5] SD206[1]	CL ≤ 0.3% SH+LW ≤ 1.0% AL+MC+C ≤ 2.0% Total: 2.0%
Utah	3.0%[1]	CL+F ≤ 3.0% C ≤ 1.0.% OI[3]	1.0%[1,4]	CL+F ≤ 2.0% CH ≤ 3.0% Total ≤ 3.0%
Wisconsin	3.5% 2.3%[12]	C ≤ 1.0% CL ≤ 1.0% SH ≤ 1.0% Others ≤ 1.0% Total ≤ 3.0%	1.5%	SH ≤ 1.0% C ≤ 1.0% CL ≤ 0.3% SF ≤ 5.0% Total ≤ 5.0%

Wyoming	3.0%[1]	CL+F ≤ 1.0% C ≤ 1.0.% OI[3]	2.0%[1]	SH+C ≤ 0.1% CL ≤ 0.5% F+TE ≤ 3.0% Total ≤ 5.0%

[1]AASHTO T11, ASTM C117 or other alternative washing test method
[2]AASHTO T27, ASTM C136 (or other alternative sieve analysis method) or not specified. However, the washing test is addressed by the standard sieve analysis as a specific method to measure the amount of fines passing No.200 sieve.
[3]AASHTO T71 and/or AASHTO T21 or modified DOT alternative
[4]May be raised to 1.5 if essentially free of clay or shale
[5]For combined FA and CA
[6]2.0% for wearing surfaces, except if Sand Equivalent value > 80, then 3.0%
[7]For carbonates: 4.0%
[8]For natural sand: 2.0%; For manufactured sand: 4.0%
[9]Permitted to increase the limit up to 3.0% if P200 in FA is less than 1.0%
[10] For washed gravel: 2.2%; For furnace slag ACBFC: 3.8%
[11]For CA #357: P200 - 1.5%
[12]For overlays and repairs on the decks
CL – Clay lumps; F – Friable particles; CH – Chert; C – Coal and lignite; OI – Organic Impurities; LW – lightweight particles; SH – Shale; SF – Soft Particles; TE – Thin and Elongated; SP – Spall; LC - Limonitic Concretions; AL – Alkali; MC – Mica; Others: shale, alkali, mica, coated grains

It can be seen that all the DOTs require the quantitative assessment of microfines and other deleterious particles, such as clay lumps, coal, organic, and others. However, almost none of them has a special requirement to distinguish between different types of microfines. It is common that the microfines amount is generally to be tested by the standard washing test method, but Kansas and Michigan DOTs introduce the procedure involving a mechanical washer, which can be more reliable when compared to the standard manual washing procedure, as it possibly enhance the detachment of adhered coatings and reduce operators' error.

Even if, in some cases, it is allowed to increase the P200 limit for aggregates essentially free from clays, there is no specific instruction to verify the absence of clays in those aggregate. It is worth noting that Michigan and Minnesota DOTs have different limits for natural and crushed stone aggregates, likely due to the fact that the presence of clays is more likely to be the case for natural aggregates, rather than for crushed stone.

NDOT requires both coarse and fine aggregates, to contain no more than 0.5% clay lumps. It is important to distinguish the term "clay lump" from the clay microfines particles described earlier. Here, clay lumps refer to "any material which can be broken with the fingers into finely divided particles when dry, or, after the initial rinsing of the material, is found to be soft, and can be extruded between the fingers when squeezed and feels greasy to the touch" and are to be regulated by means of NDOT T504, a standard method to determine clay lumps, shale and soft particles in coarse and fine aggregate. However, the actual amount of clay particles, and especially of harmful clays as montmorillonites, is not distinguished from the total amount of microfines, which is regulated to be under 3.0% for coarse and fine aggregate.

The specifications of DOTs were also checked to contain any special requirements in addition to the limits of amounts of microfines and other deleterious substances and the findings are summarized below in Table 7.

Table 7. Special aggregate dust-related requirements of DOTs.

DOT	Special Requirements for fine aggregates	Special Requirements for coarse aggregates
Nebraska	Washing requirement for all FA FA from dry pits: Sand equivalent value > 90	-
California	Sand equivalent value > 75	Cleanness value > 75 (California Test 227)
Colorado	Sand equivalent value > 80	-
Idaho	Sand equivalent value > 70	-
Illinois	Washing requirement for all FA P200 does not apply to washed stone sand	-
Minnesota	Washing requirement for all FA Strength tests at 3-d (Type III) and 7-d (Type I/II) > 90% than Ottawa Sand (AASHTO T71)	Washing requirement for all CA, except crushed quartzite, gneiss and granite
Missouri	Strength tests at 7-d (Type I) > 90% than Ottawa Sand (AASHTO T71)	Washing requirement for gravel
Nevada	Sand equivalent value > 71	Cleanness Value > 71
Ohio	-	Washing requirement for gravel
Wisconsin	The P200 washing test may be substituted by dry sieving if actual P200 is less than half of the limit (washing test should be performed on every 10^{th} sample)	-
Wyoming	Washing requirement for all FA	Washing requirement for all CA to reduce P200 at least 50%

It can be noticed that only about half of the DOTs presented earlier have additional special requirements such as a sand equivalent value, Fineness Modulus, or strength. Although, in their regulations, DOTs generally require to use coarse and fine aggregates “composed of clean, hard, durable, and uncoated particles”, which are “free from injurious quantities of dust, soft or flaky particles, loams, alkali, organic matter, paper, wood, or other deleterious matter as determined by the Engineer”, only 6 out of 20 assessed DOTs require washing of aggregates, but not specifying the exact procedure and only stating the vague requirement to wash aggregates from any coatings. The only specific requirement is demanded by Wyoming DOT, where they require to wash coarse aggregates to get rid of approximately half of the coating particles when compared to prior to the washed state.

While NDOT requires that fine aggregates from wet pits shall be washed to clean any coatings, it is additionally required to wash and check the Sand Equivalent value of the fine aggregates from dry pits. In instances where the Sand Equivalent value is less than 90, it is recommended to check if the 7-days compressive strength of the mortar cubes made of these aggregate be no less than that made of the same aggregate, but washed to have a sand equivalent value greater than 90. Although this proactive monitoring procedure is possibly sufficient to prevent strength issues of the concrete,

there is no guarantee that there will not be any durability, workability, and air entrainment problems related to the presence of the microfines, which were described earlier.

The X-ray diffraction analysis may be used as a direct method to identify the mineralogy of the microfines collected after drying off the rinse water collected after the standard washing test. Although this test requires a specific equipment setup, it was widely used by the number of researchers as it is one of the few ways to identify the exact chemical composition of the sample (Gullerud, 2002; Munoz et al., 2007; Cramer et al., 2010; Cramer et al., 2011)

Another method to assess the mineralogy of microfines is the Methylene Blue Adsorption Test (MBT). This test is based on the absorption of the methylene blue dye by clay minerals: the higher the MBV indicates the presence of the harmful clays with higher CEC. The test could be further modified by multiplying the Methylene Blue Value by the P200 value, thereby obtaining Modified Methylene Blue Value (MMBV), which could work as a better predictor of the influence of the microfines on concrete performance as it combines both: quantitative and qualitative characteristics of the examined coating (Munoz et al., 2007).

The effect of different coating particles on the function of air entrainment could be assessed by means of the modified foam index test, which is originally designed to predict required Air Entrainment Agent (AEA) dosage for concrete containing fly ash, which is known to negatively impact the amount of entrained air. Although there is a variety of test approaches, and there is no standard procedure to follow, the study of Harris et al. (2008) showed the results of the foam index test are highly subjectable to the approach. Thus, amongst four different testing setups and procedures that were studied in their paper, it was shown that the bottle shake method (using the container of 132-ml volume and 45 mm of inner diameter) ended up in the results with the best correlation to the real AEA dosage requirement of fresh concrete.

2.5. Summary

Overall, it is still not clear if the current practice is sufficient to accurately quantify aggregate microfines and use it to adequately predict the concrete performance due to the following limitations:

- While the standard washing test seems to be a simple and optimal tool to identify the number of microfines that are dispersed or weakly attached to aggregates surface, it does not take into account particles that are still firmly attached after the washing procedure. Thus, this test may result in an underestimated P200 value (unless washed with a detergent or by the mechanical washer)
- Current practices do not distinguish between different types of microfines, although it is specified to determine the amount of clay lumps and eliminate the presence of organic impurities
- The proposed compressive strength testing of mortars made of fine aggregate not passing the Sand Equivalent limit might not be enough as it does not show the effect on the durability and fresh properties of the concrete

Thus, it was proposed to modify microfines sampling and quantification procedure, as well as to introduce the qualitative analysis in order to distinguish between different coatings types and their properties, such as X-ray diffraction, methylene blue test, and others.

CHAPTER 3. MATERIALS AND TEST METHODS

3.1. Introduction

The objective of this chapter is to present the materials, which were selected to conform to the NDOT requirements of the 47B mix for concrete pavement, as well as to provide a complex study of the most commonly used aggregates across the state. The details of the mixing proportioning and batching procedure were also included in this chapter.

It was also critical to develop a reasonable experimental program for elaborate research. Thus, this chapter also describes a set of the selected testing methods and procedures for effective sampling and characterization of properties of aggregates and microfines and evaluation of concrete samples' performance.

3.2. Materials

3.2.1. Cement and Cementitious Materials

Type IP Portland-pozzolan interground/blended cement was used as the only cementitious material in this study per the NDOT standard specifications for highway construction (2017). Conforming to the material specifications of ASTM C595 (Standard Specification for Blended Hydraulic Cement) and containing 25% of Class F fly ash, the type IP cement is utilized to mitigate concrete durability issues, such as ASR.

3.2.2. Aggregate

Seven different samples of coarse and fine aggregates collected with the assistance from NDOT and one additional fine aggregate from Western Nebraska collected through a previous project were included in this study. In addition, a limestone aggregate and a sand and gravel aggregate locally available in the Eastern Nebraska region, were used as the reference coarse and fine aggregate, respectively. A list of the ten aggregate included in the present study is presented in Table 8 below. Images of appearances of the aggregate can be found in Figure 3.

Table 8. Sources and location of aggregates.

	Aggregate ID	Type	Source and Location
1	DO_WY	Dolomite	Harriman Quarry, Laramie, WY
2	GN_WY	Granite	Martin Marietta, Granite Canyon, WY
3	LS_NEE1	Limestone	Kerford Limestone, Weeping Water, NE
4	QZ_SD	Quartzite	Rapid City, SD
5	GR_NEW	Gravel	Apex Dry Pit, Gering, NE
6	SG_NEC1	Sand and Gravel	Platte River Wet Pit, Platte River, NE
7	SG_NEC2	Sand and Gravel	Grant Island, NE
8	SG_NEW*	Sand and Gravel	Ogallala, NE
9	LS_NEE2**	Limestone	Omaha, NE
10	SG_NEE2**	Sand and Gravel	Omaha, NE

*Aggregate sample collected from a previous project

**Reference aggregates: to be washed to minimize the P200 value as further described in Section 3.3.8

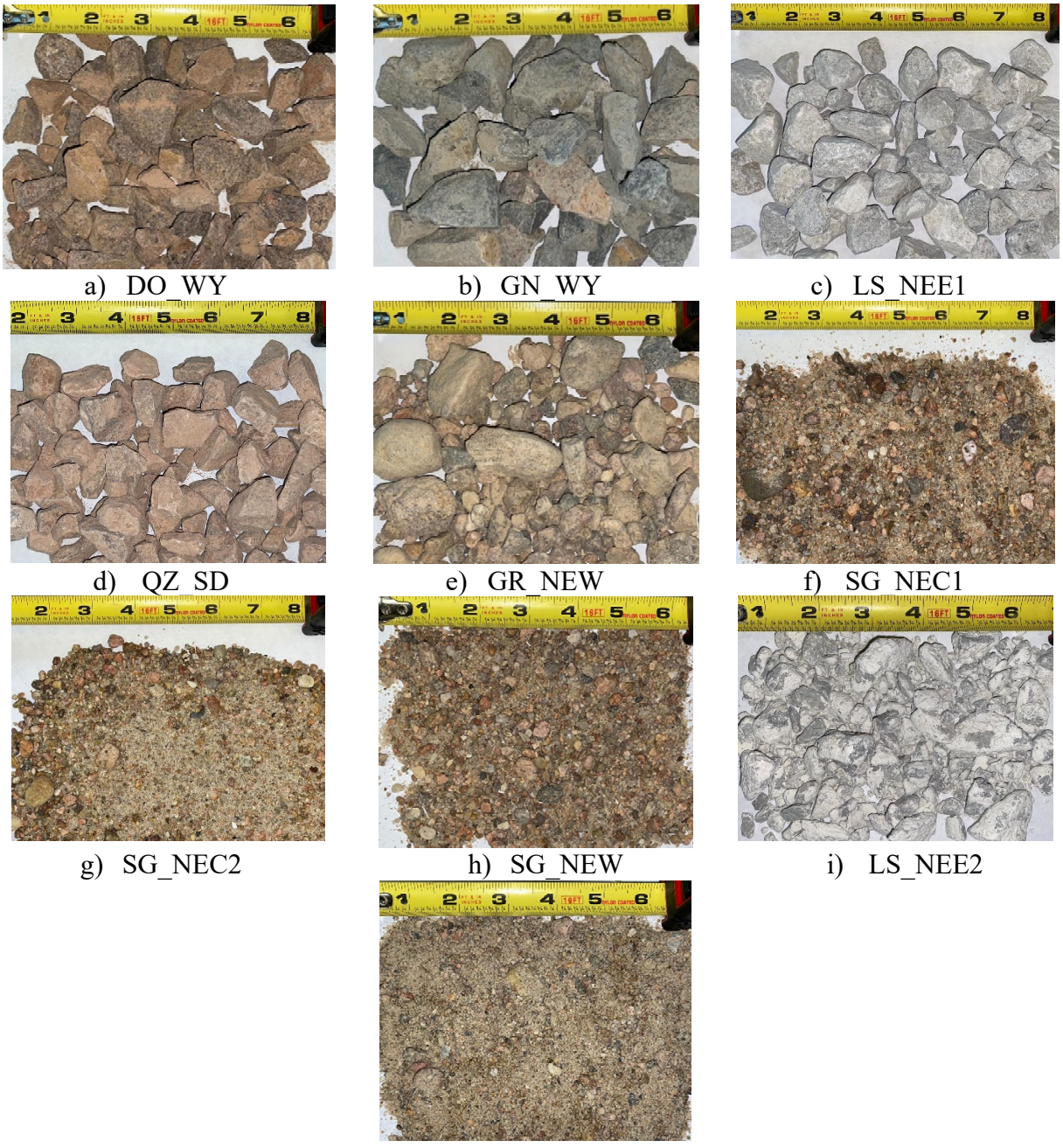

a) DO_WY b) GN_WY c) LS_NEE1

d) QZ_SD e) GR_NEW f) SG_NEC1

g) SG_NEC2 h) SG_NEW i) LS_NEE2

j) SG_NEE2

Figure 3. Appearances of aggregates in as-received condition.

3.2.3. Chemical Admixture

As it is expected that microfines will affect the workability and air content of the concrete, Master Air AE 90 was used as an air-entraining admixture (AEA) that conforms to ASTM C260 (Standard Specification for Air-Entraining Admixtures for Concrete), as well as Eucon X-15 was utilized as a mid-range water reducer (WR), which meets ASTM C494 (Standard Specification for Chemical Admixtures for Concrete) (ASTM, 2016; ASTM, 2019).

3.3. Laboratory Tests for Aggregate and Microfine Properties Evaluation

Aggregates were received in 50-lb bags. In order to obtain a representative sample of a testing size, aggregates were mixed, quartered, and sampled on a plastic blanket in accordance with ASTM C702 (Standard Practice for Reducing Samples of Aggregate to Testing Size) (ASTM, 2018).

3.3.1. Sieve Analysis

The particle size distribution of obtained coarse and fine aggregates was determined by sieve analysis following ASTM C136 (Standard Test Method for Sieve Analysis of Fine and Coarse Aggregates) (ASTM 2014). A representative aggregate sample of a required testing size was dried to a constant mass at a temperature of 110±5ºC prior to sieving in a mechanical sieve shaker, as shown in Figure 4.

Figure 4. Aggregate sieve analysis setup.

3.3.2. Washing Test

The amount of dust (material finer than 75-µm) present in each aggregate sample was identified by means of ASTM C117 (Standard Test Method for Materials Finer than 75µm (No. 200) Sieve in Mineral Aggregates by Washing) (ASTM, 2017). A representative sample of aggregates was dried at a temperature of 110±5ºC and then thoroughly washed in a clean bowl until rinse water appeared to be transparent (Figure 5b). The rinse water was drained through a 75-µm (No. 200) sieve, collected in a separate clean bowl (Figure 5c), and put in the oven until all of the water was dried off (Figure 5d). Microfines left on the bottom of the bowl were then collected and used in further aggregate characterization tests. The mass difference of the aggregate sample before and after the washing test indicated the amount of material finer than 75µm and was recorded and reported as a percent loss by weight.

a) The rinse water at the beginning of the test

b) The rinse water at the end of the test

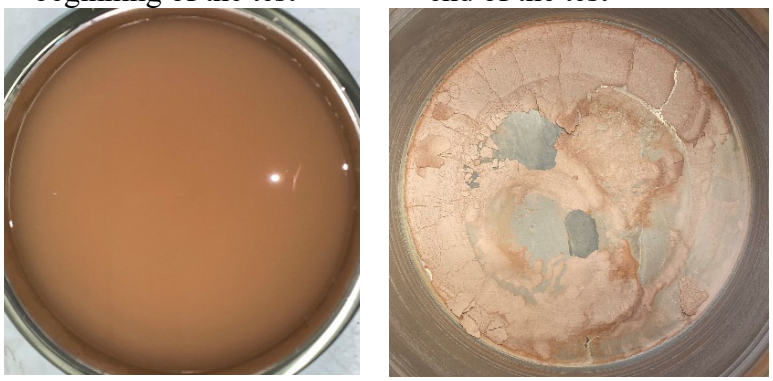

c) Collected rinse water

d) Dried off microfines

Figure 5. Example of steps for washing test.

3.3.3. Sand Equivalent Test

Another relatively quick and common test to identify aggregate dust or claylike materials content in a given set of fine aggregates is AASHTO T176 - Standard Method of Test for Plastic Fines in Graded Aggregates and Soils by Use of the Sand Equivalent Test (AASHTO, 2017). An oven-dry sample of fine aggregate was sieved through No. 4 sieve, moisturized to approximately saturated surface dry (SSD) condition, and sampled by quartering method. As shown in Figure 6, an obtained test sample was then oven-dried and put into a plastic cylinder, where it was thoroughly mixed with a calcium chloride solution. The process resulted in layers' separation of clay and sand that was further used to calculate the sand equivalent value, which quantifies relative proportions of sand versus clay in a given sample (i.e., a higher sand equivalent value indicates that there is less clay-like microfines content).

Figure 6. Sand Equivalent test apparatus and example of test result.

3.3.4. Methylene Blue Test

Another different approach of aggregate testing is to evaluate the quality of clay particles present on aggregates and predict their potential effect on concrete properties. One of the proposed test methods is AASHTO T330 (Standard Method of Test for the Qualitative Detection of Harmful Clays of the Smectite Group in Aggregates Using Methylene Blue) (AASHTO 2017). The method is based on mixing titrated Methylene Blue (5mg/ml) and water (30 ml) containing testing material (10 grams finer than 75-µm) and record how many drops of this mix will it take to form a blue ring on a filter paper, which will indicate that clay particles are not absorbing methylene blue anymore (Figure 3.5). Note that per ASTM C1777 (Rapid Determination of the Methylene Blue Value for Fine Aggregate or Mineral Filler Using a Colorimeter) (ASTM 2020), aggregate dust samples collected from sieving is to be used for MBV measurement. In this study, two types of microfine samples collected separately after dry sieving and after washing of each aggregate were used.

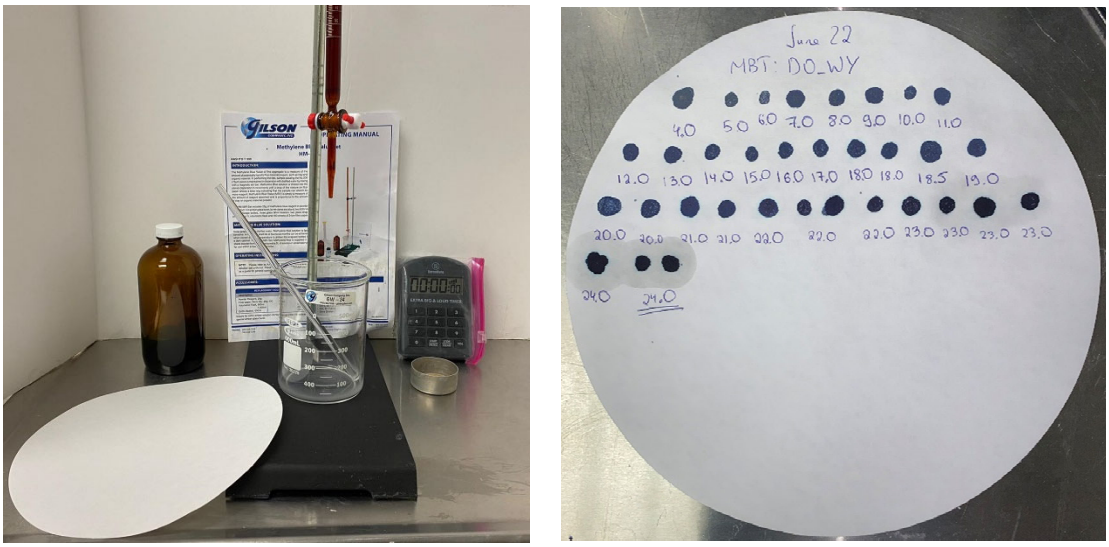

Figure 7. Methylene Blue test (MBT) equipment setup and example of test result.

3.3.5. Ultrasonic Cleaning of Aggregates

Although the amount of excess microfine materials can be assessed through the standard sieve analysis ASTM C136 (identifies the amount of loose microfines) or the washing test ASTM C117 (identifies the amount of microfines that are loose or weakly attached to aggregate surfaces), both techniques will not refer to those particles that are firmly attached to the aggregates. Thus, it was decided to introduce an additional cleaning technique – ultrasound cleaning, where a sample of washed aggregates was immersed in an ultrasound bath for complete detaching of microfines.

An approximately 1000g sample of washed aggregate was dried at a temperature of 110±5ºC and immersed into an ultrasonic bath (Figure 8) filled with 1500 mL of deionized water. The sample was then sonicated for 30 minutes at a normal (23ºC) temperature. The rinse water then was sieved through a No.200 sieve, dried off, and a sample of microfines was collected (Figure 9).

Figure 8. Ultrasound cleaner machine.

a) Aggregate immersed in an ultrasonic bath with clean deionized water

b) Aggregate after ultrasonic cleaning

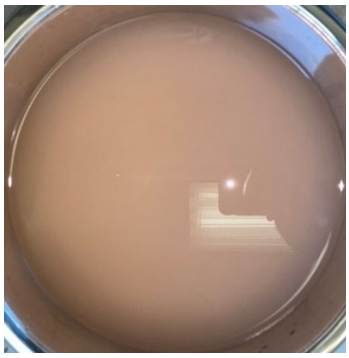

c) Collected rinse water

d) Dried off microfines

Figure 9. Example of step-by-step ultrasonic cleaning procedure.

3.3.6. Microfines Sampling Methods and Aggregate Cleanliness Conditions

It was also important to sample and distinguish between different types of fines (in case if loose and firmly attached microfine particles are of different mineralogy) and different conditions (states) of cleanness of aggregates. This was achieved by the following procedure:

Condition A. No microfines are sampled, and aggregates are used in further concrete mixing in as-received condition.

Condition B. Take aggregates in as received (state A) condition and proceed with standard sieve analysis (ASTM C136). As a result, collect microfine material that passed No.200 sieve and use it for MBT and XRD analysis.

Calculate the weight loss: $P_{200\,B} = (W_{OD\_A} - W_{OD\_B}) / (W_{OD\_A}) \times 100\%$

Label the obtained microfines as MF_ID_B (sample will represent microfine particles that were loose and dispersed in the original aggregate matrix)

Condition C. Take aggregates in as received (state A) condition and proceed with the standard washing test (ASTM C117), collect and dry off the rinse water to obtain the sample of microfines for further MBT and XRD analysis.

Calculate the weight loss: $P_{200\,C} = (W_{OD\_A} - W_{OD\_C})/ (W_{OD\_A}) \times 100\%$

Label the obtained microfines as MF_ID_C (sample will represent microfine particles that were loose or weakly attached to the aggregates' surface)

Condition D. Take the sample of the washed aggregate (state C) and clean it in an ultrasonic bath. Then, sieve the rinse water through the No.200 sieve, dry it off and collect the sample of microfines for further XRD analysis.

Calculate the weight loss: $P_{200\,D} = P_{200\,C} + (W_{OD\_C} - W_{OD\_D})/ (W_{OD\_C}) \times 100\%$

Label the obtained microfines as MF_ID_D (sample will represent microfine particles firmly attached to aggregates' surface that were not detached during the washing procedure)

As a result of the whole sampling procedure, the following should be obtained:

- Four conditions of aggregate: ID_A, ID_B, ID_C, and ID_D for as-received, dry sieved, washed, and sonicated conditions, respectively. (all four will be used for ITZ examination using SEM images and possible concrete mixing)
- Three samples of microfines: MF_ID_A, MF_ID_B, and MF_ID_C (for MBT, XRD analysis, and the foam index test)

A Summary of specimen and information to be obtained as a result of the proposed four-condition aggregate sampling procedure and proposed tests for microfines qualitative analysis can be found in Table 9 and Table 10, respectively.

Table 9. Summary of specimen and information to be obtained from the four different aggregate cleanliness conditions.

Sample	Method of Treatment	Specimen obtained	Information obtained
Condition A	None	- Agg – as-received dusty	Sand Equivalent Value
Condition B	Dry sieving through No. 200	- Agg – not very clean - Fines that are loose	Fine content - $P_{200\ B}$ (loose particles only)
Condition C	Washing	- Agg – fairly clean - Fines that are loose and weakly attached	Fine content - $P_{200\ C}$ (loose and weakly attached particles)
Condition D	Washing and ultrasonic cleaning	- Agg – very clean - Fines that are firmly attached	Fine content - $P_{200\ D}$ (firmly attached particles)

Table 10. Proposed tests for microfines qualitative analysis.

Property	Test	Sample Used
Mineralogy	X-ray Diffraction	Microfines collected after dry sieving (MF_B), washing (MF_C) and ultrasonic cleaning (MF_D)
Indirect detection of harmful clay content	Methylene Blue Test	MF_B and MF_C
Effect on interfacial transition zone (ITZ)	Visual ITZ examination	Aggregates at all four cleanness conditions: as received A, after dry sieving B, washed C, u-cleaned D

3.3.7. Reference Aggregates Preparation for Concrete Mixtures

Two of the obtained ten aggregates, from East Nebraska Limestone (LS_NEE2) and East Nebraska Sand and Gravel (SG_NEE2), were chosen to be the reference coarse and fine aggregates, respectively, which will be used in concrete batching while studying the effect of dust present in a companion aggregate sample. In order to minimize the effect of dust present in the reference aggregate matrices, they were thoroughly washed in a three cubic feet drum mixer.

During each batch of the washing of reference aggregates, approximately 77 to 88-lb for limestone (40 to 44-lb for sand and gravel) of aggregate was loaded into the mixer, and water in the amount enough to cover aggregate was then introduced into the mixer. The following aggregate washing procedure was then used:

i. Mix for 5 minutes, drain the wash water over the No.16 and 200 sieves, introduce clean water

ii. Run a few revolutions, drain the wash water over No.16 and 200 sieves, introduce clean water (repeat five times)

iii. Return the material retained on the sieves back into the mixer

An example of the step-by-step washing process is shown in Figure 10. The procedure was to be repeated three times, and by the end of the washing procedure, the rinse water should appear transparent.

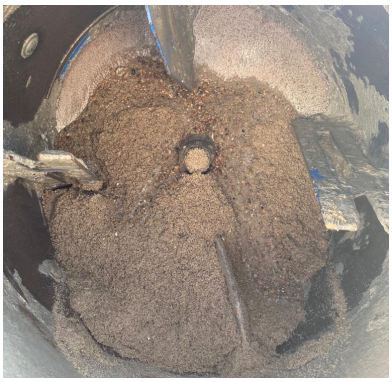

a) Loading of aggrgate in the mixer

b) Covering aggregate with clean water

c) After 1st round of 5-min washing

d) After 2nd round of 5-min washing

e) After 3rd round of 5-min washing

f) Clean aggregate covered with water

g) Draining off the rinse water

Figure 10. Step by step sand and gravel washing.

The efficiency of the washing procedure was assessed by means of the washing test (ASTM C117) and the sand equivalent test (AASHTO T176), as it was aimed to obtain the P200 values of both reference aggregates close to zero and the sand equivalent value of sand and gravel sample close to 100. The results of the tests of newly washed reference aggregates are presented in Table 11 below.

Table 11. Microfines content in the reference aggregates before and after washing.

Aggregate	P200		Sand Equivalent Value	
	Before washing	After washing	Before washing	After washing
LS_NEE2	4.72	0.11	N/A	N/A
SG_NEE2	0.77	0.03	92	100

3.3.8. X-Ray Diffraction Analysis

The X-ray diffraction (XRD) analysis of collected aggregate dust specimens is conducted in order to identify the mineralogical composition of microfine samples, where an atomic structure of the sample is identified by illuminating and capturing beams of X-rays on it. Thus, the results of this test will act as a reference point to predict the effect of microfines on concrete characteristics and the possibility of substituting this test by means of simpler and more practical Methylene Blue Test (MBT), which is used to detect harmful clays in aggregates using methylene blue solution.

Approximately one gram of oven-dried microfines was collected after the dry sieving (identified with a letter "S" at the end of the specimen ID), and washing (identified with a letter "W" at the end of the specimen ID) of different aggregate samples to perform XRD analysis. Microfine samples were dried to a constant mass at a temperature of 110±5^{o}C and then cooled to normal temperature prior to testing. AGTC XRD (Match) Powder X-Ray Diffraction data were obtained on a Bruker D8 Advance X-ray Diffraction and Scattering machine. AGTC XRD (Quant) Rietveld Analysis (Phase Quantification) of Powder X-Ray Diffraction data was calculated using the Topas software used to obtain phase identification and quantitation of mineral content of the analyzed samples of microfines.

3.3.9. ITZ Examination Specimen Preparation

This section covers the examination of the effects of different cleanliness conditions on the aggregate-paste interfacial transition zone (ITZ). Four different aggregates, i.e., sand and gravel (SG_NEC1), gravel (GR_NEW), quartzite (QZ_SD), and dolomite (DO_WY), were included in this part of the study. Previous studies on the ITZ could demonstrate its properties as a highly porous area, which acts as the weak link in the vicinity of an aggregate particle. The ITZ has a higher water-to-cement ratio due to micro-bleeding. Moreover, the wall-effect phenomena explain that due to disruption in the packing of cement grains against the aggregate particles, this zone contains mostly smaller grains, therefore presents a higher porosity. It is also known that both cement paste and aggregate show brittle behavior individually, while concrete mixtures show quasi-brittle (or quasi-ductile) behavior. The formation and propagation of microcracks within the ITZ is the governing factor of the quasi-brittle behavior and significantly affects the strength and durability of concrete (Prokopski and Halbiniak 2000; Mondal et al. 2009; Khedmati and Kim 2020; Khedmati et al. 2018; Scrivener et al. 2004). Moisture absorption capacity, aggregate size, and surface roughness are the aggregate physical properties that potentially affect the ITZ properties and were the main focus of previous studies (Khednati and Kim 2020; Elsharief et al. 2003; Tasong et al. 1998). One important factor that was not examined previously is the effect of dusty aggregates on the properties of the ITZ. The high content of dust in the aggregate (defined as particles passing a 75 μm sieve) increases the total surface area of aggregate particles, which results in a higher water requirement of the mixture to wet all the surfaces of the aggregate particles

(Celik and Marar 1996). This issue in the vicinity of the ITZ could potentially influence the ITZ properties.

For the complex visual ITZ examination samples were prepared as follows:

Step 1. Prepare a set of aggregate pieces of different cleanliness conditions (as received, after dry sieving, washed, or cleaned by ultrasound) and states of moisture condition (air-dry or saturated surface dry).

In order to obtain aggregates in SSD condition without wiping them using a towel (as dust coating will be undesirably removed), aggregate pieces were immersed in separate containers filled with water for 24-hour to avoid cross-contamination and obtain a fully saturated condition (Figure 11a). Then, aggregates were placed on top of the sieve mesh and covered with a wet towel to allow excess water to drain and receive a condition close to SSD condition after three to four hours (Figure 11b).

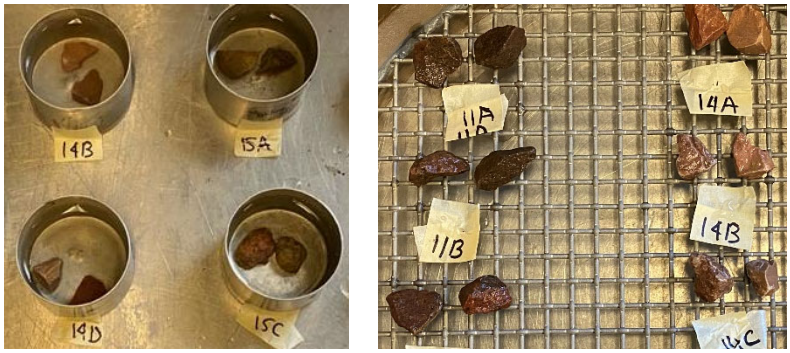

a) Immersed aggregates b) Aggregates left on a mesh

Figure 11. Aggregates SSD condition preparation.

Step 2. Prepare the cement paste of 0.41 water-to-binder ratio conforming Nebraska 47B mix and following ASTM C305 (Standard Practice for Mechanical Mixing of Hydraulic Cement Pastes and Mortars of Plastic Consistency) (ASTM, 2014). An IP cement complying with NDOT requirement was used in preparing the cement paste.

Step 3. Cast the cement paste in 1x1x11 inch prisms, dip eight aggregate pieces at a sufficient distance, and place tape-covered cardboard separators (Figure 12).

a) Aggregate placement distance and separators arrangement

b) Paste casting and aggregate dipping

c) SEM samples demolding

Figure 12. SEM samples casting procedure.

Step 4. The specimens were then cured in saturated lime water for 28 days to ensure full hydration.

Cured aggregate-paste samples (as well as samples from actual concrete batches) were then cut and confined with epoxy, so the aggregate-cement paste bonding is visible and could be assessed by SEM and Energy-dispersive X-ray spectroscopy (EDS) (Figure 13).

Figure 13. Microstructural analysis samples preparation procedure.

3.3.10. SEM and EDX Analysis

A Hitachi TM3030 tabletop scanning electron microscope (SEM), as shown in Figure 14, was utilized to assess the effect of microfines on the aggregate-cement paste bonding.

Figure 14. Hitachi TM3030 SEM and Quantax EDS unit.

In SEM and EDX analysis of each of the aggregate specimens, magnified images of three random locations of aggregate-to-cement paste bonding were obtained. An example is shown in Figure 15.

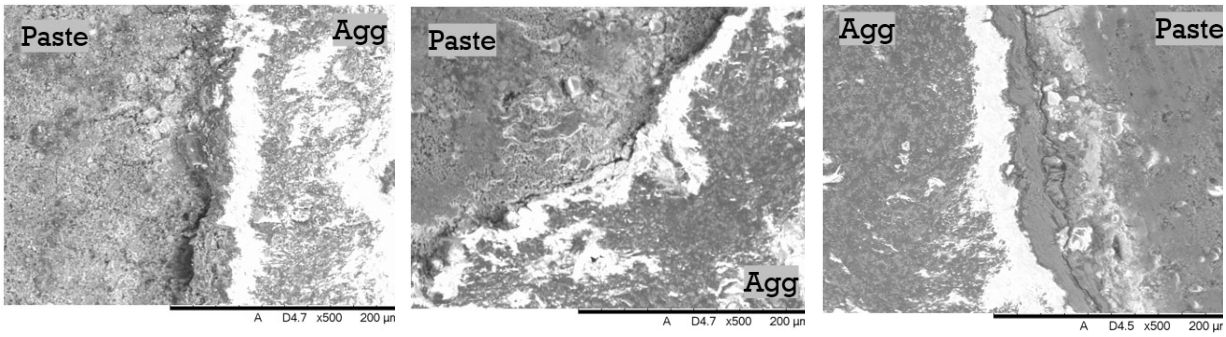

a) SEM image - location 1 b) SEM image - location 2 c) SEM image - location 3

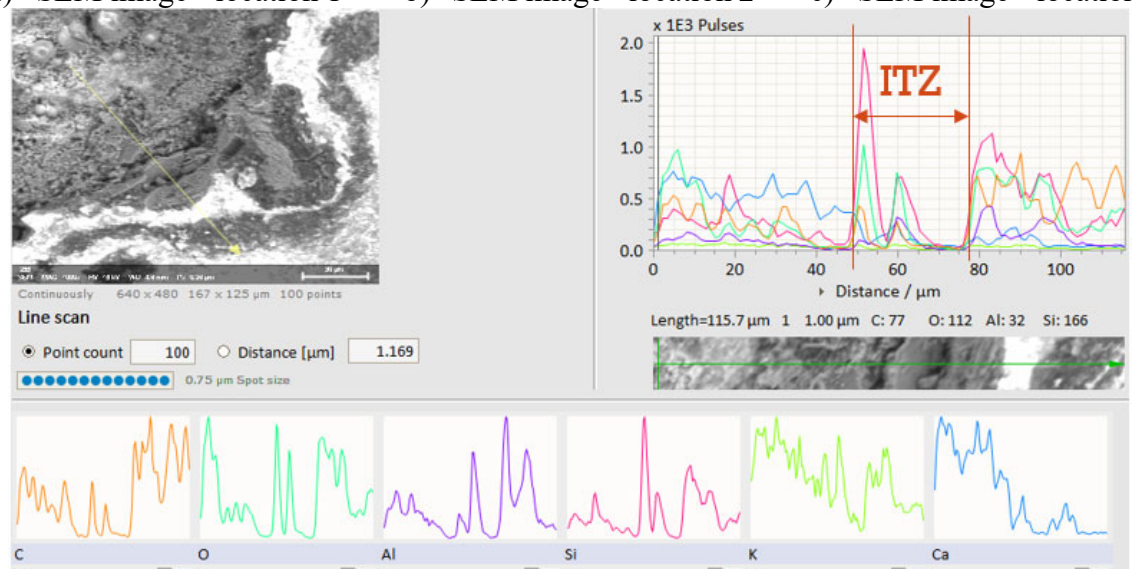

d) EDS line-scan at location 2

Figure 15. Example results of SEM and EDS analysis of the ITZ (aggregate DO_WY_A).

In addition to visual inspection, each of the locations was subjected to the EDS line-scan, aligned perpendicular to the aggregate-paste boundary to identify the width and chemical composition of the interfacial transition zone was identified using. Presumably, cement paste should mostly consist of Calcium (Ca), while aggregate piece (depending on the mineralogy) should consist of other minerals like Silicon (Si), Aluminum (Al), Potassium (K), and others. Thus, as can be seen from Figure 3.16.b, a clear boundary between cement paste and aggregate could be identified, as well as the width and the composition of the transition zone: a significant drop of Calcium content was observed at 50 µm-distance (from the beginning of line-scan) followed by a 30-µm long porous region with some spikes of Silicon, Oxygen, Carbon, and Aluminum. Thus, it can be assumed that this porous region represents the ITZ and contains some portion of the stone dust. The same analysis was performed for the other two locations, and the average result of the total three measurements was calculated. Moreover, the following ranking was introduced to visually assess the boundary condition (based on the SEM image):

- 1 [Poor] – a distinct boundary between aggregate and paste with some dust/coating particles
- 2 [Adequate] – no signs of dust particles, but the boundary is still noticeable
- 3 [Good] – a boundary layer between the aggregate piece and cement paste is almost indistinguishable.

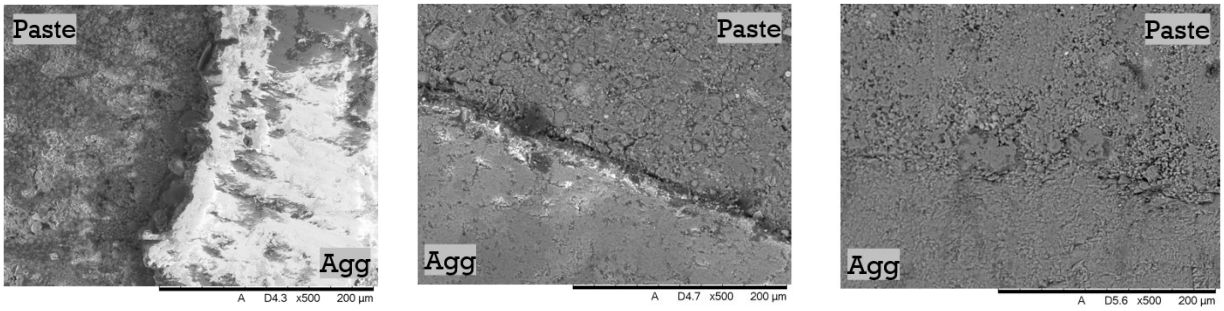

a) Poor ITZ (aggregate QZ_SD_A)
b) Adequate ITZ (aggregate GR_NEW_C)
c) Good ITZ (aggregate GR_NEW_C)

Figure 16. ITZ visual inspection ranking examples.

3.3.11. X-ray Micro Computed Tomography

With the 1-inch cubic samples as described earlier in section 3.3.9, the samples were also used for the X-ray micro-CT scanning. To provide stability for the subsequent grinding and polishing processes, the samples were embedded in an epoxy resin. The grinding and polishing process is necessary because the samples must have low (nanometer level) surface roughness, so that accurate micromechanical properties can be measured. The root mean square (RMS) roughness of surface should be less than 1/3 of the average indentation depth to avoid any surface roughness effect. The grinding process was performed by using silicon-carbide coated papers with U.S. industrial grits of 400 (22µm), 600 (15µm), and 1,200 (5µm), successively. Grinding time for each step was varied between 5-20 mins, depending on the surface conditions. Because of the difference in hardness between the aggregate and the paste in each sample, diamond lapping films with gradations of 9µm, 3µm, 1µm, and 0.5µm were used to maintain coplanarity. Lapping film

polishing was carried out for approximately 30 mins. Finally, all samples were immersed in an ultrasonic isopropanol bath to remove all residues for 5 mins. Samples were stored in a desiccator for 48 hours prior to testing to remove any trace of solvent.

X-ray micro computed tomography (CT), as shown in Figure 17, is a nondestructive technique for obtaining the three-dimensional internal microstructure of solid materials. X-ray beams are shot to the specimen by a high energy source (350 kV and 225 kV) for imaging of a wide range of materials with different densities and thicknesses. Low-density phases are typically represented by darker color contrasts, while high-density phases are represented by brighter color contrasts (Elseifi et al. 2011). In this study, more than 1,000 two-dimensional image slices were captured per specimen, and the aggregate-paste interphase was evaluated.

Figure 17. ZEISS Xradia 3D X-ray Microscopy and Computed Tomography.

Figure 18 presented examples of randomly selected internal microstructure images obtained from the Micro-CT scanning. Note that there are some small air bubbles entrapped in the cement paste due to the lack of consolidation during the specimen preparation. However, it should not have a direct impact on the interface between aggregate and paste.

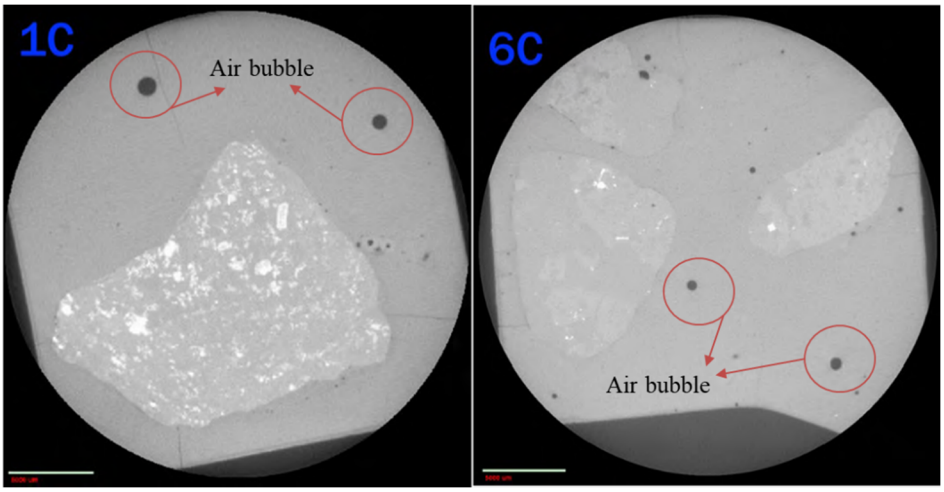

Figure 18. Example of micro-CT scanning images
(Left: Dolomite (as received); Right: Sand and Gravel (washed)).

3.3.11. Laser Scanning Confocal Microscopy

In this study, a Keyence® VK9700 laser scanning confocal microscope (LSCM), as shown in Figure 19, was used to obtain topography near the ITZ. LSCM is a type of optical microscope that uses two light sources: a white light for gathering color and a laser beam for scanning the surface and collecting detailed topography information. The result is a high-resolution, large depth-of-field, color image with nanometer-level height resolution for accurate profile and roughness measurements. In this study, LSCM was employed to obtain 3-D topography images from multiple locations over the aggregate-paste interface. 2-D profiles were also captured from one random location through a line scanning perpendicular to the interphase.

Figure 19. KEYENCE VK-9700K laser scanning confocal microscope (LSCM).

After finishing the micro-CT scanning, each sample was cut in half with a low-speed diamond saw to expose the desired interface. The topography of the interphase region was examined by LSCM for all different specimens. For each specimen, two random locations with dimensions of 1,400 µm × 1,000 µm were selected. Laser scanned image, 3D topography, and its associated 2D profile for a random single line perpendicular to the interphase were captured. An example of the 3D topography and 2D profile line from LSCM image is shown below in Figure 20.

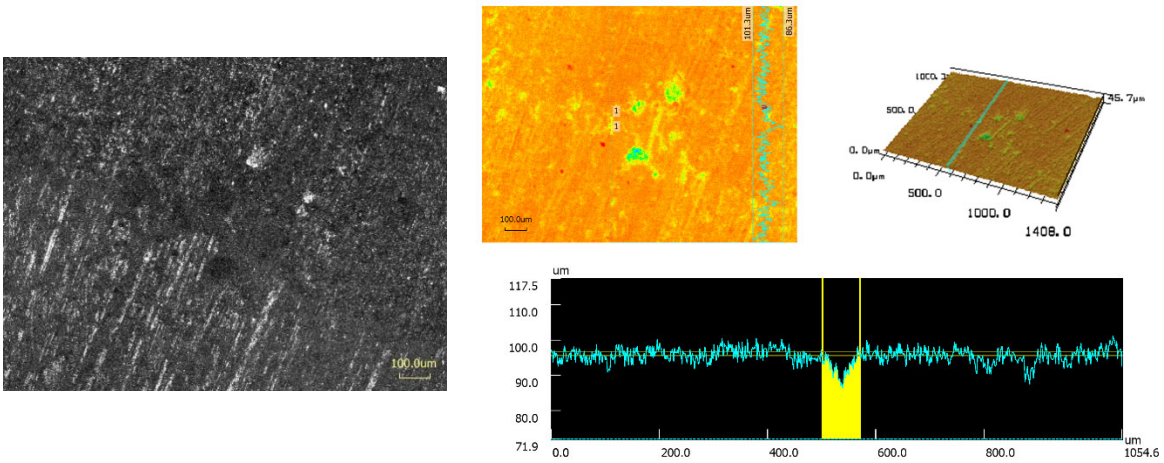

Figure 20. Example of LSCM image (Aggregate DO_WY)
(Left: 3D topography, and Right: 2D profile line Specimen).

3.3.12. Quasi-Static Nanoindentation

Nanoindentation is a popular and effective technique to obtain the micromechanical properties of various materials, including cementitious materials. In this test, a force-load path is applied to the surface of a sample using an indenter (in nanometer length scale) with precisely characterized properties. The corresponding displacement response is recorded, and the initial slope of the unloading portion of the curve is measured. For the nanoindentation testing, a Hysitron Triboindenter with a Berkovich tip (i.e., pyramidal shape), as shown in Figure 21, was used.

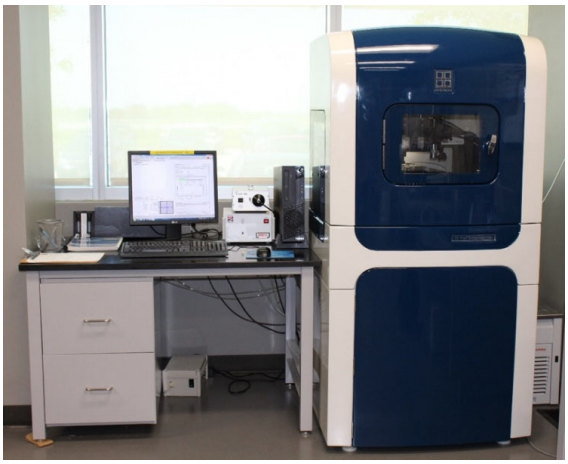

Figure 21. Bruker's TI 950 Triboindenter.

As illustrated in Figure 21, the indentation was performed using a quasi-static force-controlled mode where the loading function was defined with three steps: 10 seconds loading, 5 seconds holding, and finally 10 seconds unloading (with the same rate as loading). The holding period was considered to eliminate any creep effects. The maximum load was set to 3,000 μN.

The force-displacement data was fitted by applying contact mechanics, often with the Oliver and Pharr method (Oliver and Pharr 1992). The local hardness of the material can be determined as follows:

$$H = \frac{P_{max}}{A_c}$$

Where, P_{max} is the peak load and A_c is the projected contact area at the peak load. Using the following equations, the reduced modulus, which represents the elastic property of both the indenter tip and the testing specimen, was determined:

$$E_r = \frac{1}{\beta} \cdot \frac{S}{2} \cdot \frac{\sqrt{\pi}}{\sqrt{A_c}}$$

Where, the dimensionless correction factor β accounts for the shape of the indenter tip, and is equal to 1.081 for a Berkovich tip; the parameter S refers to the contact stiffness of the material and is defined as the initial slope of the unloading part of the load-displacement curve at $h = h_{max}$;

and A_c is the projected contact area at the peak load (P_{max}). An example of load-displacement curve from the nanoindentation test is illustrated in Figure 22.

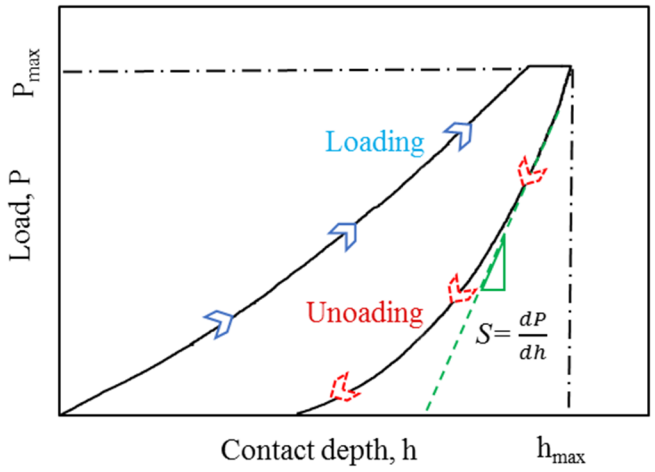

Figure 22. Typical example of load–displacement curve from nanoindentation.

The reduced modulus (E_r) is related to the elastic modulus (E_s) and Poisson's ratio (v_s) of the tested material. E_s of the material can then be calculated by the following equation:

$$\frac{1}{E_r} = \frac{1-v_s^2}{E_s} + \frac{1-v_i^2}{E_i}$$

Where, E_i and v_i are the Young's modulus and Poisson's ratio of the diamond indenter tip, respectively. The elastic modulus and the Poisson's ratio of the diamond indenter are equal to 1,140 GPa and 0.07, respectively.

A histogram of the obtained elastic moduli was plotted to show the distribution of elastic moduli within the ITZ, and an example is shown in Figure 23.

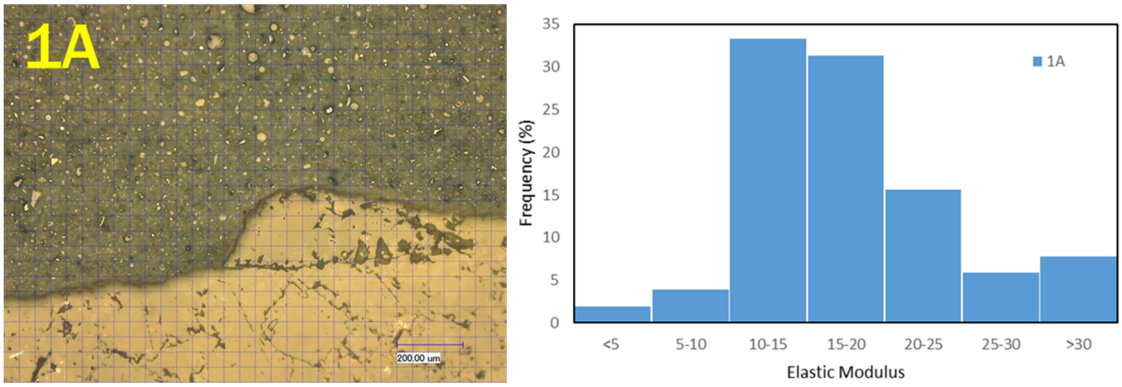

Figure 23. Example of indented region locations and correlated elastic modulus histograms (Aggregate ID: DO_WY).

3.4. Concrete Mixing Procedure

Prior to batching, the required amount of aggregates in air-dry moisture condition was obtained, and the mix proportions were adjusted based on the moisture content of aggregate. Just

prior to mixing, the inside surface of the mixer was “buttered” by mixing a batch proportioned closely to the test batch.

The mixing procedure described in ASTM C192 (Standard Practice for Making and Curing Test Specimens in the Laboratory) as described below, was followed.

- Introduce coarse aggregates and half of the mixing water (with diluted AEA – Master Air AE90)
- Start mixing, introduce fine aggregates, cement and the rest of the water (with diluted WR – Eucon x15)
  - Mix for 3-min (cover the mixer opening with a lead)
  - Allow the mix rest for 3 mins (cover the mixer opening with a lead)
  - Mix for 2 mins (cover the mixer opening with a lead)
- Immediately check for targeted values of a slump (3-4 in.) and unit weight
  - If necessary (low slump) - add WR (Eucon X-15 with range 4-15 fl oz/cwt), remix for 3 mins and check slump
  - Or if the slump is in the targeted range, but unit weight is high – add AEA (Master Air AE90 0.25-4.0 fl oz/cwt) and remix for 1 min

Immediately after finishing concrete mixing, approximately 100 grams of mortar specimen (wet-sieved though No. 4 sieve) was obtained for the heat of hydration measurement. Samples for mechanical properties and durability measures were demolded after 24±8 hours after the casting and moist-cured at 23±2.0ºC until the moment of the test.

3.5. Laboratory Tests for Fresh Concrete Properties Evaluation

3.5.1. Slump Test

To assess workability and determine the consistency of fresh concrete, ASTM C143 (Standard Test Method for Slump of Hydraulic-Cement Concrete) was followed (ASTM, 2015). The complete test was performed within 2.5 minutes right after concrete mixing. A slump (see Figure 24) was measured to the nearest quarter inch.

Figure 24. Slump test apparatus.

3.5.2. Isothermal Calorimeter Test

The hydration process was assessed by measuring the heat of hydration following ASTM C1702 (Standard Test Method for Measurement of Heat of Hydration of Hydraulic Cementitious Materials Using Isothermal Conduction Calorimetry) (ASTM, 2015). Approximately 100 grams of mortar were wet-sieved using No.4 sieve (Figure 25 a-d). The amount of heat released from the mortar sample, which was sieved from a fresh concrete mix, was captured by heat-flow sensors in the isothermal calorimeter (Figure 25 f). In addition, the initial and final setting times were estimated based on the rate of heat generated (Hu et al., 2013).

a) Placing a concrete sample on top of No.4 sieve

b) Sieving

c) Collecting mortar passed No. 4 sieve

d) Placing approximately 100 g in a cup

e) Placing a sample in calorimeter

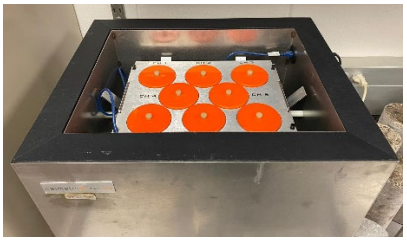

f) Take measurement using isothermal calorimeter

Figure 25. Heat of hydration sample preparation and equipment.

3.6. Laboratory Tests for Hardened Concrete Properties Evaluation

3.6.1. Compressive Strength

The compressive strength of hardened concrete was measured per ASTM C39 (Standard Test Method for Compressive Strength of Cylindrical Concrete Specimens) (ASTM, 2020). Cylindrical specimens at the dimentions of 4" diameter and 8" height were subjected to compression using the Forney compression testing machine (see Figure 26) at 7 and 28 days of age. At each testing age, three specimens were randomly selected for the test, and the average value and standard deviation were reported.

Figure 26. Compressive strength apparatus – Forney compression testing machine.

3.6.2. Modulus of Rupture

The flexural strength of hardened concrete was evaluated based on the modulus of rupture value determined by ASTM C78 (Standard Test Method for Flexural Strength of Concrete (Using Simple Beam with Third-Point Loading)) (ASTM, 2018). Thus, a 28-d cured concrete beam specimen (prism of 6”×6”×20”) was subjected to third-point loading on Forney flexural testing machine (Figure 27).

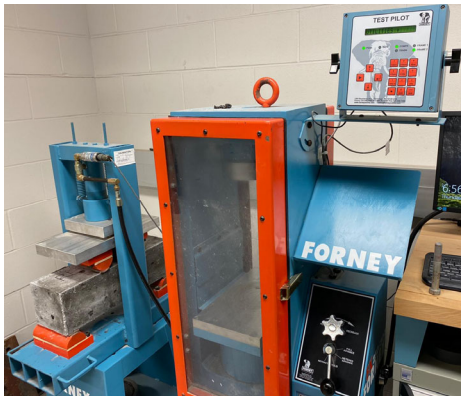

Figure 27. Flexural strength apparatus – Forney flexural testing machine.

3.6.3. Modulus of Elasticity

The static modulus of elasticity was measured per ASTM C469 (Standard Test Method for Static Modulus of Elasticity and Poisson’s Ratio of Concrete in Compression) (ASTM, 2014). 28-d cured cylindrical specimen was (4” radius and 8” height) was subjected to compression while axial and radial deformations were recorded (Figure 28). Three specimens were randomly selected for the test, and the average value and standard deviation were reported.

Figure 28. Modulus of Elasticity testing apparatus.

3.7. Laboratory Tests for Concrete Durability Evaluation

3.7.1. Freeze-Thaw Cycling Test

Freeze/Thaw resistance of hardened concrete samples was evaluated following Procedure A of ASTM C666 (Standard Test Method for Resistance of Concrete to Rapid Freezing and Thawing) (ASTM, 2015). Three 14-d cured concrete specimens (prism of 3”×4”×16”) were subjected to deterioration by 300 repeated cycles of rapid freezing and thawing in water using Humboldt’s Elite Series Freeze-Thaw Cabinet (

Figure ***29***a). After every 30 cycles, the mass loss of the samples was measured.

Figure 29. Freeze-thaw resistance testing apparatus.

3.7.2. Electrical Resistivity Test

Concrete surface resistivity was measured per AASHTO TP 95-14 (Standard Method of Test for Surface Resistivity Indication of Concrete’s Ability to Resist Chloride Ion Penetration) (AASHTO, 2014). Two fully saturated and cured concrete cylindrical specimens (4” radius and 8” height) were tested for their electrical surface and bulk resistivity characteristics using Proceq

Resipod resistivity meter at the ages of 7, 14, 28, and 90 days (Figure 30). Bulk resistivity measures the resistivity of the whole cylinder instead of just the surface, as from the surface resistivity test.

a) Surface resistivity measurement b) Bulk resistivity measurement

Figure 30. Concrete surface resistivity testing apparatus.

3.7.3. Free Shrinkage Test

The potential volumetric contraction of concrete was tested according to ASTM C157 (Standard Test Method for Length Change of Hardened Hydraulic-Cement Mortar and Concrete) (ASTM, 2017). After 28-d of lime-water curing, three concrete prisms of the dimension of 3"×3"×11.25" were placed in an environmental chamber with a temperature of 73.5±3.5ºF (23.0±2.0ºC) and relative humidity of 50±4.0%. The length change of bars was measured by length comparator after 4, 7, 14, 28 days, and after 8, 16, 32, 64 weeks of air storage (Figure 31).

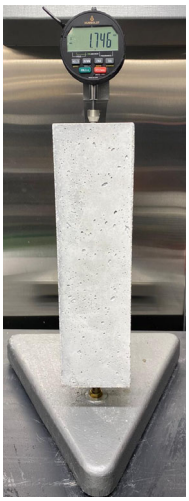

Figure 31. Free shrinkage test equipment setup.

CHAPTER 4. EXPERIMENTAL DESIGN AND RESULTS

4.1. Introduction

This chapter describes the details and results of the developed experimental study, which was divided into two parts: aggregates characterization and concrete performance evaluation. With the obtained aggregate samples, tests including microfine content (P200 value), MBT, XRD were used to identify the type, content, and properties of microfines present. Advanced tests, including XRD, EDX, micro-CT, and nano-indentation, were used to evaluate the interface between aggregate and cement paste. After the properties of aggregates and microfines were determined and evaluated, aggregates with high microfines content (P200 value) and/or presence of harmful clays (MBT and XRD results) were selected for further concrete mixing and performance evaluation. Thus, the properties of fresh and hardened concrete samples made of these aggregates were compared to the reference sample made of clean aggregates.

4.2. Aggregates and Microfines Characterization Results

4.2.1. Aggregate Gradation, Absorption Capacity, and Specific Gravity

The gradation of aggregate samples was measured through ASTM C136 (Standard Test Method for Sieve Analysis of Fine and Coarse Aggregates) (ASTM, 2020).

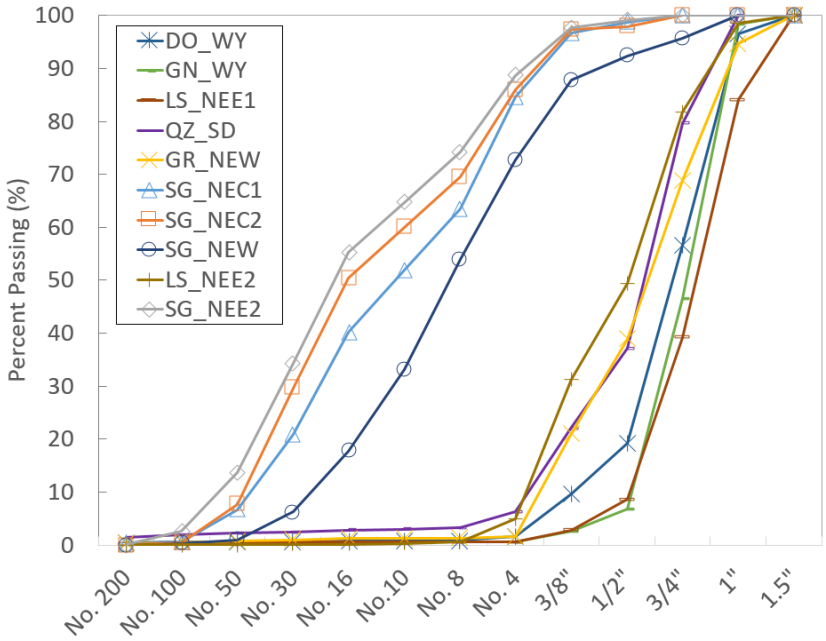

Figure 32. Gradation curves of aggregates.

The results of the sieve analysis, as shown in Figure 32, indicated that some of the aggregates, including GN_WY, DO_WY, LS_NEE1 (obtained from NDOT), and GR_NEW, were coarser than required for 47B mix.

All aggregates samples were also subjected to absorption capacity and specific gravity tests per ASTM C127 and ASTM C128 (Standard Methods for Relative Density and Absorption of

Coarse and Fine aggregates respectively) for the mixing proportions of concrete constituents. The results of absorption and specific gravity (SSD) were reported in Table 12.

Table 12. Absorption and specific gravity values of aggregates.

Aggregate ID	1 DO_ WY	2 GN_ WY	3 LS_N EE1	4 QZ_ SD	5 GR_ NEW	6 SG_N EC1	7 SG_N EC2	8 SG_N EW	9 LS_N EE2	10 SG_N EE2
Absorption (%)	0.52	0.34	1.04	0.78	0.60	0.56	0.56	1.35	1.20	0.44
Specific Gravity	2.63	2.83	2.63	2.66	2.61	2.58	2.61	2.53	2.62	2.60

4.2.2. Amount of Material Passing No.200

After following the aggregate sampling procedure as described in section 3.3.6 (Microfines sampling methods and aggregate cleanliness conditions), a set of aggregates in different cleanliness states, as presented in Appendix A-1 were obtained. The results of fine contents based on different microfine quantification methods, drying sieving, washing, and ultrasonic cleaning, are presented in Table 13 below:

Table 13. P200 value - % passing No.200 sieve (by mass).

Procedure	1 DO_ WY	2 GN_ WY	3 LS_N EE1	4 QZ_ SD	5 GR_ NEW	6 SG_N EC1	7 SG_N EC2	8 SG_N EW	9 LS_N EE2	10 SG_N EE2
Sieving $P_{200\ B}$	0.45	0.38	0.21	1.51	0.34	0.13	0.06	0.30	2.59	0.40
Washing $P_{200\ C}$	0.70	0.59	0.77	2.31	0.50	0.15	0.16	0.73	4.72	0.77
U-clean $P_{200\ D}$	0.77	0.77	1.02	2.51	0.60	0.27	0.25	0.91	4.87	0.94

As shown in Table 13, as expected, P200 values from the ultrasonic cleaning were the highest, followed by washing, and then sieving. Results confirm that microfines that were loose (sieving), loose and weakly attached (washing), loose plus weakly, and firmly attached (u-cleaned) could be different. In general, the difference between $P_{200\ C}$ and $P_{200\ D}$ was not that significant as the difference between P_{200C} and P_{200D}, but it still indicates that the standard washing test may result in an underestimated P_{200} value in the case of the aggregate washing was not performed thoroughly enough. Also, even with thoroughly washing, there are still a good amount of firmly attached microfines on aggregate surfaces. Nevertheless, as it is not practical to obtain P_{200D} values, only P_{200C} will be used as a further microfines quantity indicator.

In addition, it worthwhile to note that most of the aggregate specimens obtained from NDOT have the P200 value much lower than the NDOT limits of the maximum allowable P200 value of 3.0%, except for QZ_SD, which has a fine content (by washing) of 2.31%.

4.2.3. Results of Sand Equivalent Test

As one of the NDOT requirements for the sand and gravel samples coming from dry pits was to pass the Sand Equivalent Test, it was decided to run this test for all fine aggregate samples regardless of their source type (wet or dry pit). The results of the conducted Sand Equivalent Test are presented in Table 14 and Appendix A-2. As can be seen, all of the sand and gravel samples passed the NDOT limit of SE value to be greater than 90.

Table 14. Results of Sand Equivalent test.

Aggregate sample	6 SG_NEC1	7 SG_NEC2	8 SG_NEW	10 SG_NEE2	10w SG_NEE2 washed
Sand Equivalent Value	98	98	94	92	100

4.2.4. Results of Methylene Blue Test

As shown below in Table 15, different performance categories for the methylene blue values are recommended with the two different methods, with the MBV based on dusts collected from washing per AASHTO T330 adopting higher values compared to dusts collected from dry sieving per ASTM C1777 (Mukhopadhyay et al. 2003). For both methods, the possible problems or failure is associated with a high content of harmful clays, such as montmorillonites.

Table 15. Expected performance categories of Methylene Blue Values based on AASHTO T330 and ASTM C1777.

AASHTO T330		ASTM C1777	
Methylene Blue Value (mg/g)	Expected Performance	Methylene Blue Value (mg/g)	Performance Category
<6	Excellent	≤ 4.5	Normal
7-12	Marginally acceptable	4.5-6.5	Poor
13-19	Problems/Possible failures	≥ 6.5	Very poor
>20	Failure	-	-

The methylene blue test was conducted with microfines collected from aggregate sieving and washing procedures. The results are shown below in Table 16. Details from each test can be found in Appendix A-3.

Table 16. Summary of MBV results.

Mix ID	1 DO_ WY	2 GN_ WY	3 LS_N EE1	4 QZ_ SD	5 GR_ NEW	6 SG_N EC1	7 SG_N EC2	8 SG_N EW	9 LS_N EE2	10 SG_N EE2
MBV_C Washed (mg/g)	12.0	5.25	4.0	5.25	7.0	11.5	38.0	29.0	3.0	28.0
MBV_B Sieved (mg/g)	10.75	7.5	4.25	5.75	7.25	4.75	10.25	6.0	2.5	6.75

As was expected, both limestone dust samples (LS_NEE1 and LS_NEE2) showed the least methylene blue values, as they supposedly contain only calcium carbonates as coatings. The possible presence of harmful clays was determined in DO_WY, GR_NEW, SG_NEC1, SG_NEC2, and SG_NEE2. Moreover, it is worth noting that the SG_NEC2, SG_NEW, and SG_NEE2 showed much higher MBV when compared to the results reported in previous studies (Gullerud, 2002; Munoz, 2010), where the MBV based on AASHTO T330 was only as high as 11.5 mg/g for clay/dust microfines. The results indicate a higher portion of clay minerals, such as illite (MBV of 65 mg/g) or smectite (MBV of 260 mg/g) (Pike, 1992).

Additionally, the MBT on washed and sieved off microfines obtained from all fine aggregate samples resulted in different methylene blue values, showing the less potential presence of harmful clays in sieved off samples. However, it was not the case for coarse aggregate samples. The high MBV with dusts collected from the washing process (as compared to sieving) is likely due to the higher ratio of clay content collected from washing, which was confirmed earlier based on the XRD analysis. In addition, better dispersion of clay particles after washing could also lead to higher MBV.

4.2.5. Modified Methylene Blue Value

As the contribution of the aggregate dust in concrete does not simply rely on the type of dust, but also on the content of the dust, in order to take into account both the quantity and quality properties of the microfines, a Modified Methylene Blue Value (MMBV) was used. The concept combines P200 and MBV, which was first introduced by Gullerud (2002), can be obtained by multiplying the value of each of the characteristics. As shown in Table 17, even with the very high MBV, the MMBV from sand and gravel aggregate does not necessarily significantly higher compared to other aggregates.

$$MMBV = P200/100 \times MBV$$

Table 17. Modified Methylene Blue Value results.

	1 DO_ WY	2 GN_ WY	3 LS_ NEE1	4 QZ_ SD	5 GR_ NEW	6 SG_ NEC1	7 SG_ NEC2	8 SG_ NEW	9 LS_ NEE2	10 SG_ NEE2
MMBV_B[1](mg/g)	0.075	0.044	0.033	0.133	0.036	0.007	0.016	0.044	0.118	0.052
MMBV_C[2](mg/g)	0.084	0.031	0.031	0.121	0.035	0.017	0.061	0.212	0.142	0.216

[1]Based on the MBT of microfines collected after sieving (mg/g)
[2]Based on the MBT of microfines collected after washing (mg/g)

4.2.6. Results of XRD Analysis

The X-ray diffraction analysis was conducted on different microfine samples to identify the mineralogy and differentiate between clay minerals and stone dust fracture, as well as to note the difference in clay content in microfines collected from the same aggregate sample but using different cleaning technique. It was assumed that in the case of mixed clay and stone dust coating, the clay fraction should be bigger in microfines collected from ultrasonic cleaning, as they tend to attach more firmly. Details from the XRD analysis can be found in Appendix A-4.

Results from the XRD analysis show that the composition of the gravel samples is comparable to that of the "dolomite" samples. Moreover, as with sample DO_WY_W, the gravel sample, GR_NEW_W contains a significant amount of evaporite minerals (≈19%). The sand and gravel samples are comprised of the aforementioned mineral constituents in varying proportions. As with previous samples, SG_NEC1_W and SG_NEE2_W have substantial quantities of evaporite minerals (17.6% and 9.0%, respectively). Sample SG_NEC1_W has the highest concentration of clay minerals of all the samples. The limestone samples are predominantly calcite, with minor quartz, feldspars, dolomite, and ankerite. Phase percentages generated from the Topas Rietveld refinement are in agreement with previously reported results.

Overall, samples with "W" (dusts collected from washing) in the description contain considerable quantities of evaporite minerals, namely bassanite, halite, and thernardite. These minerals are absent from samples with "S" (dust collected from dry sieving) in the description. Furthermore, clay contents, on average, are higher in samples with "W" in the description. For a comprehensive review of the mineralogy of each sample, please see the test results as detailed in Appendix A-4.

4.2.7. Results of Visual ITZ Examination using SEM and EDS

An interfacial transition zone was examined for DO_WY, DO_SD, and GR_NEW aggregate samples in three different conditions:

- Aggregate piece dipped in the cement paste in as-received condition (presumably the worst-case scenario, as the aggregate coating is left in undisturbed "dirty" condition and may interfere with aggregate-cement boundary layer)
- Aggregate piece dipped in the cement paste after washing (supposedly should not result in any microfines-related ITZ issue)
- The sample is taken from the actual concrete mix (real-case scenario)

The analysis of each sample was performed based on the magnified images of three to four randomly selected locations: the average width of the ITZ and its chemical composition were estimated using EDS elemental line-scan. The obtained magnified images and results of EDS analysis are presented in Appendix A-5 and were summarized in Table 18.

Table 18. Summary of SEM and EDS analysis results.

Aggregate type	Sample type	ITZ width (μm)	Chemical composition	ITZ visual examination
Dolomite (DO_WY)	DO_WY_A (Aggregate dipped in cement paste (as received))	30-60	Si, O, Al, C	Poor [1.0]
	DO_WY_C (Aggregate dipped in cement paste (washed))	10-35	Porous/ Ca	Adequate to Good [2.67]
	DOWY (Taken from concrete batch (as received))	30-45	Si, O, Ca, Fe, Al	Adequate to Good [2.25]
Dolomite (DO_SD)	DO_SD_A (Aggregate dipped in cement paste (as received))	30-70	Ca, Si, O, C	Poor [1.33]
	DO_SD_C (Aggregate dipped in cement paste (washed))	20-30	Ca, O, C	Good [3.0]
	DOSD (Taken from concrete batch (as received))	20-35	Si, O, Ca, Al	Adequate [2.0]
Gravel (GR_NEW)	GR_NEW_A (Aggregate dipped in cement paste (as received))	30-65	Si, O, Al, C	Poor [1.33]
	GR_NEW_C (Aggregate dipped in cement paste (washed))	20-30	Ca, Si	Adequate to Good [2.67]
	GR_NEW (Taken from concrete batch (as received))	20-40	Si, O, Al, Ca	Adequate [2.0]

Overall, the visual examination using SEM imaging and EDS elemental analysis showed consistent results as all samples prepared by dipping the aggregate pieces in the cement paste in

as-received condition (DO_WY_A, DO_SD_A, and GR_NEW_A) ended up the widest ITZ with poor appearance (distinct boundary with distinguishable dust particles) and the better condition for aggregate-paste samples made of clean aggregate pieces (DO_WY_C, DO_SD_C, and GR_NEW_C). However, there is no conclusive evidence to justify if the extent to which aggregate-cement paste bond is worse for unwashed samples when compared to washed ones is significant.

In addition, based on the analysis of the lab-casted concrete specimens, the major portion of microfine coating is being washed off during the first stage of concrete mixing (when coarse aggregates are being mixed with water for 30 seconds), as the analysis of the samples taken from the actual concrete batches (DOWY, DOSD, and GRNEW) produced the results comparable to the samples when washed aggregates were dipped in the cement paste.

4.2.8. Micro-CT Scanning Results

It can be observed visually that the interphase region between the aggregate and the paste did not change considerably before and after washing, although the interphase region of "as-received" cases is somewhat more susceptible to clustering of extremely fine voids. This phenomenon was exhibited in case 4A (quartzite) and with a lower concentration in case 5A (gravel). In particular, specimens with quartzite aggregate developed marginal debonding from the cement paste for both "as-received" and "washed" cases, and the cleanliness appears to matter, although it was not significant. The result is likely due to the relatively high fine content (P200-C of 2.31%). Images from all the eight different specimens evaluated captured by X-Ray CT are present in Appendix A-6.

4.2.9. 3D Interphase Topography Results

Images from the 3D interphase topography analysis are shown in Appendix A-7, and an example is shown in Figure 33. As shown in the figure, Specimen 4A (quartzite) exhibited clear debonding (or gap) at the interfacial line. For the other cases, it could be seen that a few local deboning sites might exist at the interphase line, but it was not consistent all through the interphase. Aggregates such as dolomite or sand and gravel were very well bonded with surrounded paste. The vertical distance and lateral distance for any of the gaps were not greater than 20 μm and 100 μm, respectively.

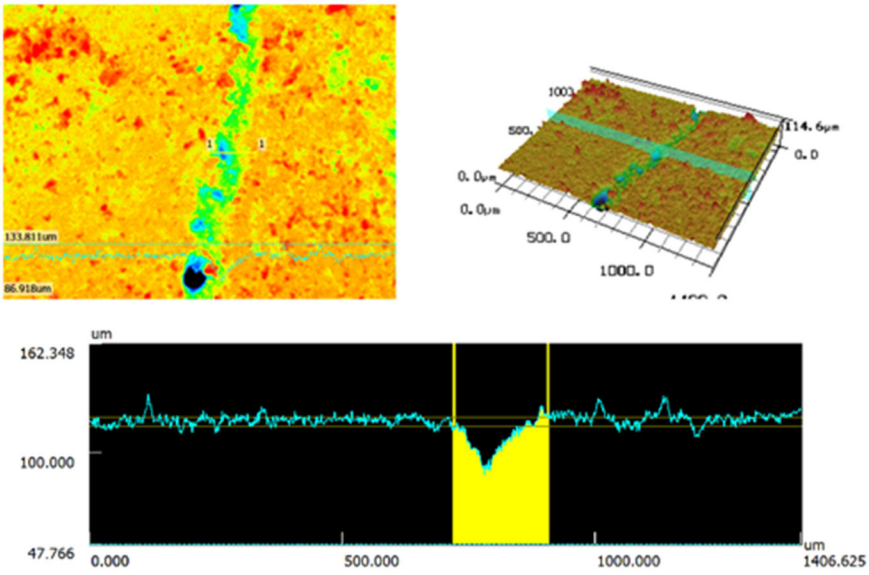

Figure 33. LSCM image (Aggregate ID: QZ_SD).

4.2.10. Nanoindentation Results

Although the ITZ does not have its distinct boundary from the aggregate surface, it can be examined by taking a reasonable distance from the surface of aggregates. In this study, it was assumed that a distance up to approximately 50μm from the surface of the aggregate could be examined for the mechanical properties of ITZ. Based on the assumption, the nanoindentation was performed in that region as a grid indentation, which yielded a total of 64 indents within a square grid of 52.5μm, with a spacing of 7.5μm (horizontally and vertically) between indents. After deriving the reduced modulus, the subsequent calculations were operated, and the elastic modulus per each indent was determined. As can be seen in Appendix A-8, the highest peak of the histogram mostly falls into the 10-20 GPa range, which can be interpreted as low-density C-S-H gel. No significant difference was observed regarding the micromechanical properties before and after aggregate washing. One possible reason could be that the dust content was not beyond the maximum threshold; thus, it did not disrupt the water demand in the vicinity of the aggregate.

As the results shown in the above sections, a noticeable difference in aggragates' basic physical characteristics, such as gradation, absorption capacity, and specific gravity, as well as the difference in microfines type present, emphasizes a complete mineralogical difference of aggregates. In order to identify questionable aggregate samples, which could potentially have issues with concrete fresh or hardened properties, aggregates with both high P200 value or high MBV were both selected for further concrete performance evaluation. The following four aggregates were identified:

- DO_WY – coarse aggregate with small P200, but marginally acceptable MBV (possible presence of harmful clays)
- QZ_SD – coarse aggregate with high P200, but acceptable MBV (possibly stone dust)

- GR_NEW – coarse aggregate with small P200, but marginally acceptable MBV (possible presence of harmful clays)
- SG_NEC1 – fine aggregate with marginally acceptable MBV

4.3. Evaluation of Influence of Microfines on Concrete Performance

Based on information collected from the aggregate characterization, three coarse aggregates, namely DO_WY, QZ_SD, GR_NEW, and one sand and gravel aggregate, SG_NEC1, were selected to prepare concrete batches using aggregate in as-received condition and compare their fresh and hardened properties with the requirements of the NDOT 47B concrete pavement mix. A reference mix (REF1) with washed east Nebraska Limestone as coarse aggregate and sand and gravel as fine aggregate was also prepared for comparison. In order to evaluate the concrete performance and identify possible issues, a comprehensive evaluation including fresh and early-age properties, mechanical and durability of hardened concrete performance as listed in Table 19, was conducted on each of the prepared concrete batches.

Table 19. Summary of tests for concrete performance evaluation.

	Property	Test Method
Fresh/ Early-age	Workability	Slump test
	Air content	Unit Weight
	Setting and Hydration	Isothermal calorimeter
Mechanical	Strength	Compressive strength
	Strength	Modulus of rupture
	Stiffness	Modulus of elasticity
Durability	Durability	Freeze-thaw cycling
	Durability	Surface resistivity
	Drying shrinkage	Free shrinkage

4.3.1. Mix Proportions

The following five concrete mix proportions, as indicated in Table 20, confirming NDOT 47B mix design, were prepared in order to evaluate the effect of aggregate dust on the concrete performance. To focus on the impact of aggregate, cement and water content were kept the same, while the contents of coarse and fine aggregate were slightly adjusted due to the different specific gravities. Contents of WR and AEA were adjusted during batching to ensure an air content and slump value that meet NDOT requirements.

Table 20. Mix proportions of the prepared concrete batches.

Mix ID	Coarse Aggregate	Fine aggregate	Cement (pcy)	Water (pcy)	CA (pcy)	FA (pcy)	WR (fl.oz/cwt)	AEA (fl.oz/cwt)
REF1	LS_NEE2w	SG_NEE2w	564	231	900	2040	8.0	2.5
DO_WY	DO_WY	SG_NEE2w	564	231	904	2041	8.0	2.5
QZ_SD	QZ_SD	SG_NEE2w	564	231	908	2047	6.0	2.5
GR_NEW	GR_NEW	SG_NEE2w	564	231	902	2035	10.0	2.5
SG_NEC1	LS_NEE2w	SG_NEC1	564	231	899	2028	8.0	2.5

The combination aggregate gradations of coarse and fine aggregates of DO_WY, QZ_SD, GR_NEW, SG_NEC1, and REF1, plotted in 0.45 Power curve, were also used to evaluate the gradation of the combined gradation.

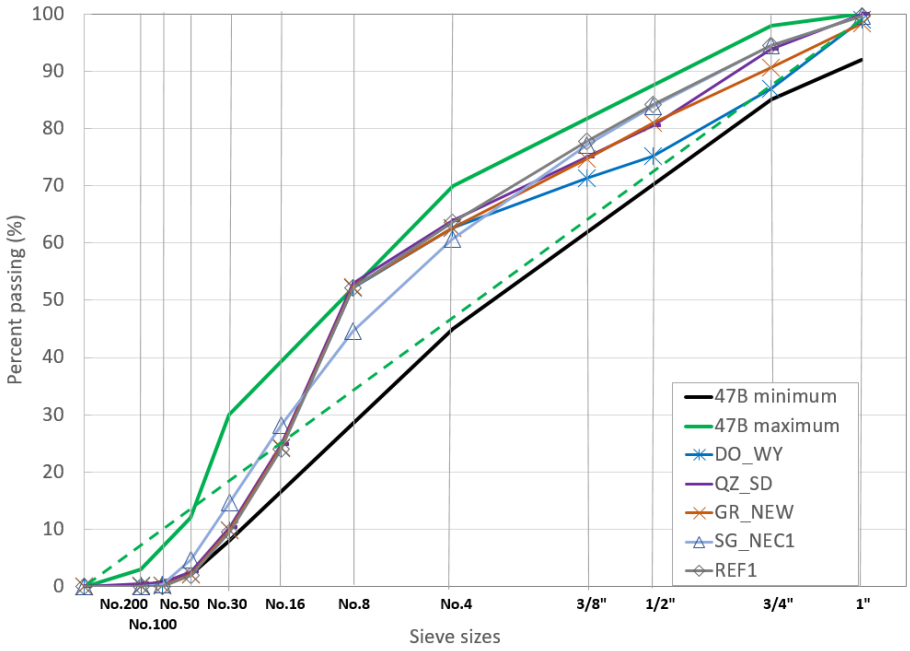

Figure 34. Combined gradation (0.45 Power chart).

As can be seen from the combined gradation chart (0.45 Power Chart, as shown in **Error! Reference source not found.**), the combined aggregate gradations vary from each other. While the combined gradations of all aggregate included in Figure 33 fall within the upper and lower limits per NDOT specification, the four coarse aggregates (DO_WY, QZ_SD, GR_NEW, and REF1) all have a fairly high amount of aggregate portion retained on No. 8 sieve that is very close to the upper limit.

4.3.2. Results of Concrete Fresh Properties Testing

Immediately after finishing the mixing procedure, slump and unit weight tests were performed, and the results are summarized in Table 21. Noted that due to the limited amount of aggregate available for this study, air content was not measured directly. Rather, the air content was estimated based on the unit weight of the concrete per ASTM C138.

Table 21. Fresh and early-age concrete properties results.

Mix ID	Slump (in)	Air content (%)	Set time (hrs)		Heat of hydration (J/g)	
			Initial	Final	24 hrs	48 hrs
REF1	4.25	8.8	8.53	11.65	177.9	235.7
DOWY	3.00	7.2	8.81	11.60	185.1	243.5
QZSD	3.75	8.9	7.69	10.79	161.1	213.6
GRNEW	4.25	8.1	9.88	12.98	180.4	241.4
SGNEC1	3.25	8.5	9.69	12.63	167.5	223.6

Results from the heat of hydration measurement and key thermal properties, including cumulated heat of hydration generated within the first 24 and 48 hours and the thermal set time, are presented in Table 21 and Figure 35, respectively.

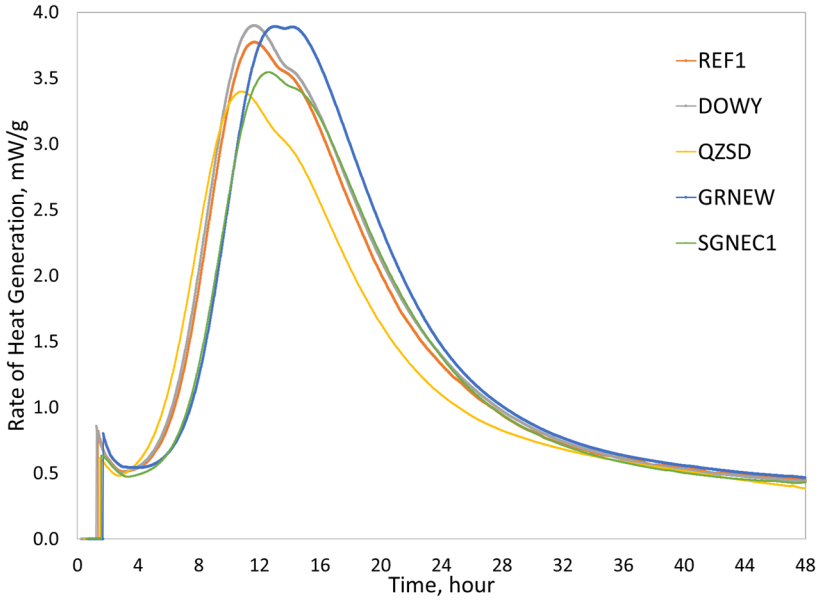

Figure 35. Heat of hydration of concrete prepared with different aggregates.

As can be seen from Table 21, no apparent workability and air content issues were identified as slump, and air content values were both in the target range (3-4 inch for slump and 6.5-9.0% for air content). However, given the same WR dosage as in the reference mix, DOWY and SGNEC1 mixes resulted in a slightly lower slump value, and it could indicate on possible workability issues. Analyzing the hydration process of the batches, one could notice that QZSD ended up with a faster setting time and lower total generated heat, which might be associated with a lower WR dosage.

4.3.3. Results of Mechanical Properties of Concrete

The results of concrete strength and stiffness characteristics tests are presented in Figure 36.

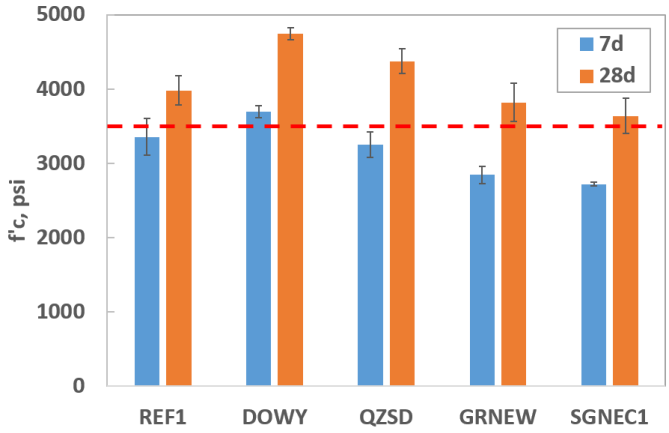

a) Compressive strength

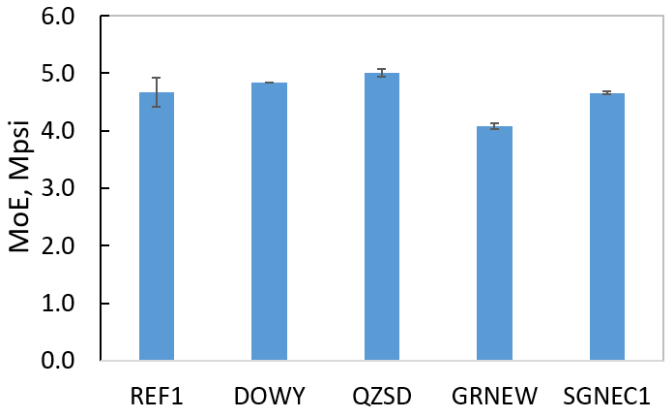

b) Modulus of elasticity

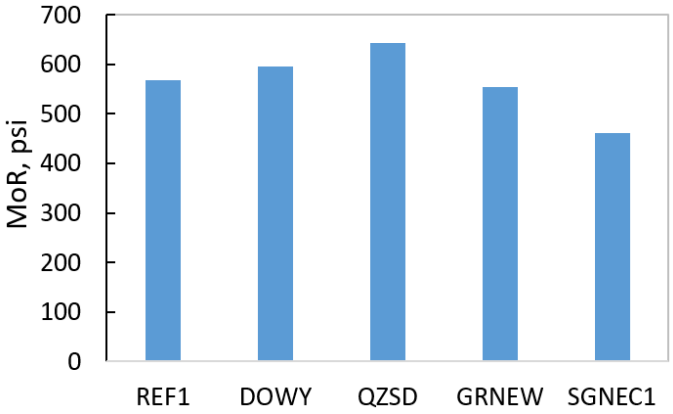

c) Modulus of rupture

Figure 36. Effect of aggregate on mechanical properties of concrete.

As shown in Figure 36, all mixes met the minimum 28-day compressive strength requirement of 3500 psi for the 47B mix (NDOT, 2017). However, it could be noticed that the compressive strength of SG_NEC1 mix (3637 psi) relatively low and that it was also the only mix to have a

modulus of rupture value less than 500 psi. In addition, from the figures of the cross-section of the MoR samples after fracturing (Figure 108 in Appendix B-1), it could be noticed that for DO_WY (to a lesser extent) and for GRNEW (more apparent), most of the fracture happened at aggregate-cement bonding. The results could be an indication of the potential issue of mechanical properties due to the aggregate dust.

Nevertheless, there is no conclusive evidence to directly correlate the difference in strength characteristics with the difference in microfines type and content between the mixes, as there are a number of other factors affecting hardened concrete properties, such as aggregate mineralogy and gradation that can be observed from Figure 107 of the cross-section of the prepared samples presented in Appendix B-1.

4.3.4. Results of Concrete Durability Evaluation

The results of the electrical resistivity per AASHTO TP95-14 and freeze/thaw resistance test per ASTM C666 are presented in Figure 37 and Figure 38, respectively. Results showed a steady growth of the resistivity of concrete specimens over time. At 90 days, the resistivity of the mixes were found to be between 30 and 40 kΩ·cm, which represents low to very low chloride ion penetrability, according to Layssi et al. (2015). Overall, no significant difference in concrete durability properties between the mixes was observed. However, it worthwhile to note that the previously questioned SG_NEC1 mix ended up with slightly lower surface and bulk resistivity values (Figure 37). Results from the bulk and surface resistivity tests followed a very similar trend, and no significant difference between the two tests was observed.

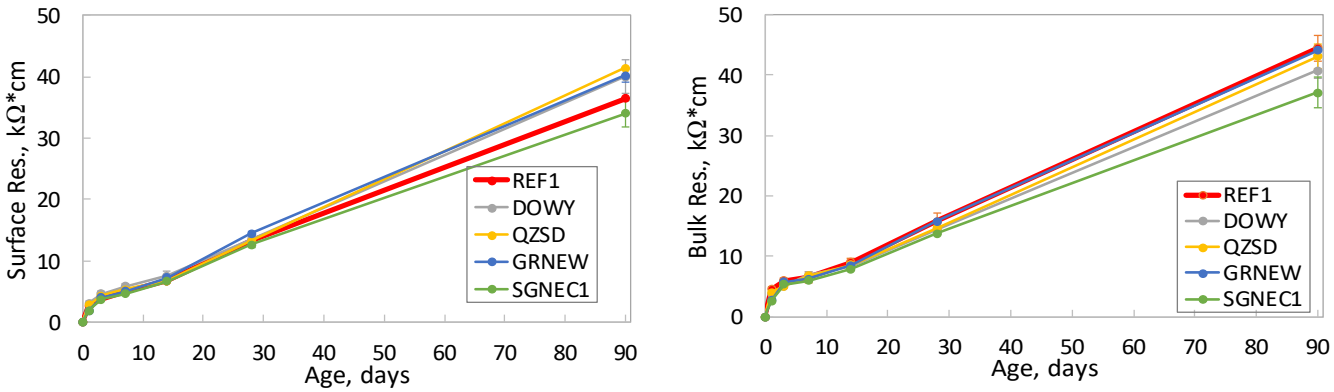

a) Effect of microfines on surface resistivity

b) Effect of microfines on bulk resistivity

Figure 37. Effect of microfines on resistivity.

No apparent difference in freeze/thaw resistance was observed with the concrete mixtures prepared with the different aggregate included in this study. Results showed that all mixes meet the NDOT requirement of relative mass loss lower than 5% after 300 freeze/thaw cycles in accordance with ASTM C666 Procedure A. Information presented in Table 26 in Appendix B-1 also confirmed that there was no apparent difference in the surface scaling level after 300 freeze/thaw cycled.

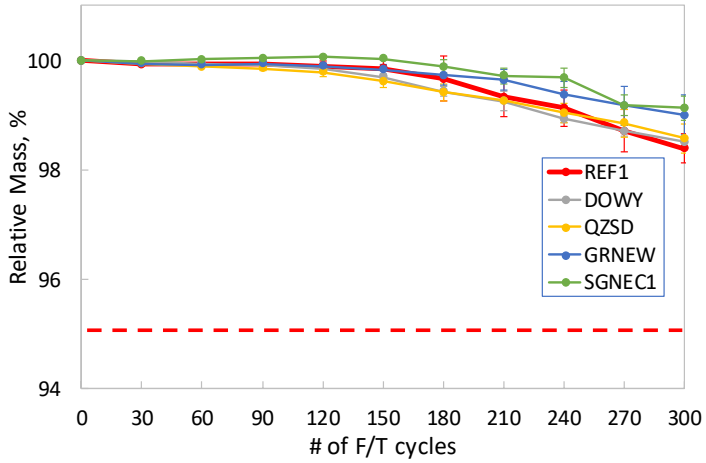

Figure 38. Effect of microfines on freeze-thaw resistance (mass loss).

Figure 38 demonstrates the results of the free shrinkage test per ASTM C157. As expected, the drying shrinkage of all specimens increased over time, with the shrinkage rates are fairly close with the different mixes. While there is no clear trend observed among the mixture prepared with different types of aggregates, it appears that there is no negative impact on drying shrinkage with the aggregate dust included in this study.

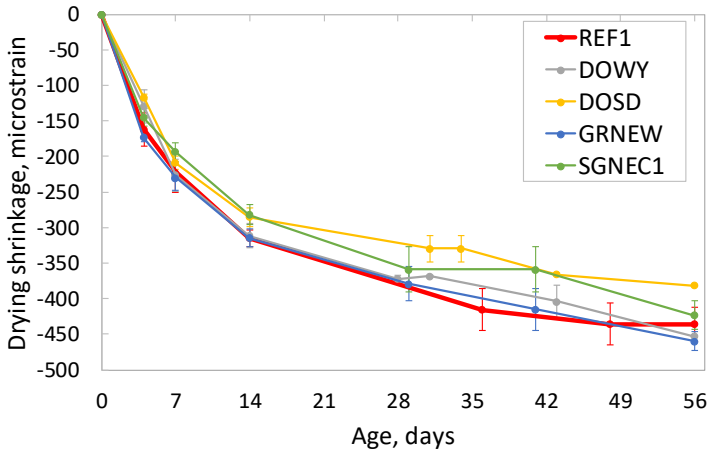

Figure 39. Effect of microfines on drying shrinkage

4.3.5. Summary of Concrete Performance Evaluation

Overall, no significant problems associated with the performance of the concrete made with aggregates with the relatively high MMBV (values compared between aggregates presented in this study) were identified, as all of the prepared batches confirmed to the requirements of the NDOT 47B mix (slump, air content, compressive strength, and freeze/thaw resistance). Moreover, it might be necessary to account for the difference in the aggregate fraction in the whole concrete mix volume, i.e., to account for properties of microfines present in both coarse and fine aggregates in an actual concrete mixture. Thus, a concept of weighted modified methylene blue value (WMMBV) can be obtained in the following:

$$\text{Weighted MMBV} = \frac{\text{MMBV\_FA} \times \text{Mass of FA (pcy)} + \text{MMBV\_CA} \times \text{Mass of CA (pcy)}}{\text{Total Mass of Batch (pcy)}}$$

Based on the above equation, the weight MMBV is calculated base on the mix design, and the results are presented below in Table 22.

Table 22. Results of weighted modified methylene blue value (WMMBV) calculation.

MIX ID	REF1	DO_WY	QZ_SD	GR_NEW	SG_NEC1
FA (pcy)	2036	2035	2042	2028	2023
CA (pcy)	898	901	906	899	897
Total mass (pcy)	3729	3731	3743	3722	3715
WMMBV_B (mg%/g)[1]	0.0018	0.0193	0.0333	0.0099	0.0045
WMMBV_C (mg%/g)[2]	0.0054	0.0249	0.0339	0.0130	0.0102

[1]Based on the MBT of microfines collected after sieving (mg/g)

[2]Based on the MBT of microfines collected after washing (mg/g)

Due to the limited amount of data available through this study, it is not feasible to directly correlate microfines with the properties of concrete made with completely different aggregates. Based on the information collected from other studies (Ahn and Fowler, 2001; Gullerud, 2002; Munoz et al., 2007), a summary of MMBV and calculated WMMBV, as well as the impact on fresh concrete, concrete strength (compressive strength f'_c, and splitting tensile strength f'_{sp}), and durability performance (shrinkage), can be found in Table 23 and Figure 40.

Table 23. Effect of microfines on various concrete performance characteristics based on previous studies.

Sample #	MMBV (mg/g)	WMMBV (mg%/g)	Effect on fresh concrete properties	Effect on concrete strength characteristics	Effect on concrete durability characteristics
1[1] Carbonate coating	0.0024	0.0011	3" to 1.75" slump drop	19% increase in f'_c	no apparent effect
2[1] dust/clay	0.0703	0.0337	2.5" to 1" slump drop	no significant effect	26% increase in free shrinkage
3[1] dust/clay	0.1218	0.0582	2.5" to 0.25" slump drop	no significant effect	30% increase in free shrinkage
4[1] dust/clay	0.1482	0.0707	2.5" to 1.5" slump drop	10% decrease in f'_{sp}	41% increase in free shrinkage
5[2] dust/clay	0.0061	0.0029	3" to 2.75" slump drop	no significant effect	no significant effect
6[2] dust/clay	0.0980	0.0466	3" to 1.75" slump drop	no significant effect	no significant effect
7[2] Illite	0.0267	0.0127	3" to 2.75" slump drop	no significant effect	no significant effect
8[2] Kaolin	0.0460	0.0219	3" to 2.75" slump drop	no significant effect	15% increase in free shrinkage
9[2] NaM[3]	0.2291	0.1089	3" to 0" slump drop	88% f'_c drop 80% f'_{sp} drop	42% increase in free shrinkage
10[2] CaM[4]	0.8429	0.4007	3" to 0.75" slump drop	75% f'_c drop 65% f'_{sp} drop	142% increase in free shrinkage

[1]Gullerud, 2002
[2]Munoz, 2007
[3]sodium montmorillonite
[4]Calcium montmorillonite

When comparing to the results of the previous studies (Table 23), based on the comparison of WMMBV (where the values with the current mixes do not exceed 0.035 as indicated in Table 22), the presence of microfines in the set of aggregates included in the current study should not be significant to have any noticeable effect on concrete performance indicators. However, it is possible that if the quantity of microfines reaches a certain threshold, it might end up in poor concrete performance, as was the case for specimen No. 3, 4, 9, and 10 from Table 23. In that case, MMBV (or WMMBV) could possibly work as a proper monitoring/prediction tool, as it did in the study of Ahn and Fowler (2001), where it had a significant statistical correlation with drying shrinkage and flexural strength characteristics (Figure 40). However, as properties such as shrinkage and flexural strength of concrete depend on various factors, including the type and amount of cement and aggregate used in the mixtures, more data is needed to establish a similar relationship, as shown in Figure 39.

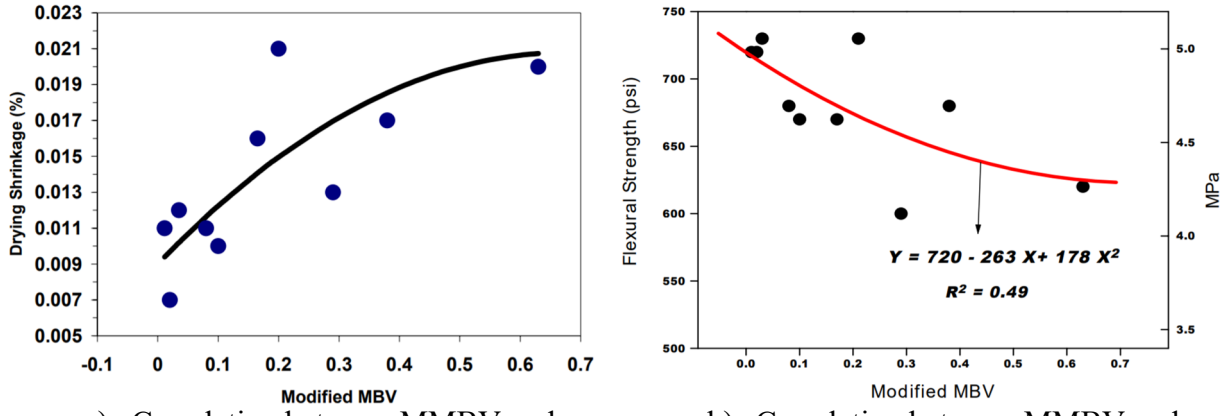

a) Correlation between MMBV and drying shrinkage

b) Correlation between MMBV and flexural strength

Figure 40. MMBV as a predictor of concrete performance (adapted from Ahn and Fowler, 2001).

4.6. Petrographic Analysis of Concrete Core samples

4.6.1. Visual Inspection

Eight concrete core samples were received from NDOT Materials Lab at the University of Nebraska-Lincoln (UNL) (Figure 41). The cores were approximately 4" in diameter and at different depths. A visual inspection of the cores showed no cracks or other visible surface deteriorations of each core, except core specimen R3 and R4 seems to have more air voids compared to other cores.

Figure 41. Core samples obtained from NDOT projects for inspection.

The main focus of the visual inspection was to indicate possible distress problems, due to dust coating from the aggregates, if any. The detailed results of the visual examination of each sample are shown in Table 27 in Appendix B-2. In addition, all samples were cut in a vertical plane in order to obtain a high-quality image of the cross-section of the sample to identify possible internal cracks, and assess the quality of aggregate-paste bonding. The results of the vertical cross-section of each of the obtained core specimens can be found in Appendix B-2. As can be seen from Figure 108, no apparent cracks or any other deteriorations were detected on the cross-section of each sample. An optical microscope was used to perform a more in-depth visual examination. As examples shown in Figure 42, the results of the core samples' visual examination revealed a possibility of aggregate dust coating appearance in sample R2, where no apparent dust coating was observed in sample R4.

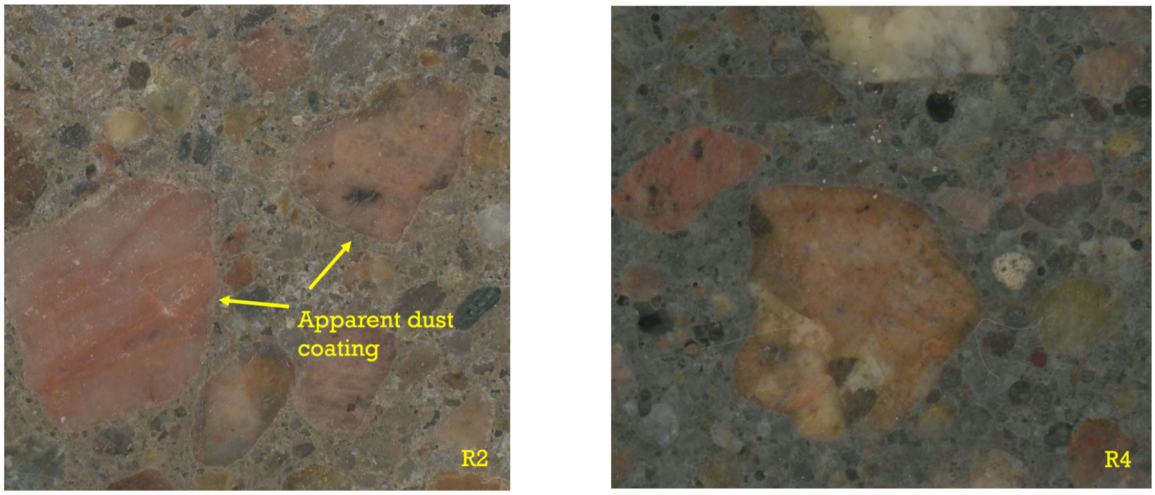

a) Core sample R2 b) Core sample R4

Figure 42. Microscope images of aggregate-cement paste bonding of core sample.

Further investigation by gently striking a portion of specimens with a hammer revealed that there might be some aggregate-cement paste bonding problems associated with samples R1 and R2, as the fracture mainly happened around aggregates particles. It was possible to separate aggregate pieces from cement paste with bare hands in core specimen R1 and R2, while the fracture of other samples (R3-R8) ended up breaking the aggregate pieces instead of the boundary (Figure 43).

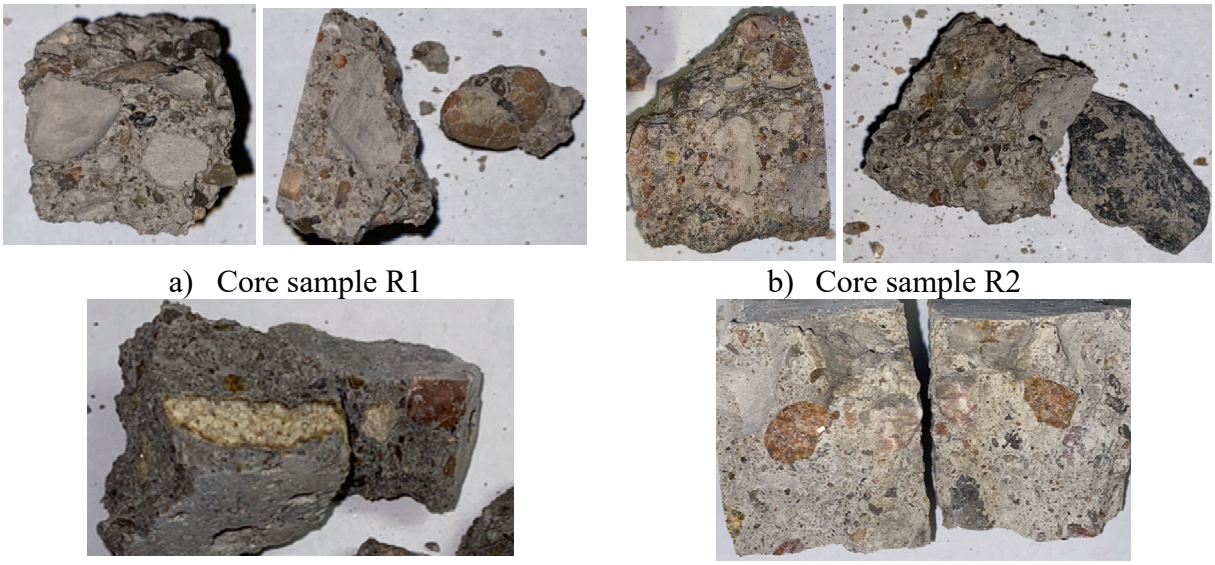

a) Core sample R1 b) Core sample R2

c) Core sample R3 d) Core sample R7

Figure 43. Examples of crushing patterns of core concrete specimens.

In addition, it was noted that R1 specimen tends to absorb water faster. Although it may be just due to different absorption properties of the aggregates, a higher permeability can also be attributed to more porous ITZ due to the dust coating of aggregate. For this investigation, R1 and R3 concrete samples were simultaneously immersed in water for approximately one second, and then removed from water and left to let the surface water dry/be absorbed. As can be seen from the results presented in Table 24 below, it is apparent that samples R1 tend to absorb the surface water at a higher rate, which could indicate a higher permeability that might be associated with more porous ITZ.

Table 24. Water permeability test of samples R1 and R3.

	Sample R1	Sample R3
Before immersion in water		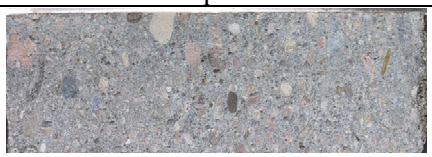
Immediately after immersion		
30 s after immersion		
60 s after immersion		
90 s after immersion		
2 min after immersion		
3 min after immersion		
4 min after immersion		
5 min after immersion		
10 min after immersion		

4.7. Summary and Discussion based on Aggregate Characterization, and Concrete Performance Analysis

In summary, the comprehensive evaluation of the aggregate dusts and contents revealed that while all aggregate collected for the present study meet the NDOT criteria of P200 less than 3% and sand equivalent value higher than 90%, the type and content of aggregate dusts varies among different aggregate sources. The quartzite coarse aggregate was found to have a fairly low Methylene Blue Test (MBV), but a higher P200 content. On the other hand, the dolomite and gravel-based coarse aggregate tend to have higher MBV, yet the total dust content is low. A parameter such as Modified Methylene Blue Test (MMBV) V that combines both fine content and MBV could be a more rational parameter in controlling the dust in aggregate.

The study of the interface between aggregate and cement paste shows that thoroughly washing the aggregate can help to improve the interface. However, based on the analysis of the lab-casted concrete specimens, no apparent issues of the aggregate-paste interface or fresh and hardened concrete behavior was observed with the concrete prepared with as-received aggregate. The result is likely due to the fact that the major portion of microfine coating on aggregate was washed off or diluted during the concrete mixing. Also, all aggregate included in this study appears to exhibit fairly low MMBV and Weighted Modified Methylene Blue Test (WMMBV) compared to previously published studies.

The results from the petrographic analysis from the core specimens collected from the field suggested that all fine aggregate included in the present study meet the NDOT sand equivalent requirement. However, the coarse aggregate shows some dust coating, which can lead to potential mechanical and durability issues. Based on the current study, a modification of current limits might not be necessary for fine aggregates. However, it might be necessary to conduct the methylene blue test for the coarse aggregate to ensure the absence of harmful dust content. Future investigation looking at NDOT requirement of P200 for coarse aggregate and obtaining the MBV to calculate MMBV and correlated to concrete performance in the field might be needed.

CHAPTER 5. CONCLUSIONS

Based on the results from the comprehensive experimental study of aggregate dust and the performance of pavement concrete prepared with different types of aggregate collected for this study, the following conclusions can be drawn:

- While aggregate collected in this study all appear to meet the current NDOT criteria of coarse aggregate fine content and fine aggregate sand equivalent value, additional test such as methylene blue value could provide more insights into the type of dust on aggregate surface, especially the coarse aggregate.
- Likely due to the relatively low fine (P200) contents, most concrete prepared with the collected aggregate included in this study exhibited acceptable fresh concrete and hardened properties.
- Petrographic analysis of core specimens collected from the field indicated that with high dust content in the coarse aggregate, shoed debonding issues between aggregate and cement paste.
- While the current NDOT specification of the P200 limit (<3.0%) appears to provide reasonable control of aggregate dust, depends on the type of dust and the modified methylene blue value, a lower limit (1.5% or 2.0%) could potentially be proposed for coarse aggregate to better prevent potential issues associated with aggregate dusts.
- Modified Methylene blue value could potentially be used to control the coarse aggregate dust. However, more data is needed to set up criteria for quality control.

REFERENCES

AASHTO T 11. (2020). Standard method of test for materials finer than 75-µm (no. 200) sieve in mineral aggregates by washing. *American Association of State and Highway Transportation Officials*

AASHTO T 21M/T 21. (2020). Standard method of test for organic impurities in fine aggregates for concrete. *American Association of State and Highway Transportation Officials*

AASHTO T 27. (2020). Standard method of test for sieve analysis of fine and coarse aggregate. *American Association of State and Highway Transportation Officials*

AASHTO T 71. (2008). Standard method of test for effect of organic impurities in fine aggregate on strength of mortar. *American Association of State and Highway Transportation Officials*

AASHTO T 95-14. (2014). Standard method of test for surface resistivity indication of concrete's ability to resist chloride ion penetration. *American Association of State and Highway Transportation Officials*

AASHTO T 176-17. (2017). Standard method of test for plastic fines in graded aggregates and soils by use of the sand equivalent test. *American Association of State and Highway Transportation Officials*

AASHTO T 330-07. (2019). Standard method of test for the qualitative detection of harmful clays of the smectite group in aggregates using methylene blue. *American Association of State and Highway Transportation Officials*

Ahn, N. S., & Fowler, D. W. (2001). An experimental study on the guidelines for using higher contents of aggregate microfines in Portland cement concrete (Report No. ICAR 102-1F). *International Center for Aggregates Research, University of Texas at Austin*.

Antoni, Chandra, L., & Hardjito, D. (2015). The impact of using fly ash, silica fume and calcium carbonate on the workability and compressive strength of mortar. *Procedia Engineering*, *125*, 773-779.

ASTM C33. (2018). Standard specification for concrete aggregates. *ASTM International.*

ASTM C39. (2020). Standard test method for compressive strength of cylindrical concrete specimens. *ASTM International.*

ASTM C40. (2020). Standard test method for organic impurities in fine aggregates for concrete. *ASTM International.*

ASTM C78. (2018). Standard test method for flexural strength of concrete (using simple beam with third-point loading). *ASTM International.*

ASTM C117. (2017). Standard test method for materials finer than 75-µm (no. 200) sieve in mineral aggregates by washing. *ASTM International.*

ASTM C127. (2015). Standard test method for relative density (specific gravity) and absorption of coarse aggregate. *ASTM International.*

ASTM C128. (2015). Standard test method for relative density (specific gravity) and absorption of fine aggregate. *ASTM International.*

ASTM C136. (2019). Standard test method for sieve analysis of fine and coarse aggregates. *ASTM International.*

ASTM C143. (2020). Standard test method for slump of hydraulic-cement concrete. *ASTM International.*

ASTM C157. (2017). Standard test method for length change of hardened hydraulic-cement mortar and concrete. *ASTM International.*

ASTM C192. (2019). Standard practice for making and curing concrete test specimens in the laboratory. *ASTM International.*

ASTM C260. (2016). Standard specification for air-entraining admixtures for concrete. *ASTM International.*

ASTM C305. (2020). Standard practice for mechanical mixing of hydraulic cement pastes and mortars of plastic consistency. *ASTM International.*

ASTM C494. (2019). Standard specification for chemical admixtures for concrete. *ASTM International.*

ASTM C469. (2014). Standard test method for static modulus of elasticity and Poisson's ratio of concrete in compression. *ASTM International.*

ASTM C595. (2020). Standard specification for blended hydraulic cements. *ASTM International.*

ASTM C666. (2015). Standard test method for resistance of concrete to rapid freezing and thawing. *ASTM International.*

ASTM C702. (2018). Standard practice for reducing samples of aggregate to testing size. *ASTM International.*

ASTM C1702. (2017). Standard test method for measurement of heat of hydration of hydraulic cementitious materials using isothermal conduction calorimetry. *ASTM International.*

Bigas, J. P., & Gallias, J. L. (2002). Effect of fine mineral additions on granular packing of cement mixtures. *Magazine of Concrete Research*, *54*(3), 155-164.

California Department of Transportation. (2018). Standard Specifications.

Caliskan, S., Karihaloo, B. L., & Barr, B. I. G. (2002). Study of rock–mortar interfaces. Part I: surface roughness of rock aggregates and microstructural characteristics of interface. *Magazine of Concrete Research*, *54*(6), 449-461.

Celik, T., & Marar, K. (1996). Effects of crushed stone dust on some properties of concrete. *Cement and Concrete research*, *26*(7), 1121-1130.

Chan, S. Y., Tsang, M. K., & Feng, N. Q. (1997). Effect of aggregate dust content on the workability and workability retention of concrete. *HKIE Transactions*, *4*(1), 1-5.

Colorado Department of Transportation. (2019). Standard specifications for road and bridge construction.

Cramer, S. M., Anderson, M. A., Silva, J. M. S., Tejedor, M. I., & Muñoz, J. F. (2011). Role of Dirty Aggregates in the Performance of Concrete Exposed to Airfield Pavement Deicers (Report No. IPRF-01-G-002-06). *Innovative Pavement Research Foundation.*

Cramer, S. M., Anderson, M. A., Tejedor, M. I., Muñoz, J. F., Effinger, J., & Kropp, R. (2010). Detecting Deleterious Fine Particles in Concrete Aggregates and Defining Their Impact (Report No. SPR# 0092-07-02). *University of Wisconsin-Madison.*

Darwin, D. (1999). Concrete in compression. *American Concrete Institute.*

Désiré, T. J., & Léopold, M. (2013). Impact of clay particles on concrete compressive strength. *International Research Journal on Engineering, 1 (2)*, 049-056.

Elseifi, M. A., Mohammad, L. N., Kassem, E., Ying, H., & Masad, E. (2011). Quantification of damage in the dynamic complex modulus and flow number tests using X-ray computed tomography. *Journal of materials in civil engineering*, *23*(12), 1687-1696.

Elsharief, A., Cohen, M. D., & Olek, J. (2003). Influence of aggregate size, water cement ratio and age on the microstructure of the interfacial transition zone. *Cement and concrete research*, *33*(11), 1837-1849.

Federal Highway Administration. (2014). Standard specifications for construction of roads and bridges on Federal Highway projects.

Fernandez, R., Martirena, F., & Scrivener, K. L. (2011). The origin of the pozzolanic activity of calcined clay minerals: A comparison between kaolinite, illite and montmorillonite. *Cement and concrete research*, *41*(1), 113-122.

Goldbeck, A. T., Miesenhelder, P. D., & Kelley, E. F. (1932). The nature and effects of surface coatings on coarse aggregates. *Highway Research Board Proceedings*, 25, 305-319.

Gullerud, K. J. (2002). *The effects of aggregate coatings on the performance of Portland cement concrete* (Master Thesis, University of Wisconsin-Madison).

Harris, N. J., Hover, K. C., Folliard, K. J., & Ley, M. T. (2008). The use of the foam index test to predict AEA dosage in concrete containing fly ash: Part I—Evaluation of the state of practice. *Journal of ASTM International*, *5*(7), 1-15.

Idaho Transportation Department. (2018). Standard specifications for highway construction.

Illinois Department of Transportation. (2016). Standard specifications for road and bridge construction.

Indiana Department of Transportation. (2020). Standard specifications.

Iowa Department of Transportation. (2015). Standard specifications for highway and bridge construction.

Kansas Department of Transportation. (2015). Standard specifications for state road and bridge construction.

Khedmati, M., & Kim, Y. R. (2020). Multiscale Characterization to Examine the Effects of Aggregate Properties on Aggregate-Paste Interphase in Cement Concrete Mixtures. *Journal of Materials in Civil Engineering*, *32*(4), 04020059.

Khedmati, M., Kim, Y. R., Turner, J. A., Alanazi, H., & Nguyen, C. (2018). An integrated microstructural-nanomechanical-chemical approach to examine material-specific characteristics of cementitious interphase regions. *Materials Characterization*, *138*, 154-164.

Layssi, H., Ghods, P., Alizadeh A.R., and Salehi M. (2015). Electrical Resistivity of Concrete – Concepts, Applications, and Measurement Techniques, *Concrete International*, 41-46.

Michigan Department of Transportation. (2012). Standard specifications for construction.

Minnesota Department of Transportation. (2018). Standard specifications for construction.

Missouri Highway and Transportation Commission. (2018). Standard specifications for highway construction.

Mondal, P., Shah, S. P., & Marks, L. D. (2009). Nanomechanical Properties of Interfacial Transition Zone in Xoncrete. In *Nanotechnology in Construction 3* (pp. 315-320). Springer, Berlin, Heidelberg.

Montana Department of Transportation. (2020). Standard and supplemental specifications for road and bridge construction.

Mukhopadhyay A.K., Brandon P., Russell A., Arambula E., Estakhri C., and Deng Y. (2013). *Treatments for Clays in Aggregates used to Produce Cement Concrete, Bituminous Materials, and Chip Seals*. Texas Department Transportation (0-6444).

Munoz, J.F, Tejedor M.I., Anderson M.A., & Cramer, S.M. (2007). Expanded Study on the Effects of Aggregate Coating and Films on Concrete Performance (Report No. SPR # 0092-04-12). *University of Wisconsin-Madison.*

Munoz, J. F., Gullerud, K. J., Cramer, S. M., Tejedor, M. I., & Anderson, M. A. (2010). Effects of coarse aggregate coatings on concrete performance. *Journal of Materials in Civil Engineering*, *22*(1), 96-103.

Nebraska Department of Transportation. (2017). Standard specifications for highway construction.

Nevada Department of Transportation. (2014). Standard specifications for road and bridge construction.

Noble, D. F., & Plaster, R. W. (1970). *Reactions in Portland cement-clay mixtures* (No. VHRC 70-R13). Virginia Transportation Research Council.

North Dakota Department of Transportation. (2019). Standard specifications for road and bridge construction.

Ohio Department of Transportation. (2019). Construction and material specifications.

Oklahoma Department of Transportation. (2009). Construction specifications.

Oliver, W. C., & Pharr, G. M. (1992). An improved technique for determining hardness and elastic modulus using load and displacement sensing indentation experiments. *Journal of materials research*, *7*(6), 1564-1583.

Pera, J., Husson, S., & Guilhot, B. (1999). Influence of finely ground limestone on cement hydration. *Cement and Concrete Composites*, *21*(2), 99-105.

Pike, D. C. (1992). *Methodologies for assessing the variability of fines in sands used for concretes and mortars* (Doctoral dissertation, University of Reading).

Prokopski, G., & Halbiniak, J. (2000). Interfacial transition zone in cementitious materials. *Cement and Concrete Research*, *30*(4), 579-583.

Schmitt, J. W. (1990). Effects of mica, aggregate coatings, and water-soluble impurities on concrete. *Concrete International*, *12*(12), 54-58.

Scrivener, K. L., Crumbie, A. K., & Laugesen, P. (2004). The interfacial transition zone (ITZ) between cement paste and aggregate in concrete. *Interface science*, *12*(4), 411-421.

South Dakota Department of Transportation. (2015). Standard specifications for roads and bridges.

Stewart, J. G., Norvell, J. K., Juenger, M. C., & Fowler, D. W. (2007). Influence of microfine aggregate characteristics on concrete performance. *Journal of materials in Civil Engineering*, *19*(11), 957-964.

Sumner, M. E., & Miller, W. P. (1996). Cation exchange capacity and exchange coefficients. *Methods of Soil Analysis: Part 3 Chemical Methods*, *5*, 1201-1229.

Tasong, W. A., Lynsdale, C. J., & Cripps, J. C. (1998). Aggregate-cement paste interface. II: Influence of aggregate physical properties. *Cement and Concrete Research*, *28*(10), 1453-1465.

Utah Department of Transportation. (2017). Standard specifications for road and bridge construction.

Wisconsin Department of Transportation. (2020). Standard specifications for highway and structure construction.

Winslow, D. N., Cohen, M. D., Bentz, D. P., Snyder, K. A., & Garboczi, E. J. (1994). Percolation and pore structure in mortars and concrete. *Cement and concrete research*, *24*(1), 25-37.

Wyoming Department of Transportation. (2010). Standard specifications for road and bridge construction.

APPENDIX A - AGGREGATES CHARACTERIZATION

A-1. Aggregate Samples at Different Cleanliness Conditions

a) Before washing b) After washing c) After ultrasonic cleaning

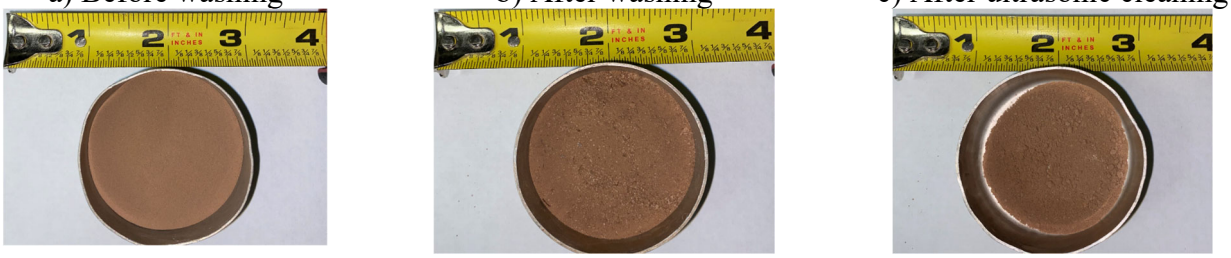

d) Microfines collected after dry sieving e) Nicrofines collected after washing f) Microfines collected after ultrasonic cleaning

Figure 44. Dolomite sample from Harriman quarry, Laramie, WY (DO_WY).

a) Before washing b) After washing c) After ultrasonic cleaning

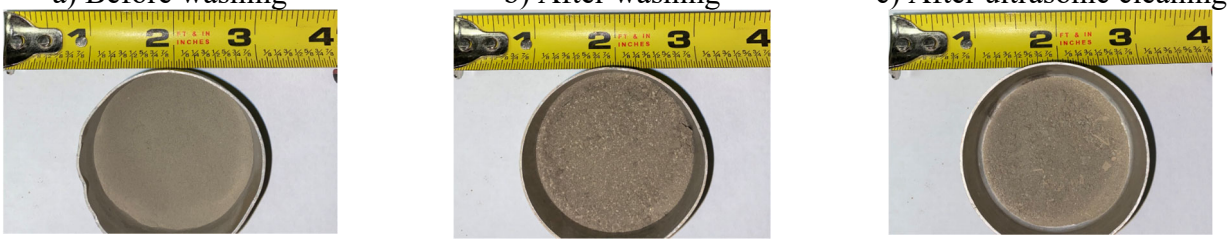

d) Microfines collected after dry sieving e) Nicrofines collected after washing f) Microfines collected after ultrasonic cleaning

Figure 45. Granite sample from Martin Marietta, Granite Canyon, WY (GN_WY).

a) Before washing

b) After washing

c) After ultrasonic cleaning

d) Microfines collected after dry sieving

e) Nicrofines collected after washing

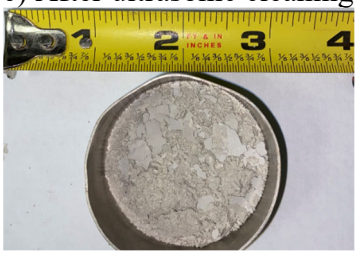

f) Microfines collected after ultrasonic cleaning

Figure 46. Limestone sample from Weeping Water, NE (LS_NEE1).

a) Before washing

b) After washing

c) After ultrasonic cleaning

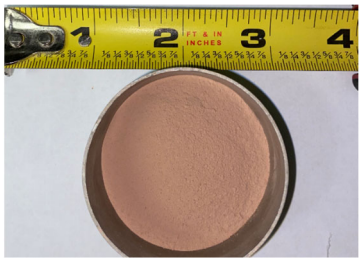

d) Microfines collected after dry sieving

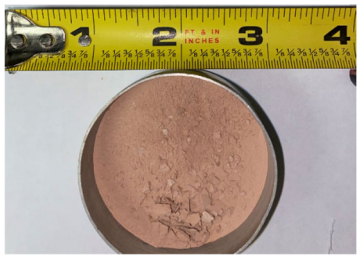

e) Nicrofines collected after washing

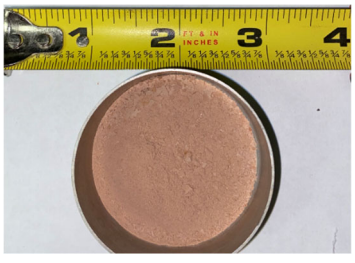

f) Microfines collected after ultrasonic cleaning

Figure 47. Quartzite sample from Rapid City, SD (QZ_SD).

a) Before washing

b) After washing

c) After ultrasonic cleaning

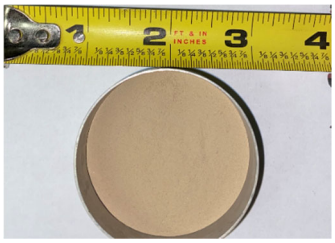

d) Microfines collected after dry sieving

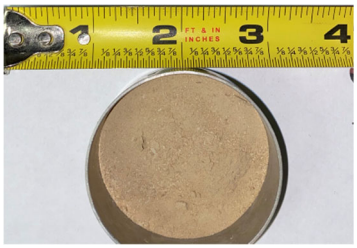

e) Nicrofines collected after washing

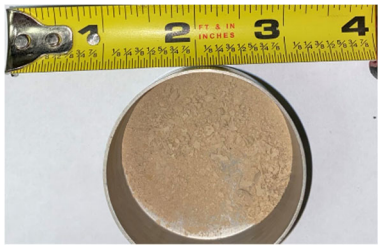

f) Microfines collected after ultrasonic cleaning

Figure 48. Gravel sample from Apex Dru Pit, Gering, NE (GR_NEW).

a) Before washing

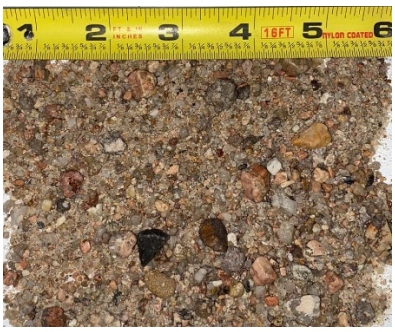

b) After washing

c) After ultrasonic cleaning

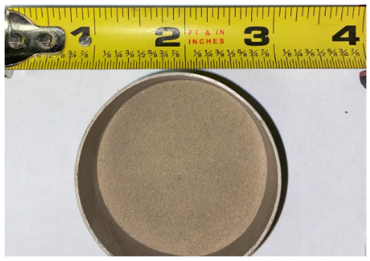

d) Microfines collected after dry sieving

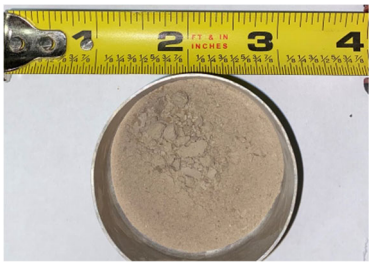

e) Nicrofines collected after washing

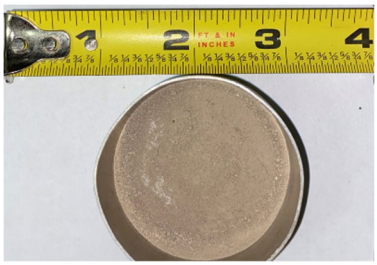

f) Microfines collected after ultrasonic cleaning

Figure 49. Sand and Gravel sample from Platte River Wet Pit, Platte River, NE (SG_NEC1).

a) Before washing

b) After washing

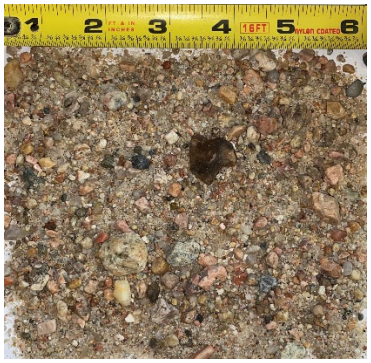

c) After ultrasonic cleaning

d) Microfines collected after dry sieving

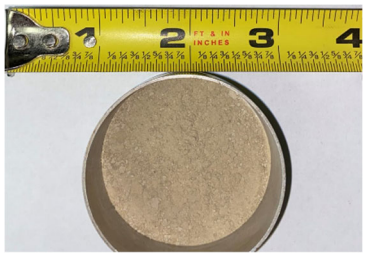

e) Nicrofines collected after washing

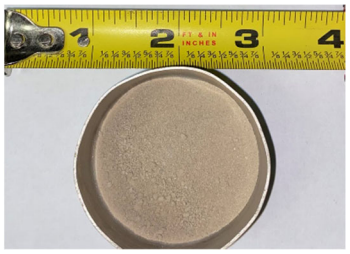

f) Microfines collected after ultrasonic cleaning

Figure 50. Sand and Gravel sample from Grant Island, NE (SG_NEC2).

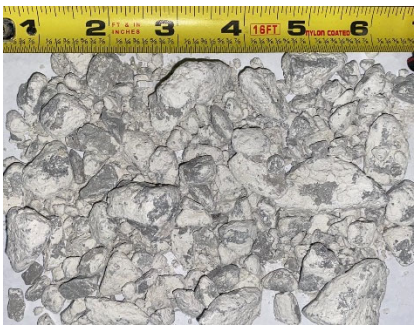

a) Before washing

b) After washing

c) After ultrasonic cleaning

d) Microfines collected after dry sieving

e) Nicrofines collected after washing

f) Microfines collected after ultrasonic cleaning

Figure 51. Limestone sample from East Nebraska (LS_NEE2).

a) Before washing SG_NEW_A

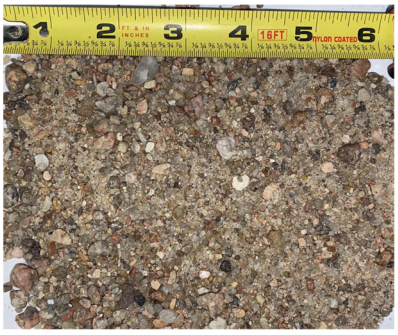

b) After washing SG_NEW_C

c) After ultrasonic cleaning SG_NEW_D

d) Microfines collected after dry sieving

e) Nicrofines collected after washing

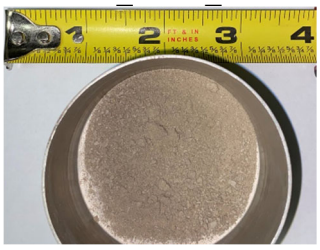

f) Microfines collected after ultrasonic cleaning

Figure 52. Sand and Gravel sample from West Nebraska

a) Before washing CS_NV_A

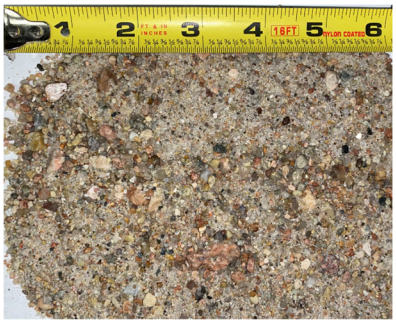

b) After washing CS_NV_C

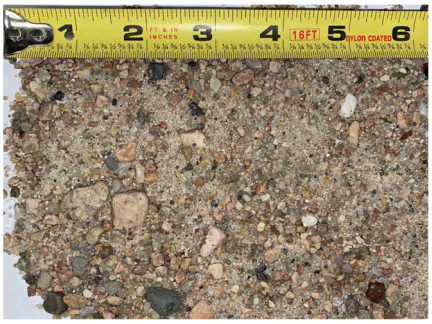

c) After ultrasonic cleaning CS_NV_D

d) Microfines collected after dry sieving

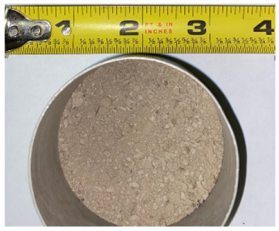

e) Nicrofines collected after washing

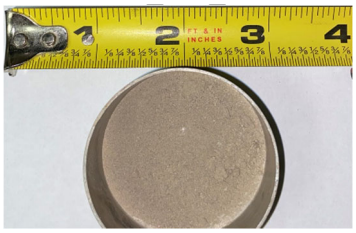

f) Microfines collected after ultrasonic cleaning

Figure 53. Sand and Gravel sample from East Nebraska

A-2. Results of Sand Equivalent Test

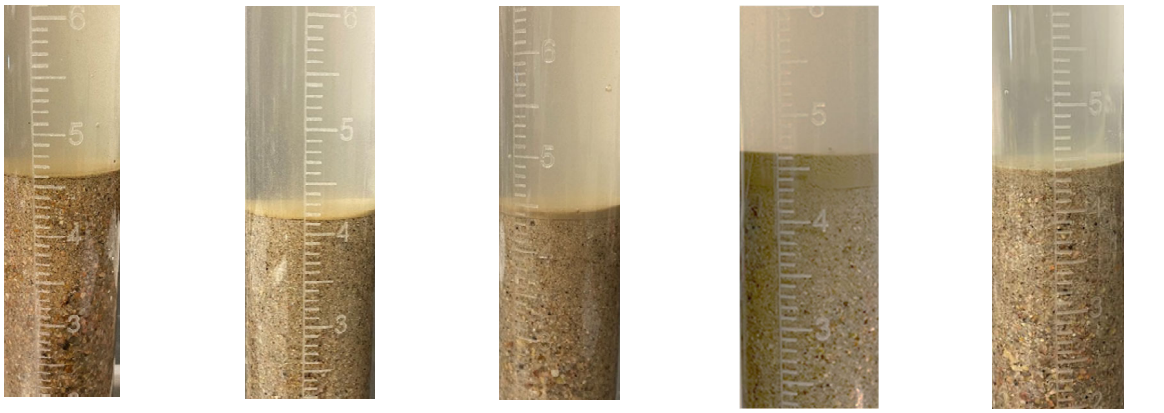

a) SG_NEC1 b) SG_NEC2 c) SG_NEE d) SG_NEE2 e) SG_NEE2_C (after washing)

Figure 54. Results of the sand equivalent test of fine aggregates.

A-3. Results of Methylene Blue Test

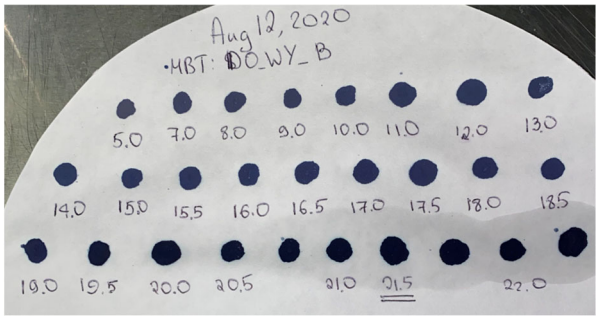

a) MBV of microfines collected after dry sieving

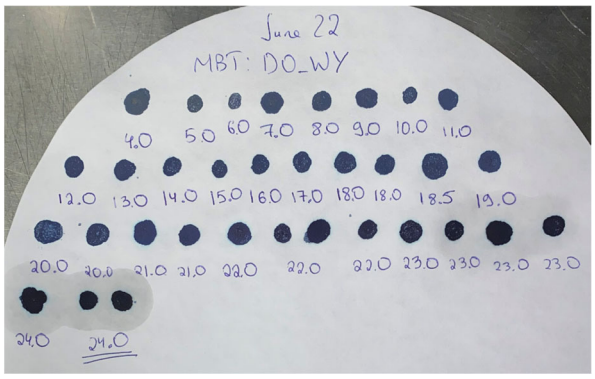

b) MBV of microfines collected after washing

Figure 55. Methylene Blue Value (MBV) of microfines collected from DO_WY.

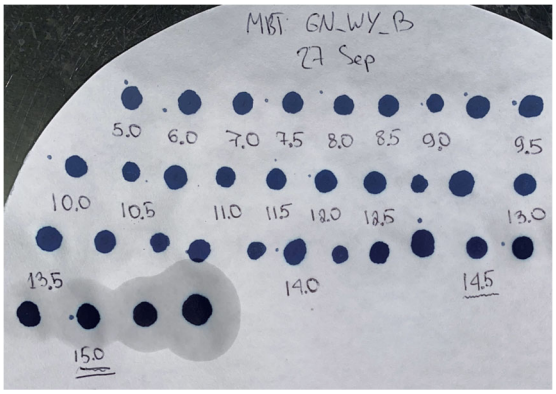

a) MBV of microfines collected after dry sieving

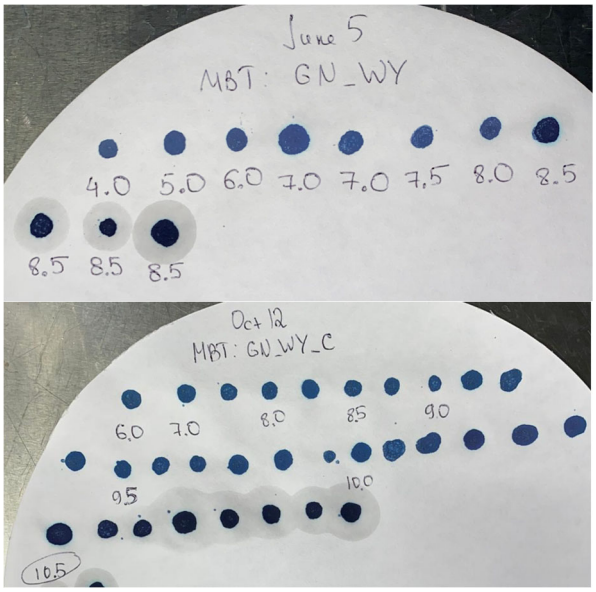

b) MBV of microfines collected after washing

Figure 56. Methylene Blue Value (MBV) of microfines collected from GN_WY.

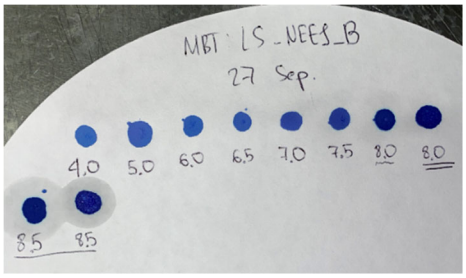

a) MBV of microfines collected after dry sieving

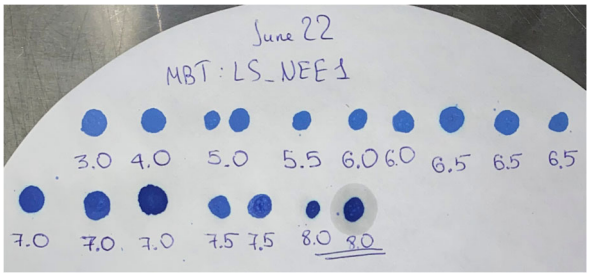

b) MBV of microfines collected after washing

Figure 57. Methylene Blue Value (MBV) of microfines collected from LS_NEE1.

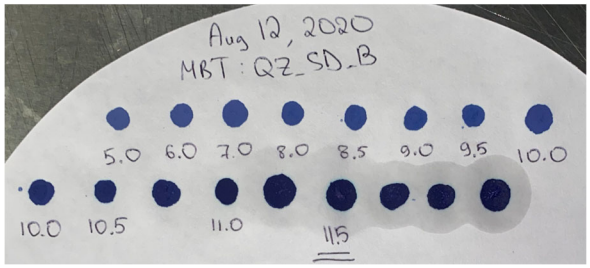

a) MBV of microfines collected after dry sieving

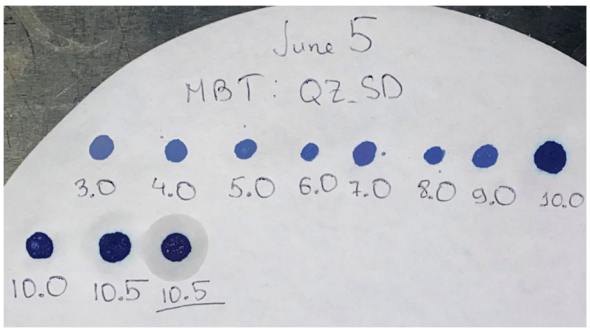

b) MBV of microfines collected after washing

Figure 58. Methylene Blue Value (MBV) of microfines collected from QZ_SD.

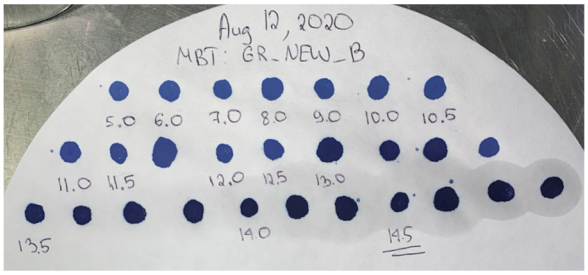

a) MBV of microfines collected after dry sieving

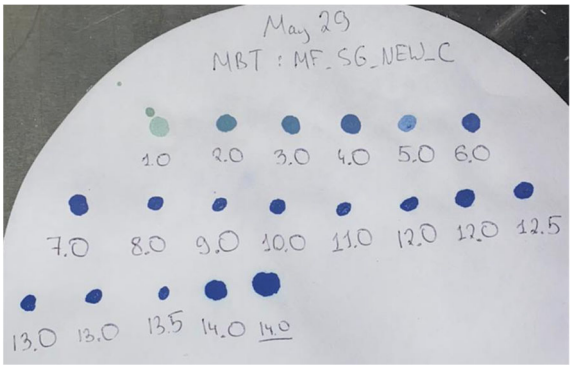

b) MBV of microfines collected after washing

Figure 59. Methylene Blue Value (MBV) of microfines collected from GR_NEW.

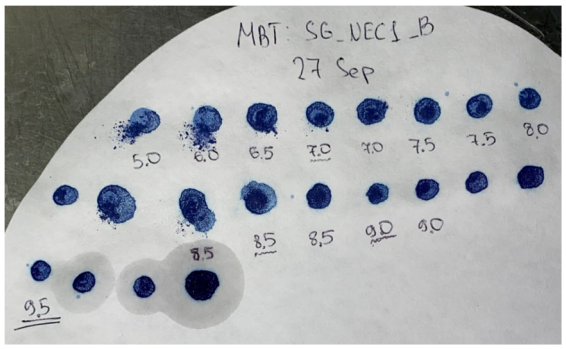

a) MBV of microfines collected after dry sieving

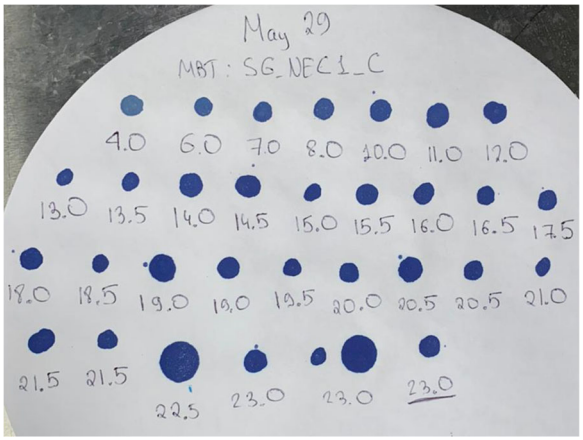

b) MBV of microfines collected after washing

Figure 60. Methylene Blue Value (MBV) of microfines collected from SG_NEC1.

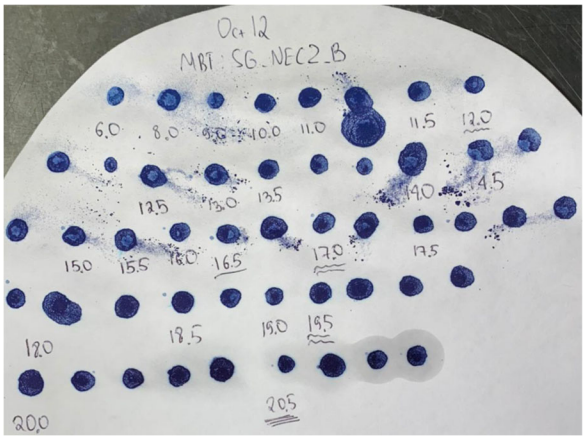

a) MBV of microfines collected after dry sieving

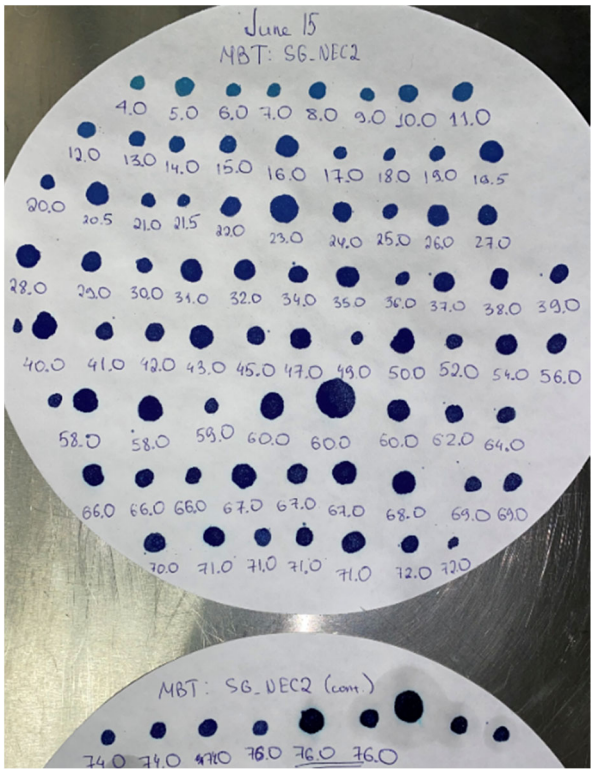

b) MBV of microfines collected after washing

Figure 61. Methylene Blue Value (MBV) of microfines collected from SG_NEC2.

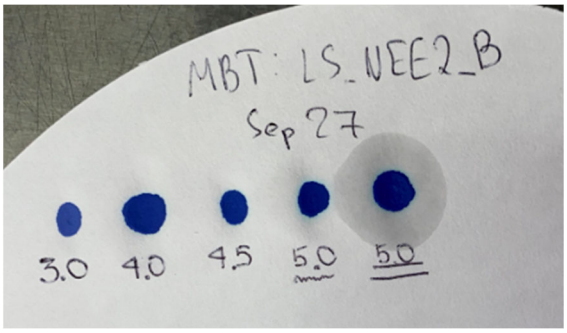

a) MBV of microfines collected after dry sieving

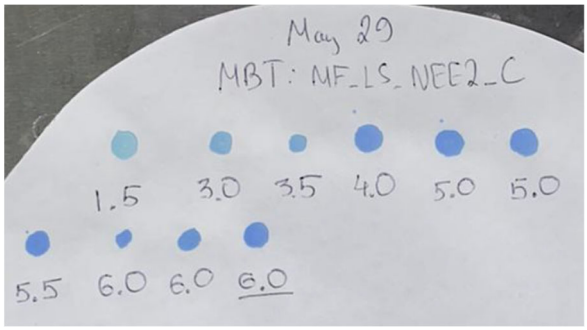

b) MBV of microfines collected after washing

Figure 62. Methylene Blue Value (MBV) of microfines collected from LS_NEE2.

Photo not available

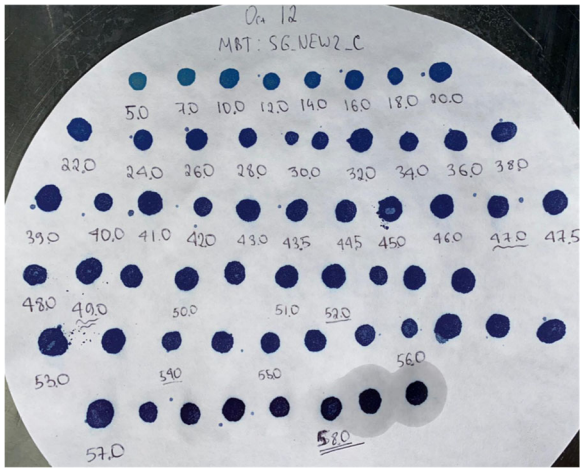

a) MBV of microfines collected after dry sieving

b) MBV of microfines collected after washing

Figure 63. Methylene Blue Value (MBV) of microfines collected from SG_NEW.

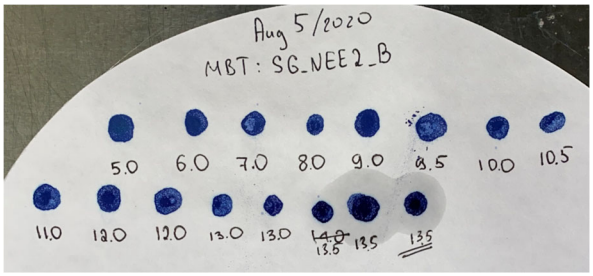

a) MBV of microfines collected after dry sieving

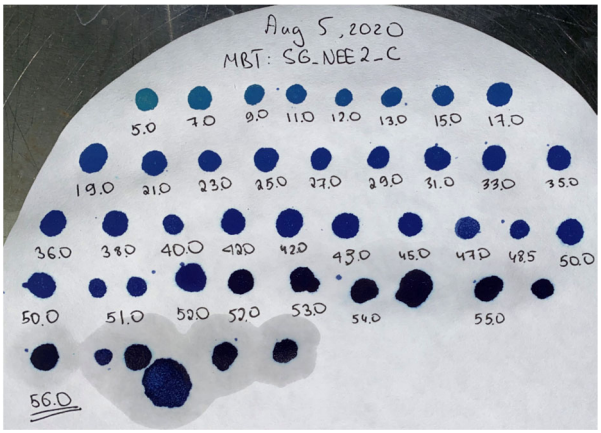

b) MBV of microfines collected after washing

Figure 64. Methylene Blue Value (MBV) of microfines collected from SG_NEE2.

A-4. Results of XRD Analysis

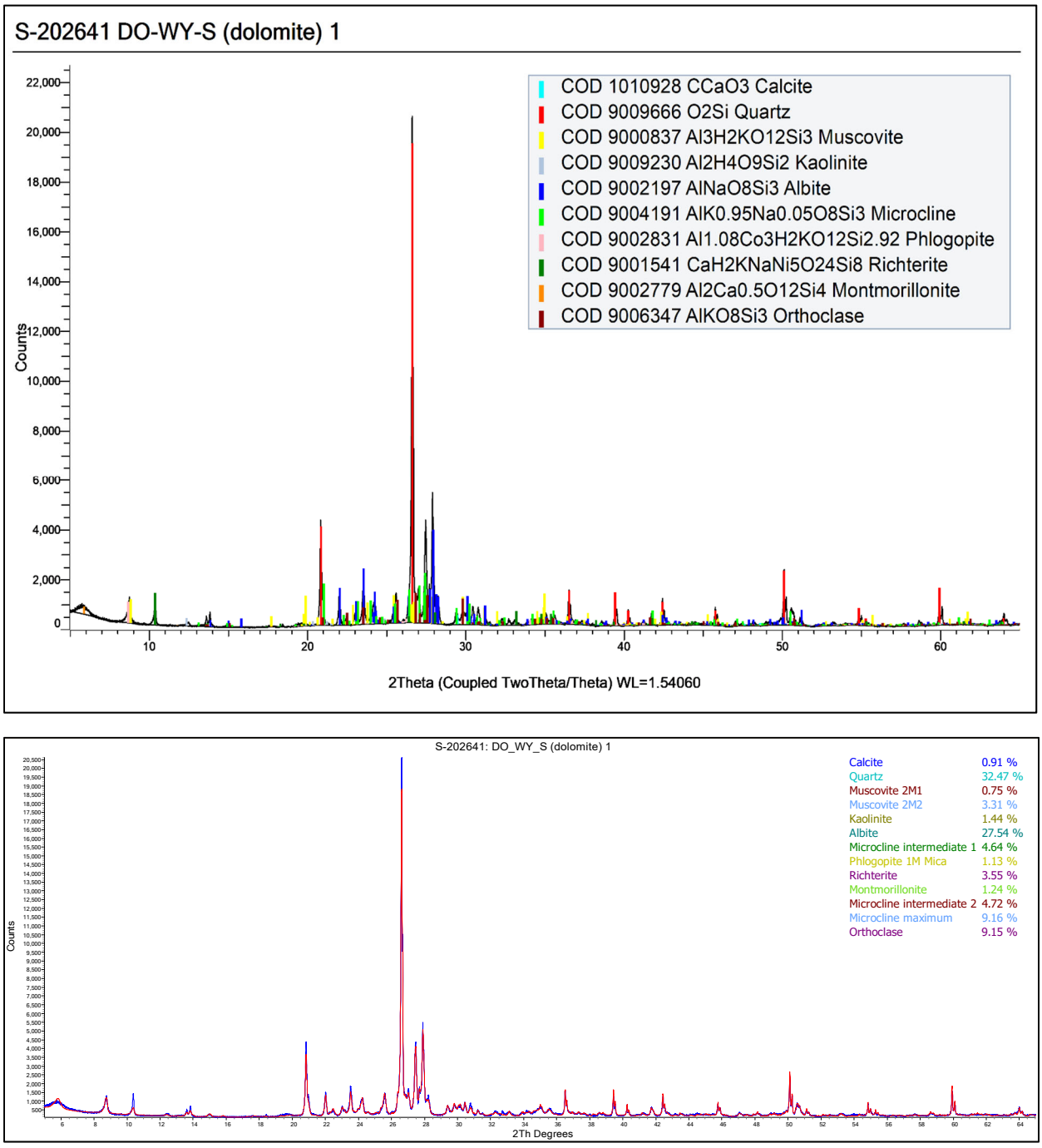

Figure 65. XRD results from DO-WY-S.

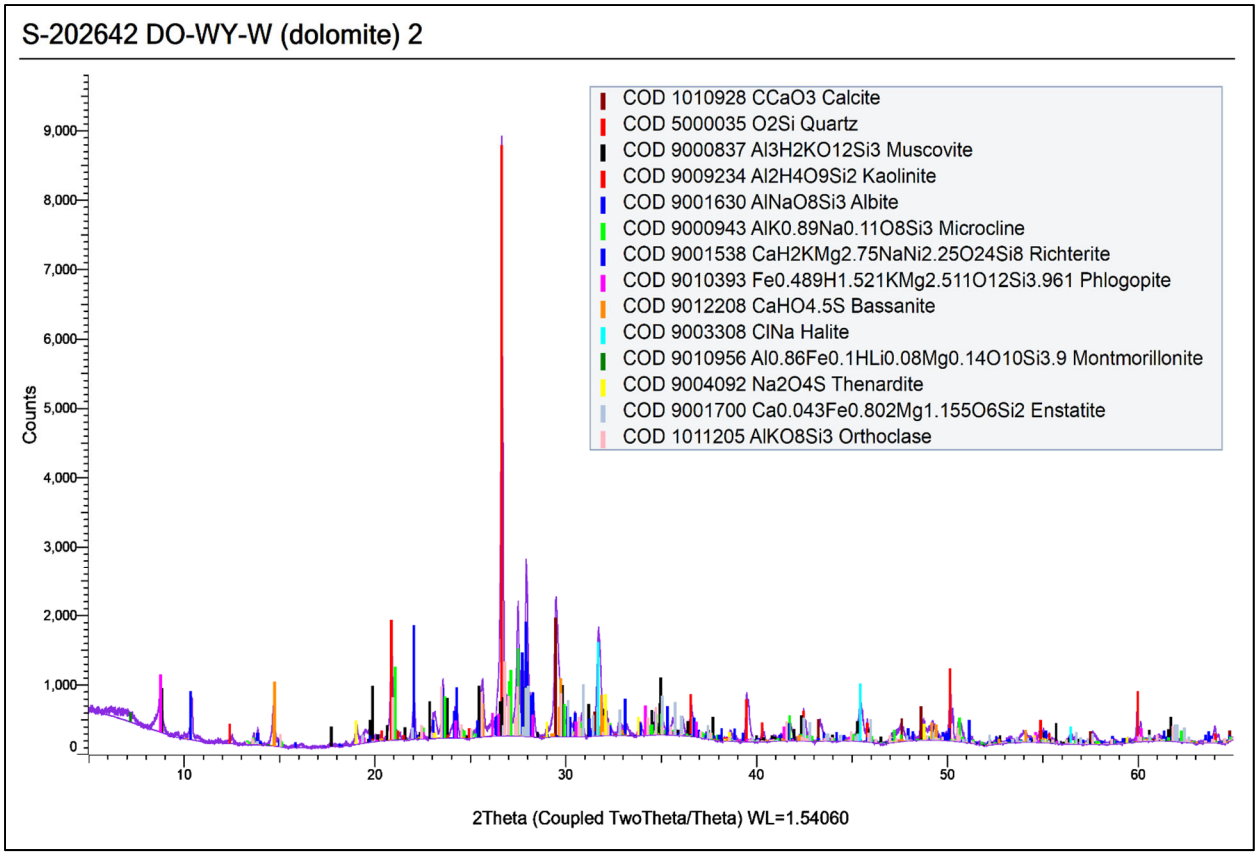

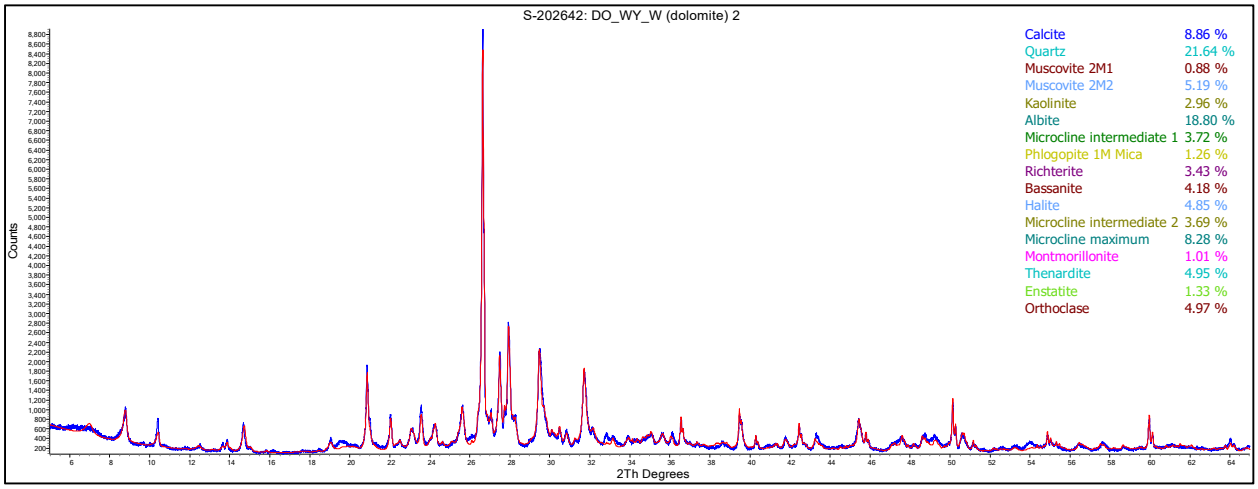

Figure 66. XRD results from DO-WY-W.

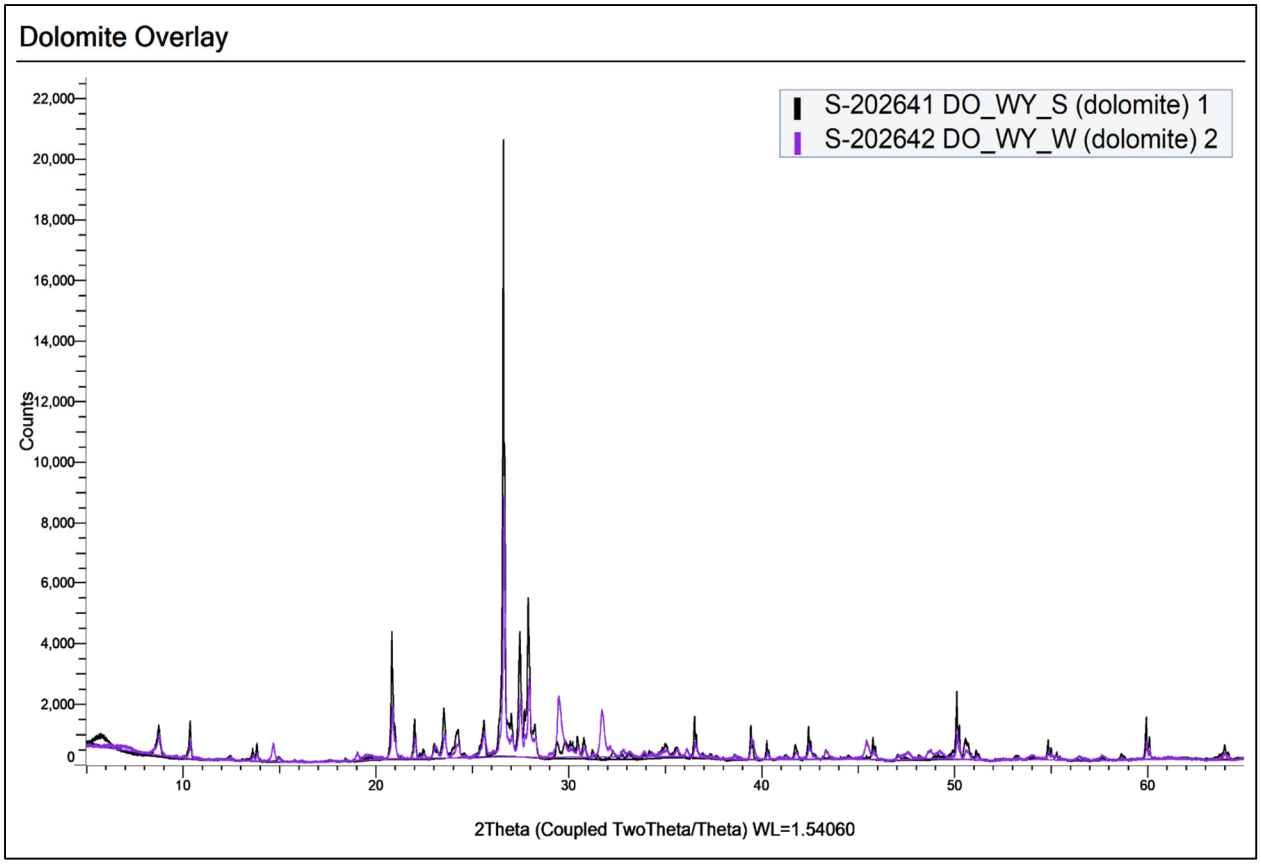

Figure 67. Comparison of XRD results from DO_WY_S and DO-WY_W.

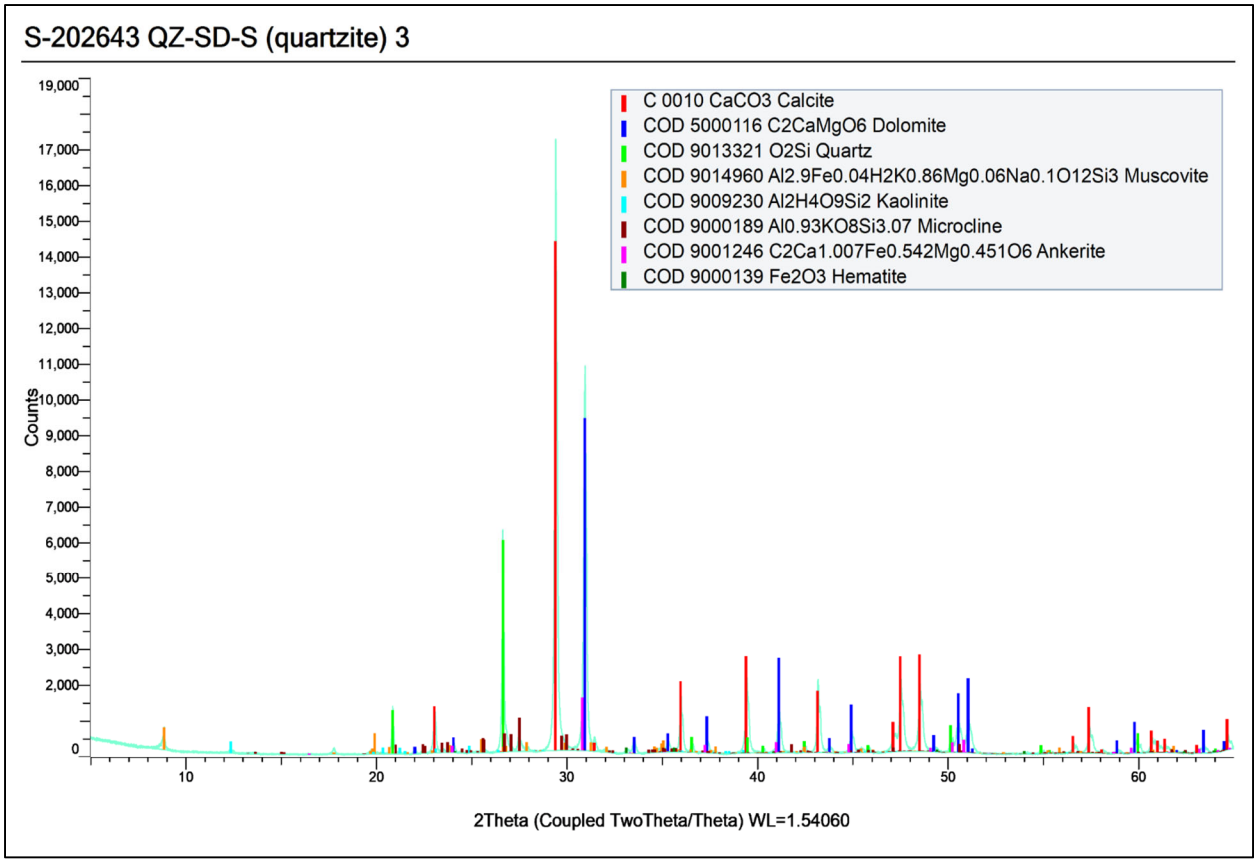

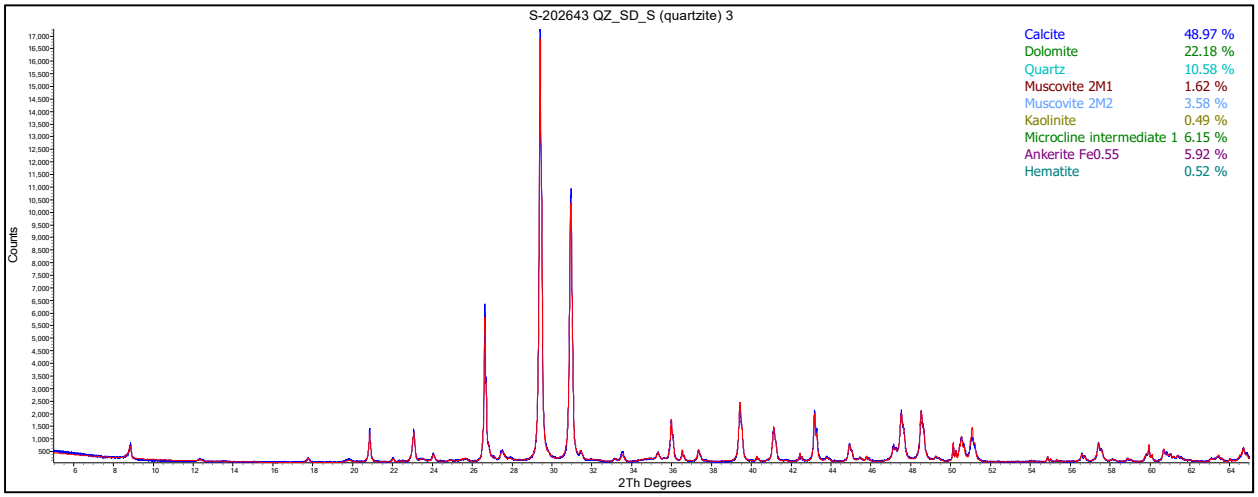

Figure 68. XRD results from QZ_SD_S.

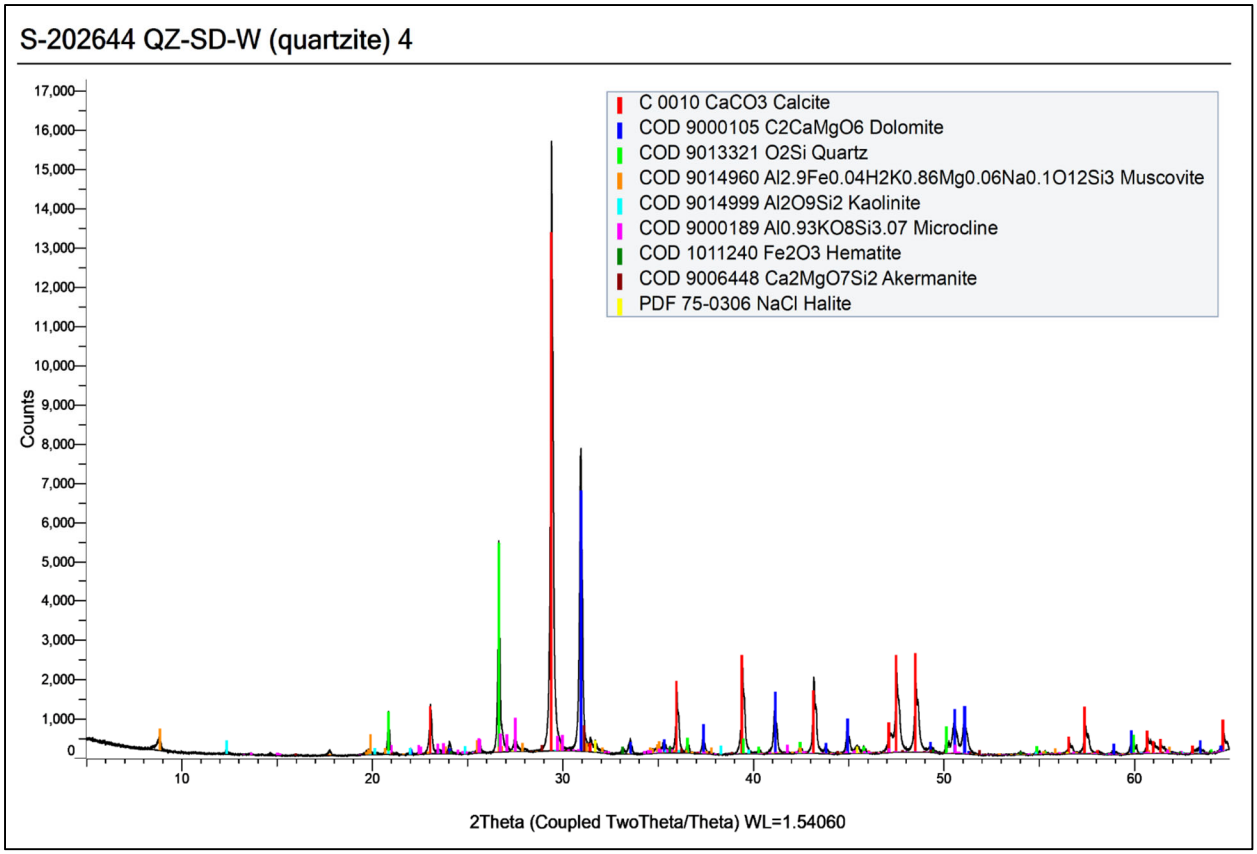

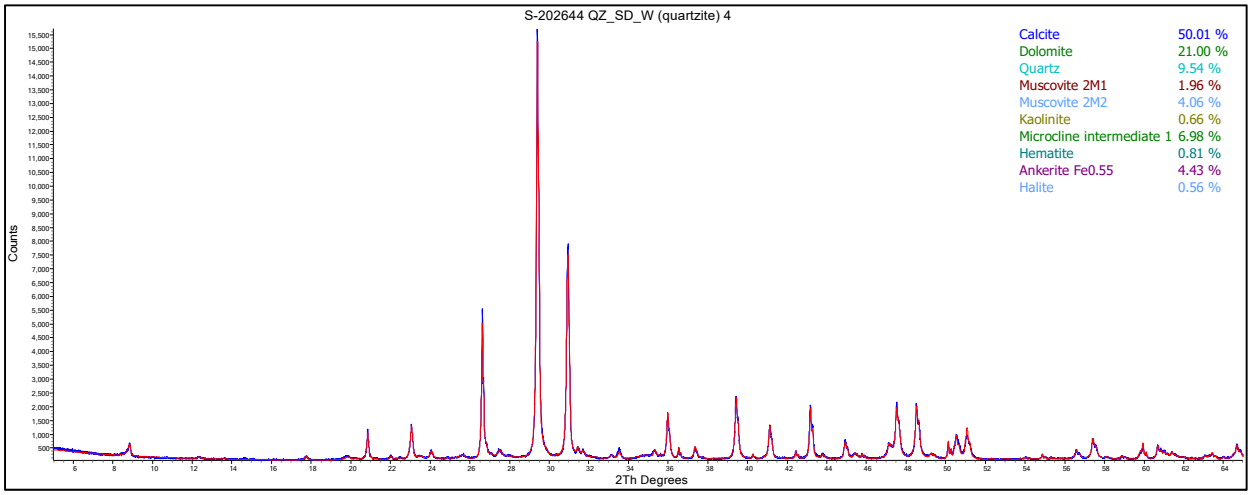

Figure 69. XRD results from QZ_SD_W.

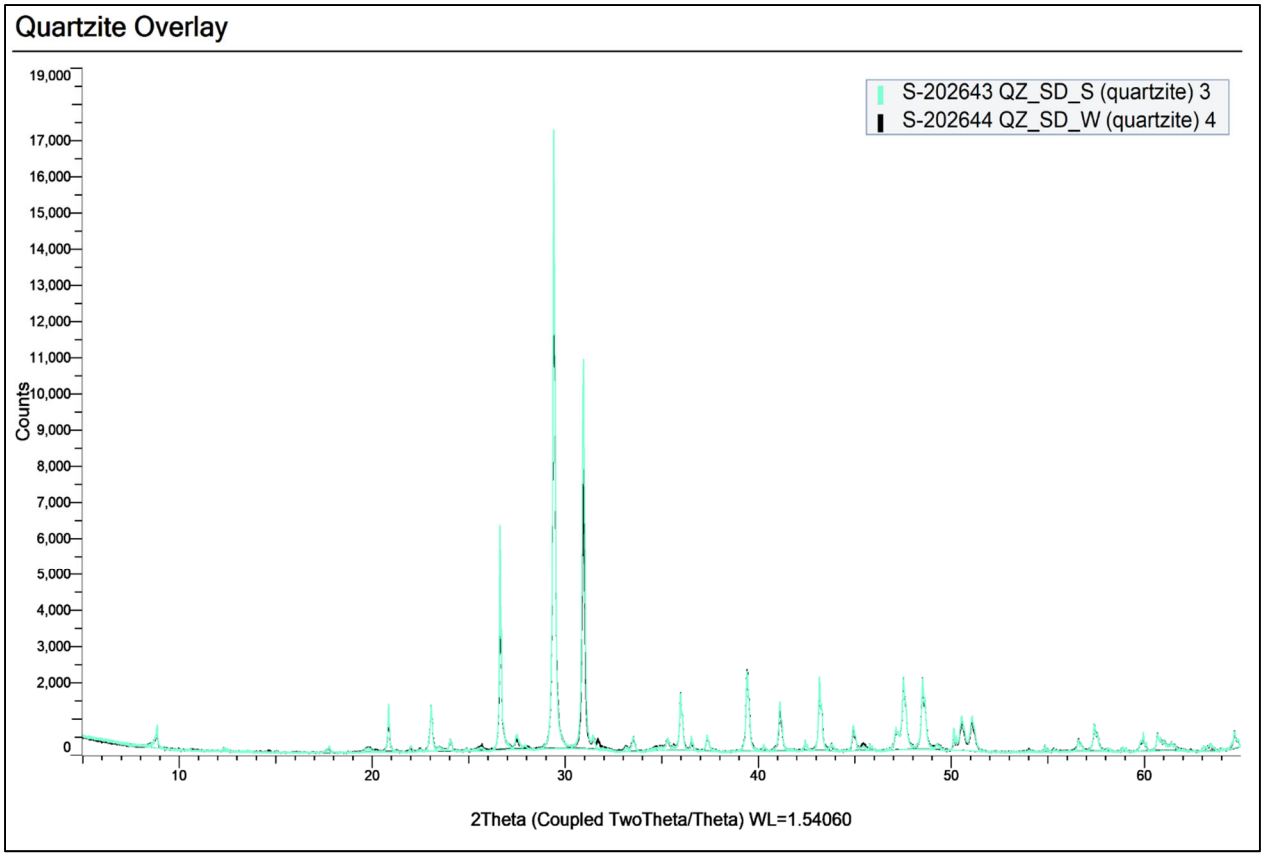

Figure 70. Comparison of results from QZ_SD_S and QZ_SD_W.

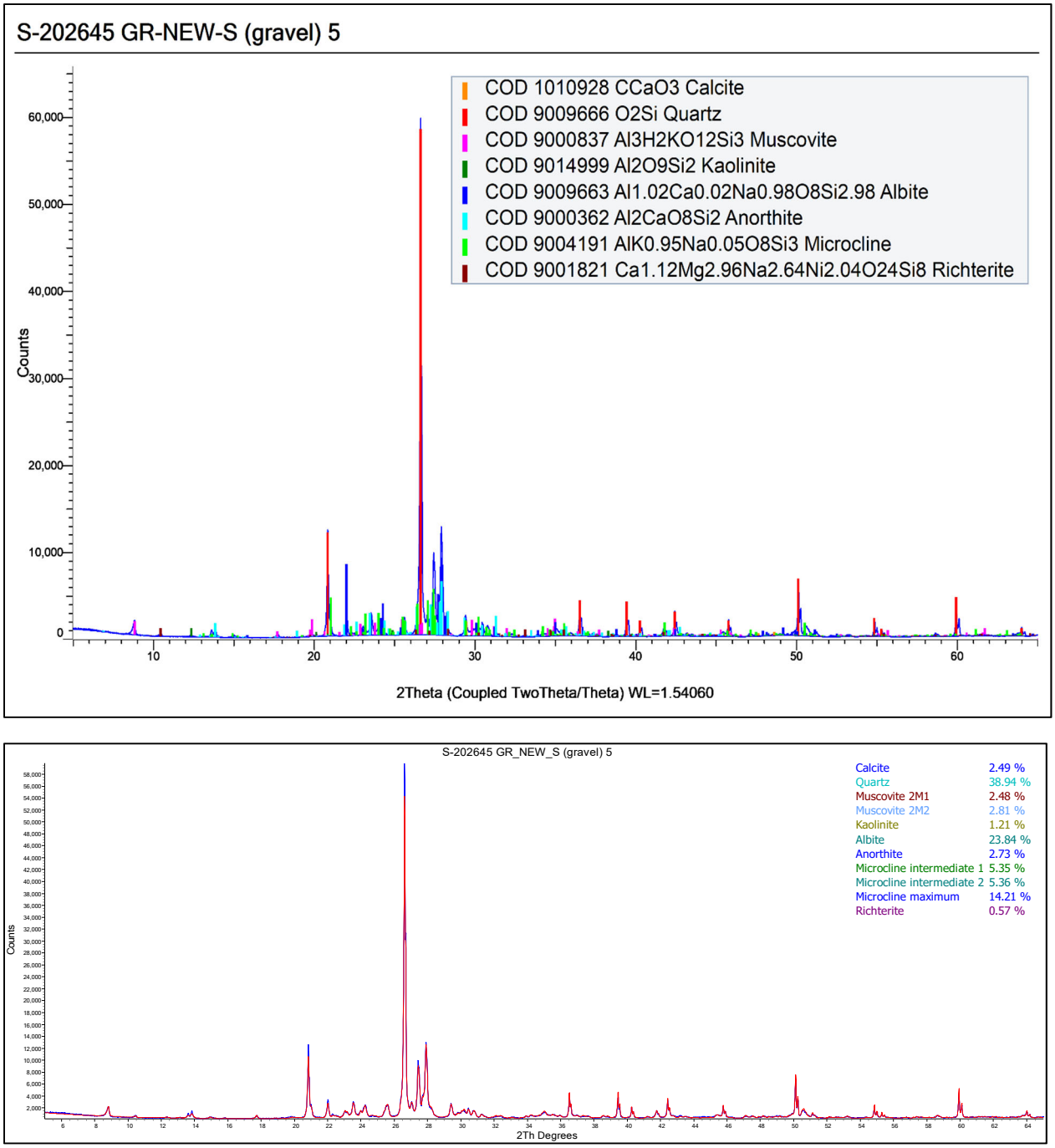

Figure 71. XRD results from GR_NEW_S.

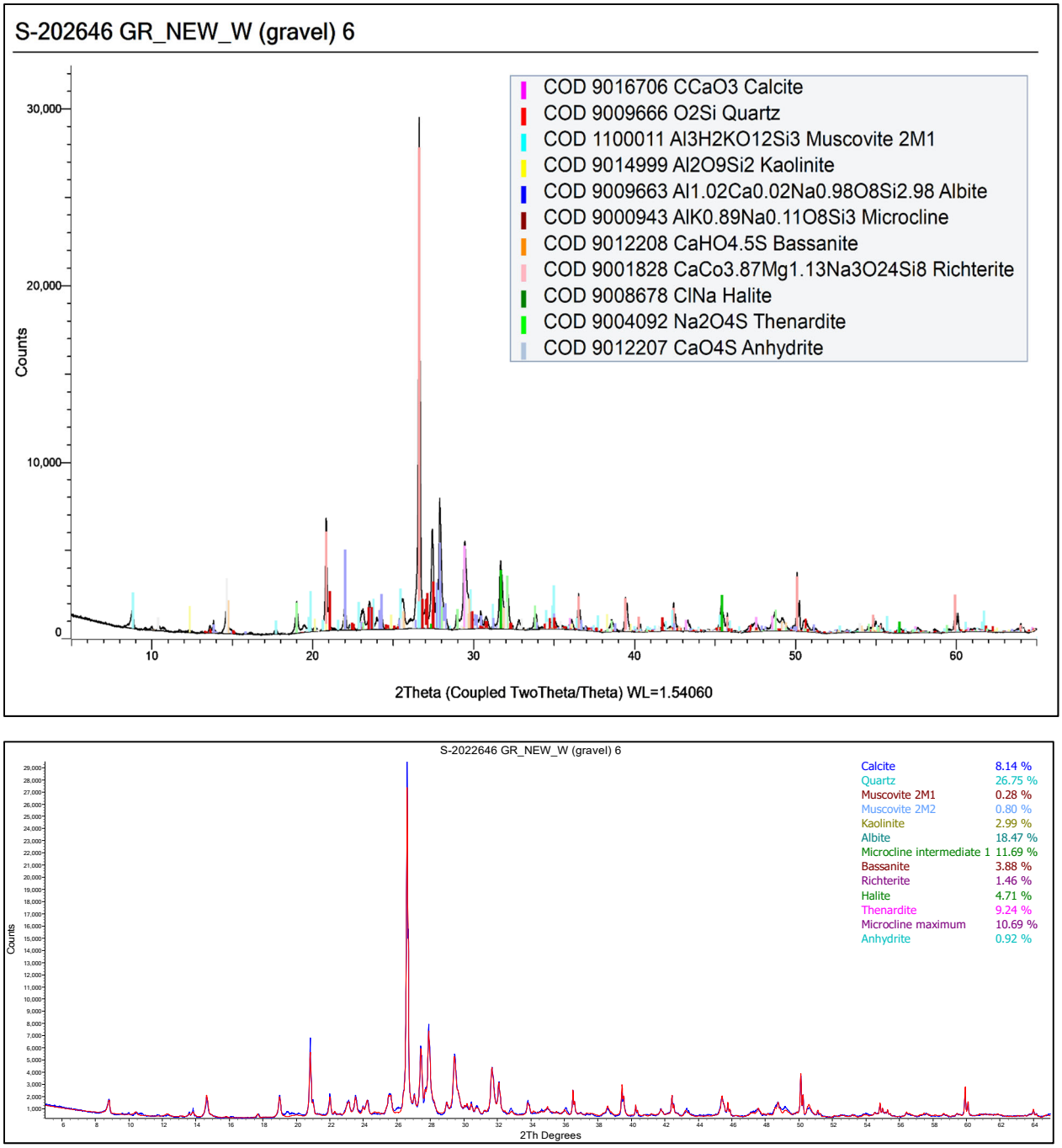

Figure 72. XRD results from GR_NEW_W.

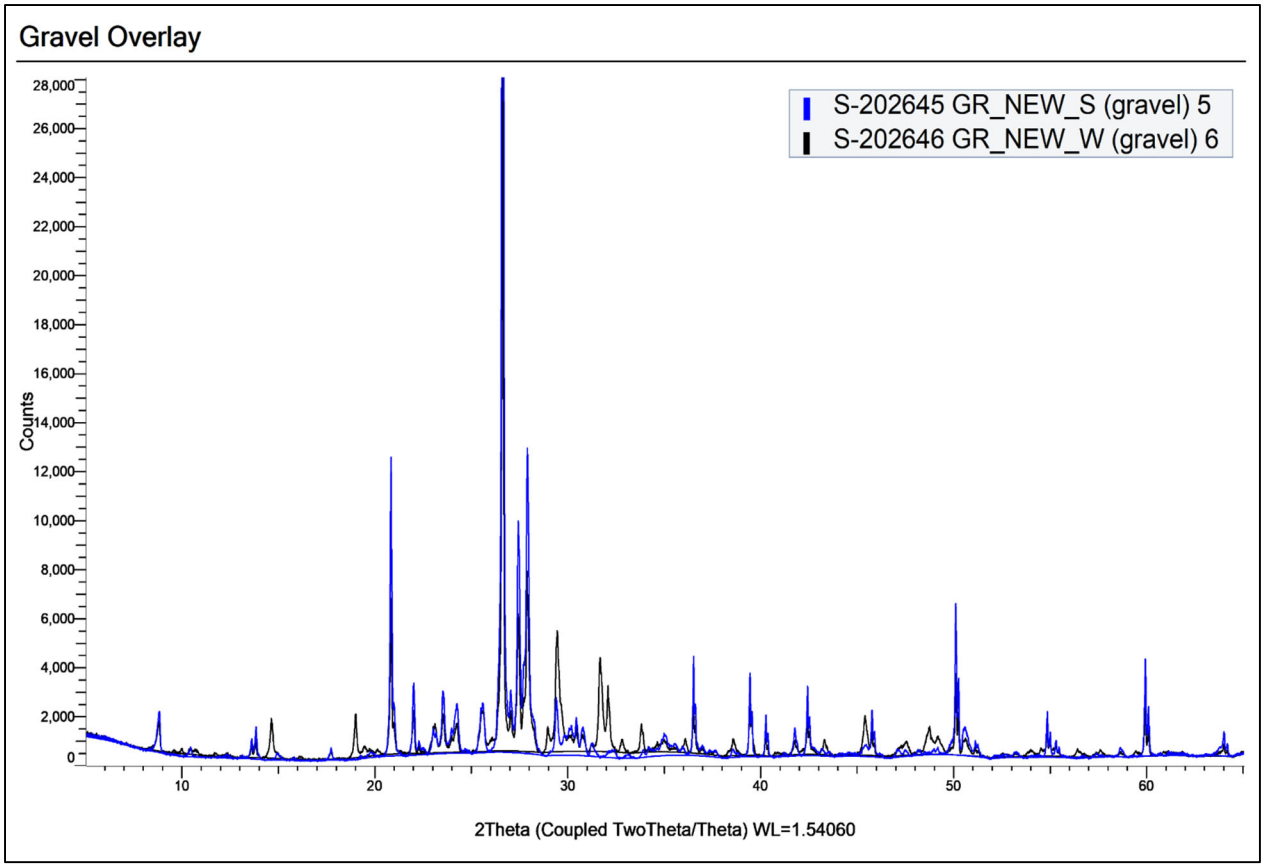

Figure 73. Comparison of XRD results from GR_NEW_S and GR_NEW_W.

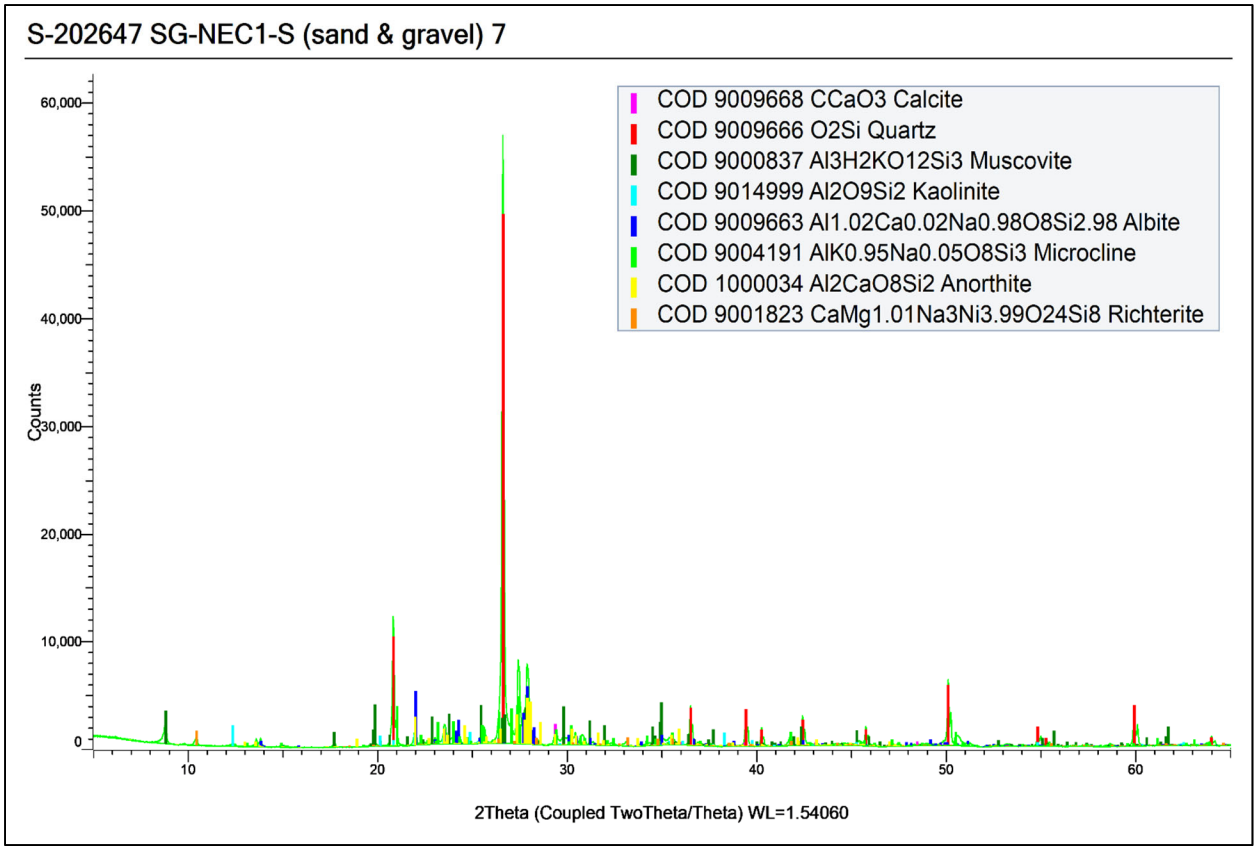

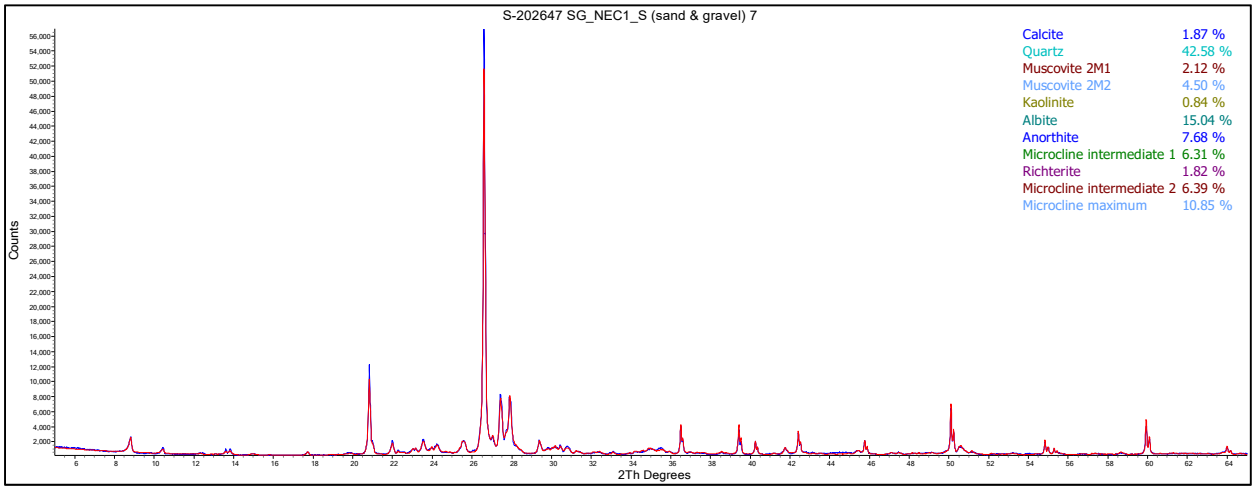

Figure 74. XRD results from SG_NEC1_S.

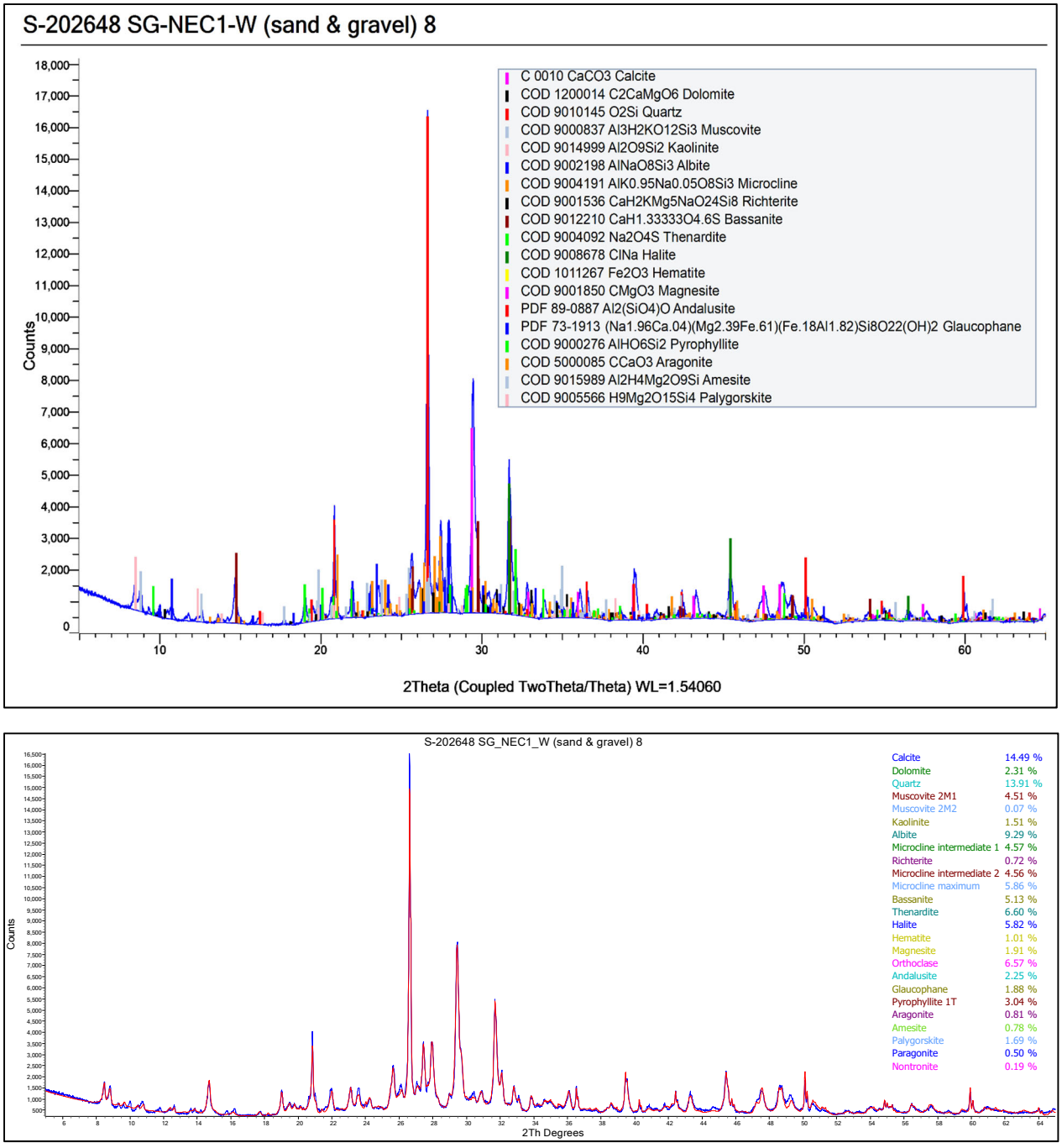

Figure 75. XRD results from SG_NEC1_W.

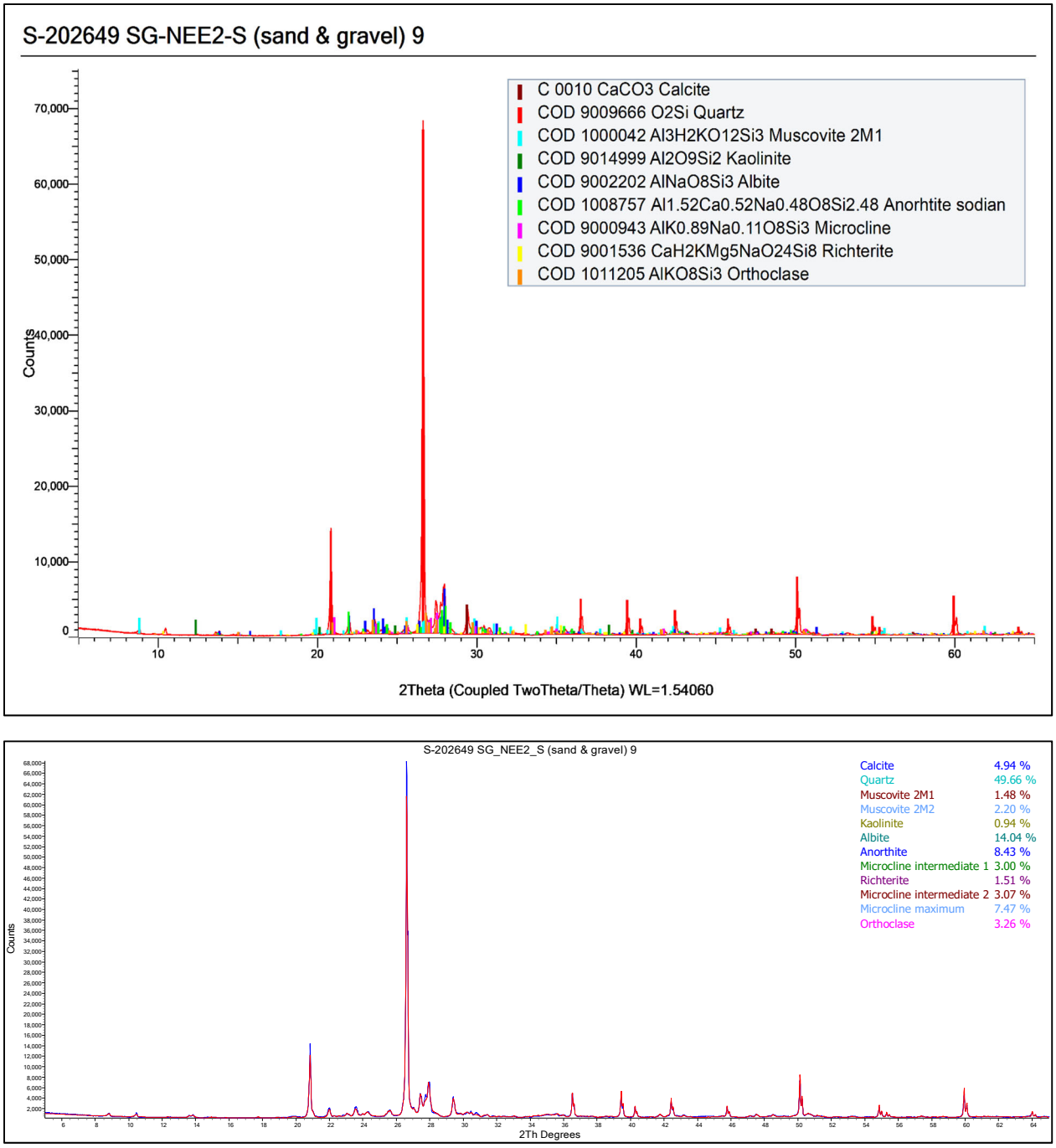

Figure 76. XRD results from SG_NEE2_S.

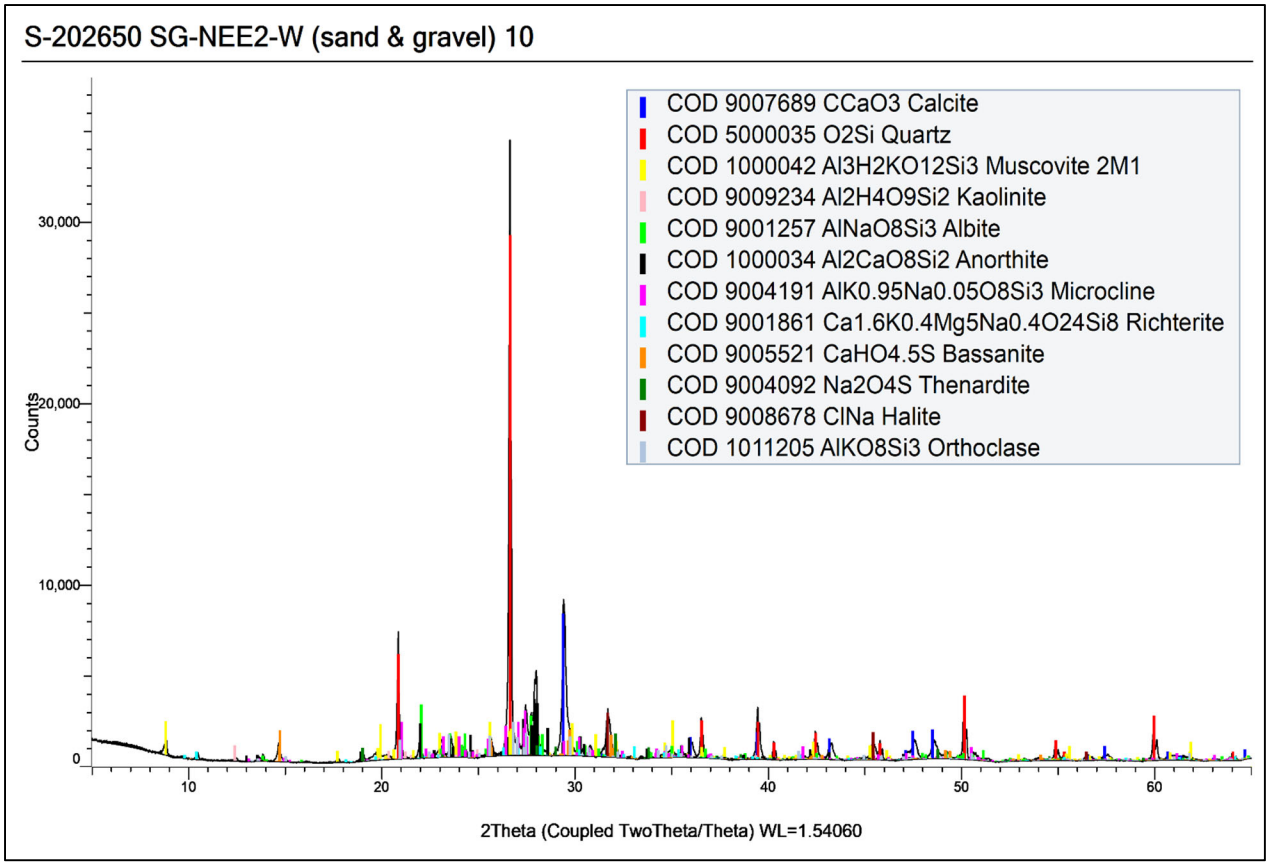

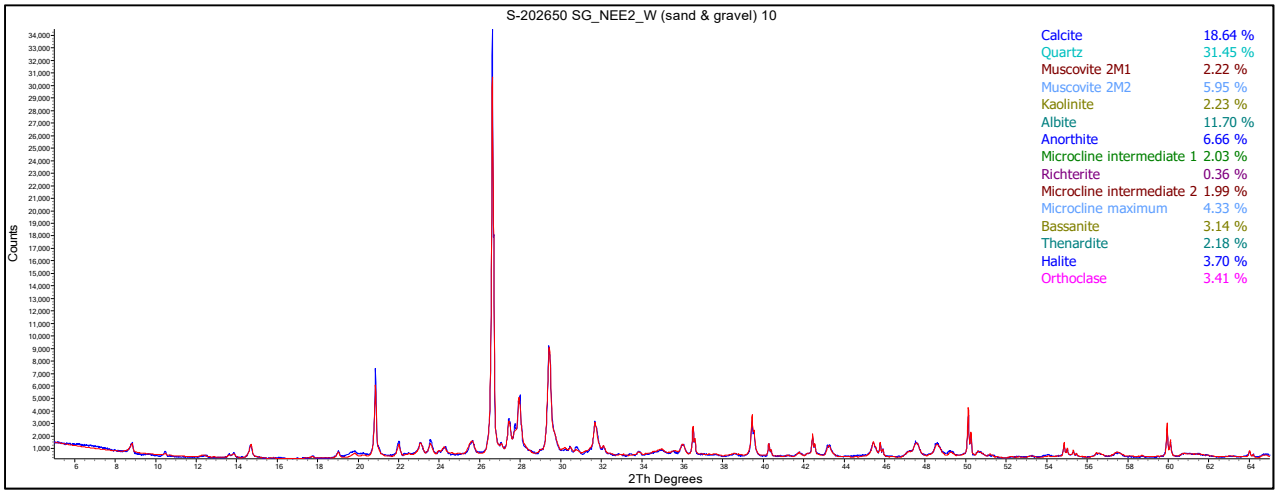

Figure 77. XRD results from SG_NEE2_W.

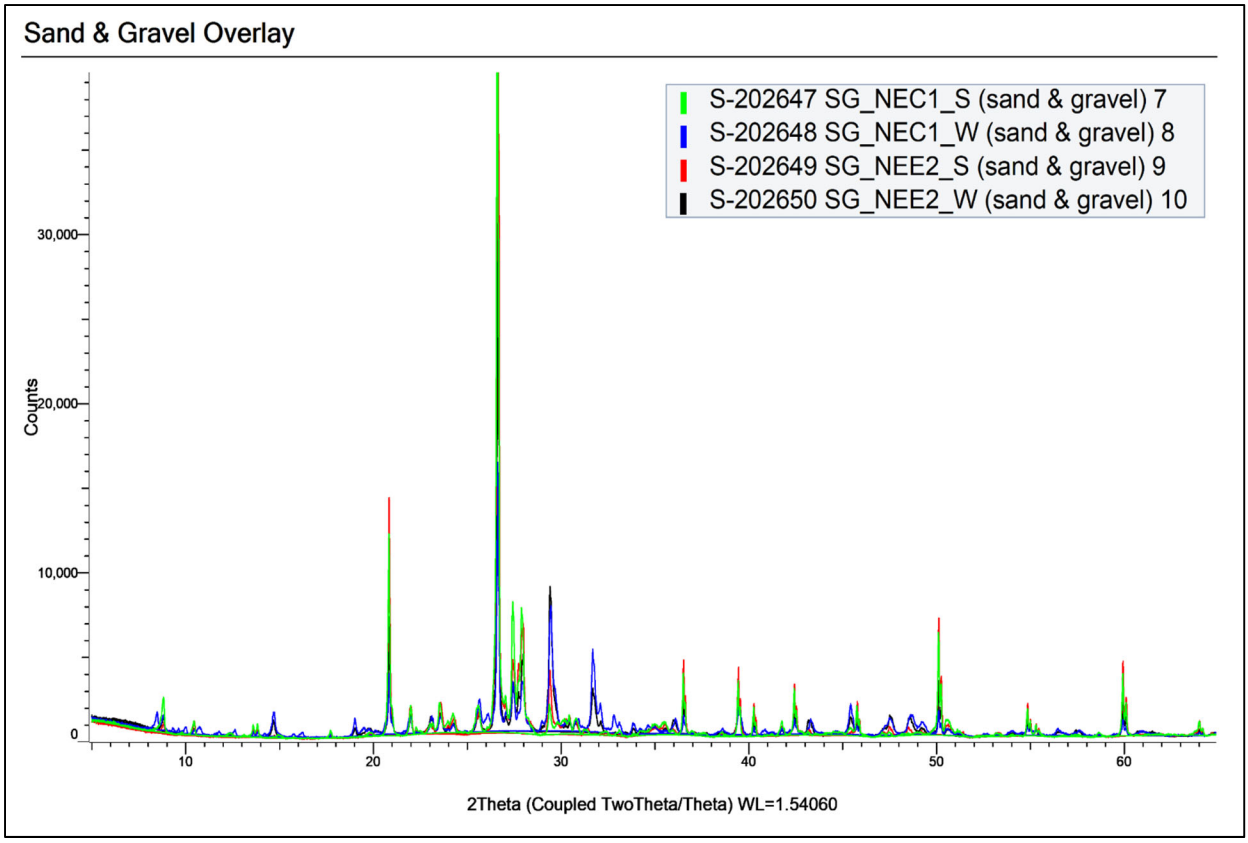

Figure 78. Comparison of XRD results from SG_NEC1_S, SG_NEC1_W, SG_NEE2_S, SG_NEE2_W.

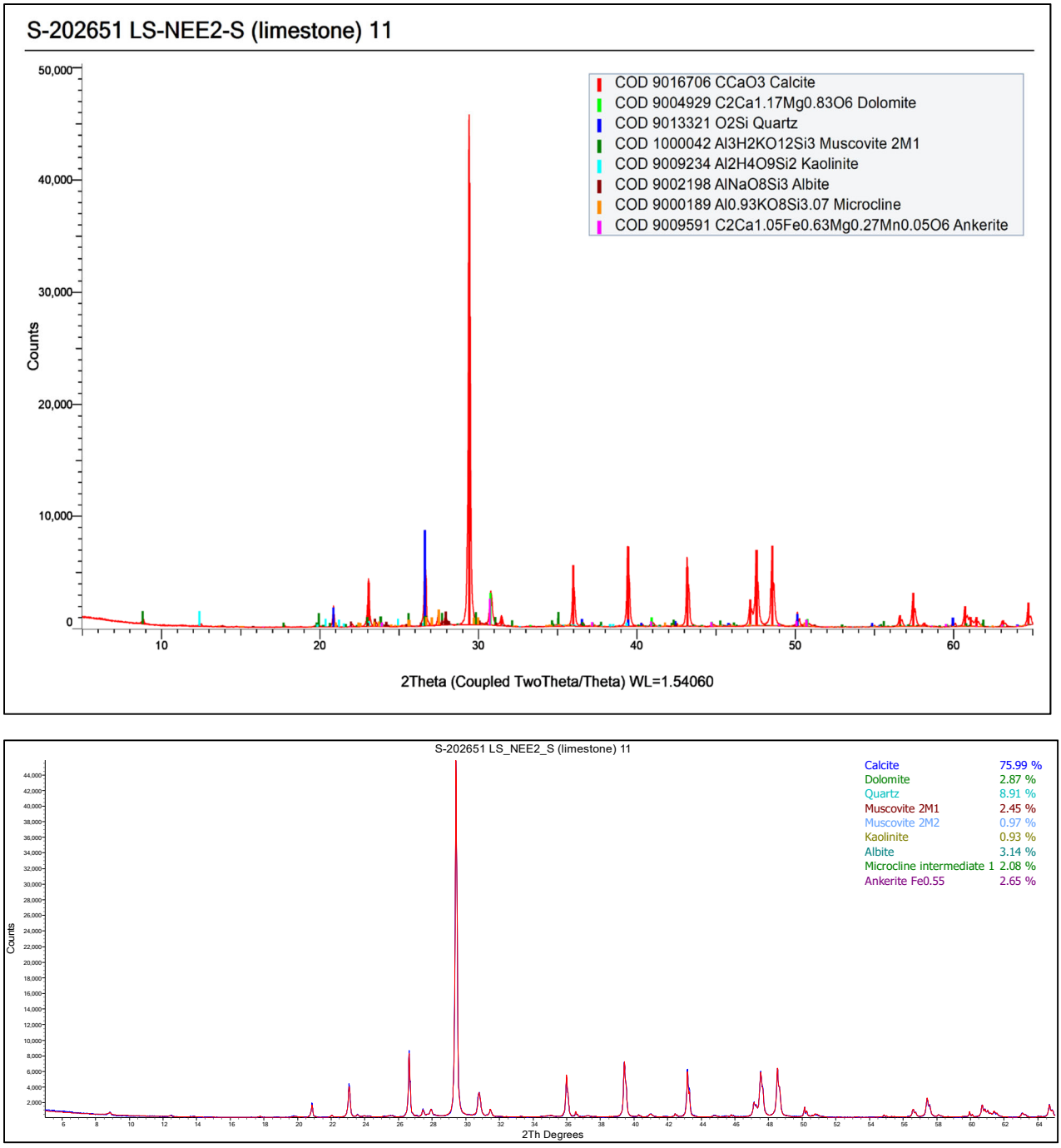

Figure 79. XRD results from LS_NEE2_S.

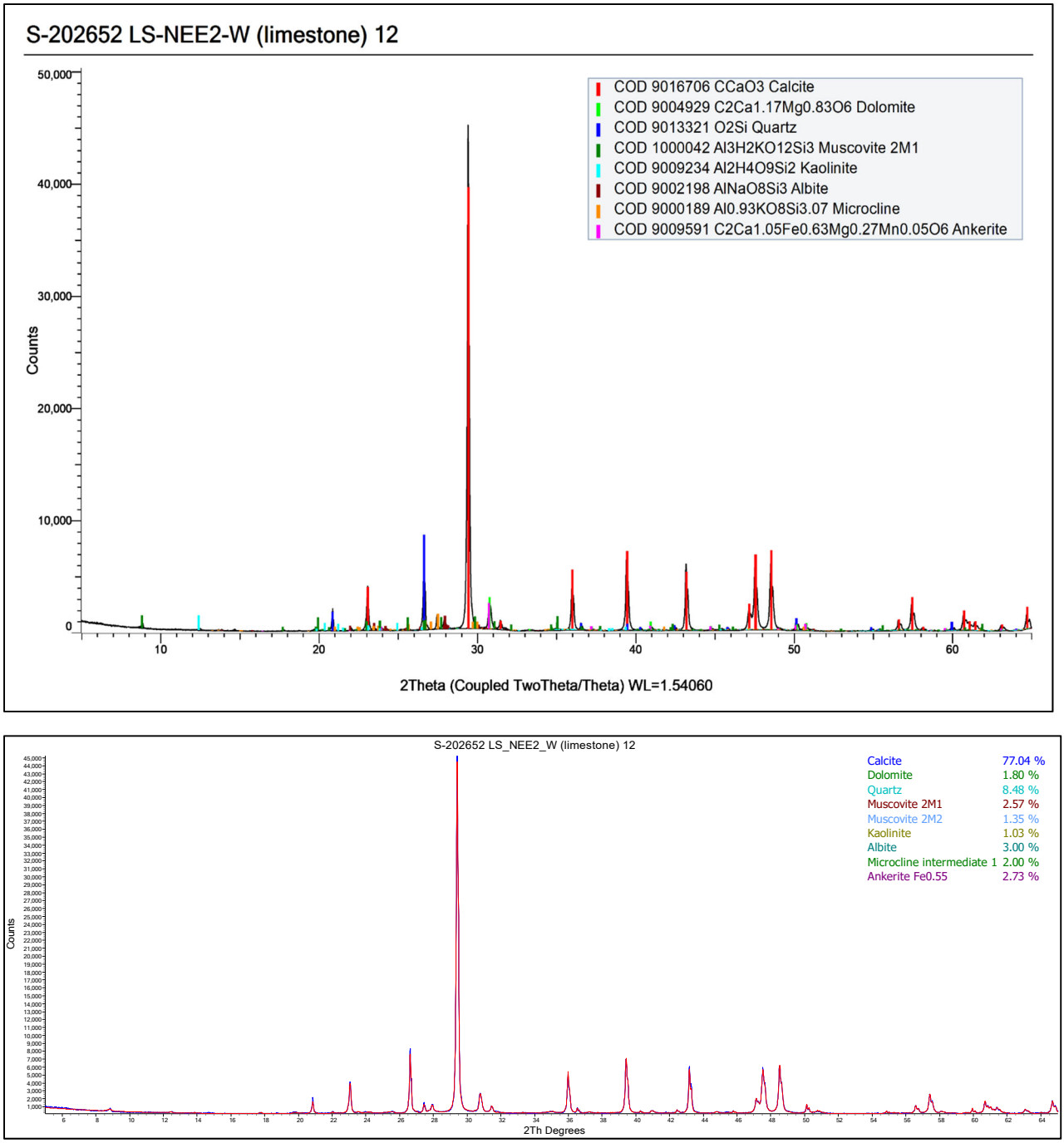

Figure 80. XRD results from LS_NEE2_W.

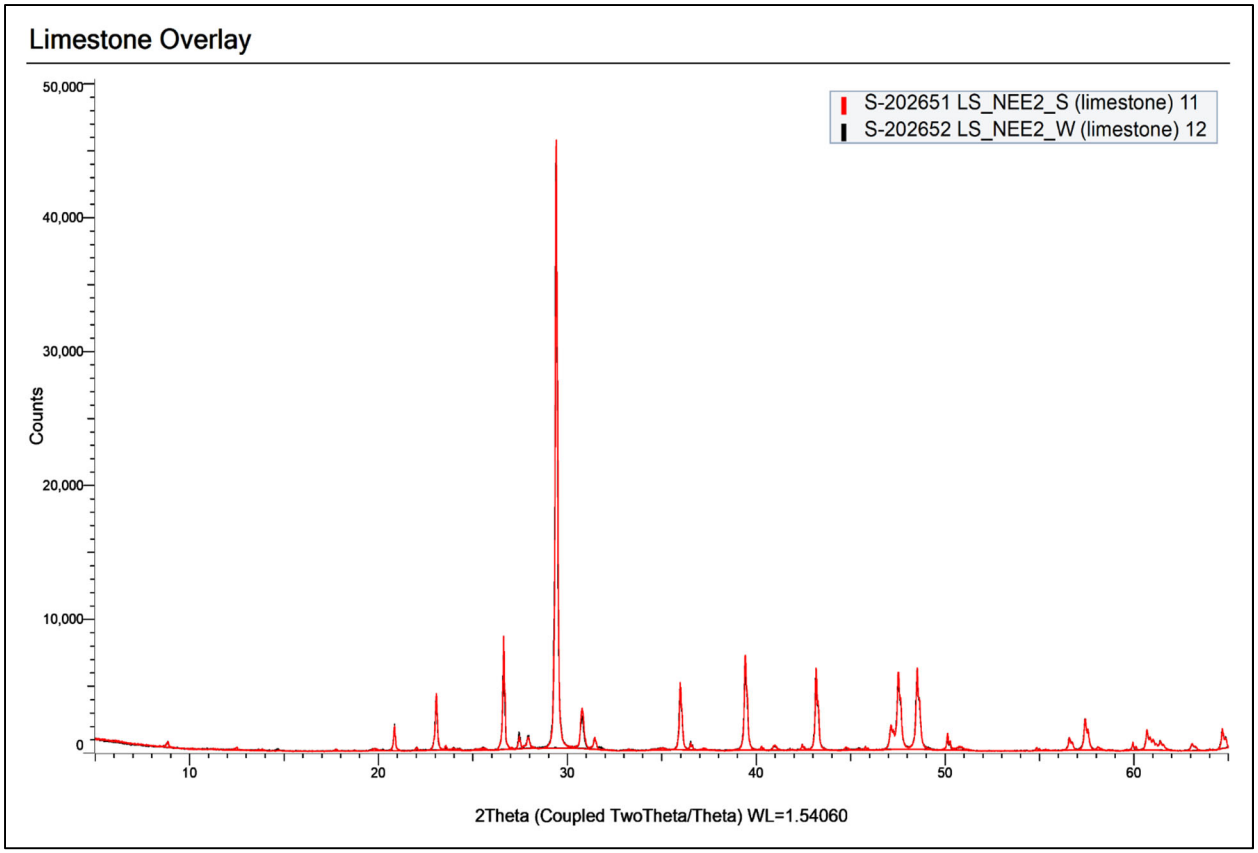

Figure 81. Comparison of XRD results from LS_NEE2_S and LS_NEE2_W.

Table 25. XRD Quant summary.

	S-202641 DO_WY_S (dolomite) 1	S-202642 DO_WY_W (dolomite) 2	S-202643 QZ_SD_S (quartzite) 3	S-202644 QZ_WY_W (quartzite) 4	S-202645 GR_NEW_S (gravel) 5	S-202646 GR_NEW_W (gravel) 6	S-202647 SG_NEC1_S (sand & gravel) 7	S-202648 SG_NEC1_W (sand & gravel) 8	S-202649 SG_NEE2_S (sand & gravel) 9	S-202650 SG_NEE2_W (sand & gravel) 10	S-202651 LS_NEE2_S (limestone) 11	S-202652 LS_NEE2_W (limestone) 12
Quartz	***32.5***	***21.6***	***10.6***	***9.5***	***38.9***	***26.8***	***42.6***	***13.9***	***49.7***	***31.5***	***8.9***	***8.5***
Calcite	0.9	8.9	49.0	50.0	2.5	8.1	1.9	14.5	4.9	18.6	76.0	77.0
Dolomite	0.0	0.0	22.2	21.0	0.0	0.0	0.0	2.3	0.0	0.0	2.9	1.8
Ankerite/Magnesite	0.0	0.0	5.9	4.4	0.0	0.0	0.0	2.7	0.0	0.0	2.7	2.7
Total Carbonates	***0.9***	***8.9***	***77.1***	***75.4***	***2.5***	***8.1***	***1.9***	***19.5***	***4.9***	***18.6***	***81.5***	***81.6***
Albite	27.5	18.8	0.0	0.0	23.8	18.5	15.0	9.3	14.0	11.7	3.1	3.0
Anorthite	0.0	0.0	0.0	0.0	2.7	0.0	7.7	0.0	8.4	6.7	0.0	0.0
Microcline	18.5	15.7	6.2	7.0	24.9	22.4	23.6	15.0	13.5	8.4	2.1	2.0
Orthoclase	9.2	5.0	0.0	0.0	0.0	0.0	0.0	6.6	3.3	3.4	0.0	0.0
Total Feldspars	***55.2***	***39.5***	***6.2***	***7.0***	***51.5***	***40.9***	***46.3***	***30.9***	***39.3***	***30.1***	***5.2***	***5.0***
Muscovite	4.1	6.1	5.2	6.0	5.3	1.1	6.6	4.6	3.7	8.2	3.4	3.9
Phlogopite	1.1	1.3	0.0	0.0	0.0	0.0	0.0	0.0	0.0	0.0	0.0	0.0
Paragonite	0.0	0.0	0.0	0.0	0.0	0.0	0.0	0.5	0.0	0.0	0.0	0.0
Total Micas	***5.2***	***7.3***	***5.2***	***6.0***	***5.3***	***1.1***	***6.6***	***5.1***	***3.7***	***8.2***	***3.4***	***3.9***
Kaolinite	1.4	3.0	0.5	0.7	1.2	3.0	0.8	1.5	0.9	2.2	0.9	1.0
Montmorillonite	1.2	1.0	0.0	0.0	0.0	0.0	0.0	0.2	0.0	0.0	0.0	0.0
Other Clays	0.0	0.0	0.0	0.0	0.0	0.0	0.0	5.5	0.0	0.0	0.0	0.0
Total Clays	***2.7***	***4.0***	***0.5***	***0.7***	***1.2***	***3.0***	***0.8***	***7.2***	***0.9***	***2.2***	***0.9***	***1.0***
Bassanite	0.0	4.2	0.0	0.0	0.0	4.8	0.0	5.1	0.0	3.1	0.0	0.0
Halite	0.0	4.9	0.0	0.6	0.0	4.7	0.0	5.8	0.0	3.7	0.0	0.0
Thenardite	0.0	5.0	0.0	0.0	0.0	9.2	0.0	6.6	0.0	2.2	0.0	0.0
Total Sulfates, Salts, & Sulfate Salts	***0.0***	***14.0***	***0.0***	***0.6***	***0.0***	***18.8***	***0.0***	***17.6***	***0.0***	***9.0***	***0.0***	***0.0***
Total Other *	***3.6***	***4.8***	***0.5***	***0.8***	***0.6***	***1.5***	***1.8***	***5.9***	***1.5***	***0.4***	***0.0***	***0.0***

* total other includes various pyroxenes, amphiboles, other silicates

A-5. Results of SEM and EDS Analysis

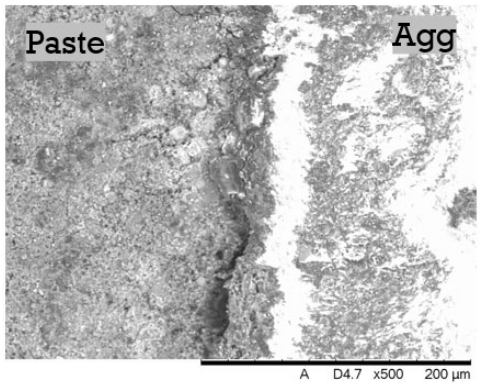

a) SEM image - location 1

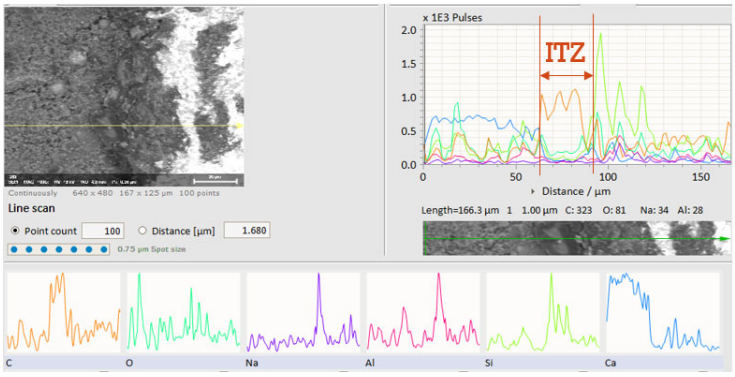

b) EDS line scan – location 1

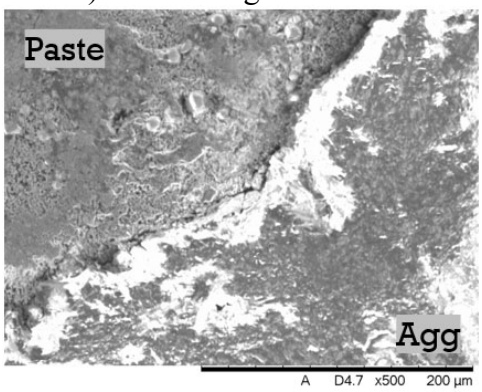

c) SEM image - location 2

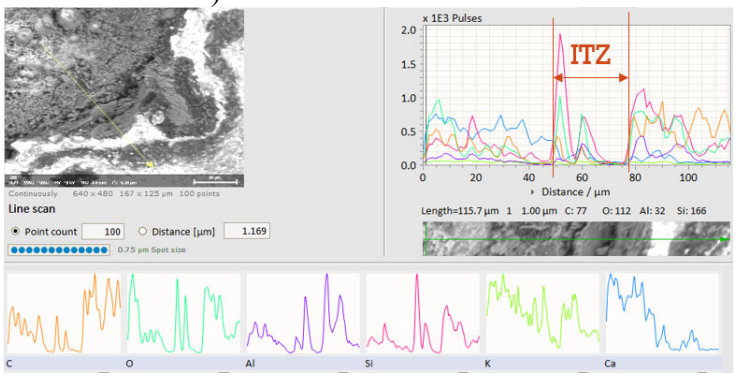

d) EDS line scan – location 2

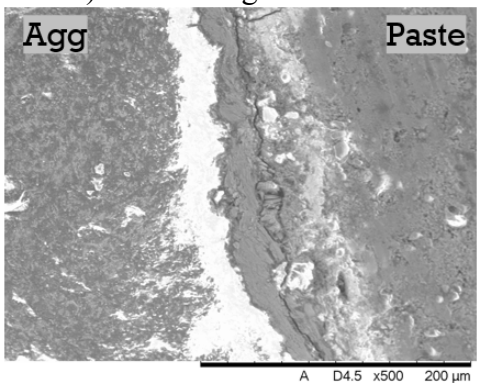

e) SEM image - location 3

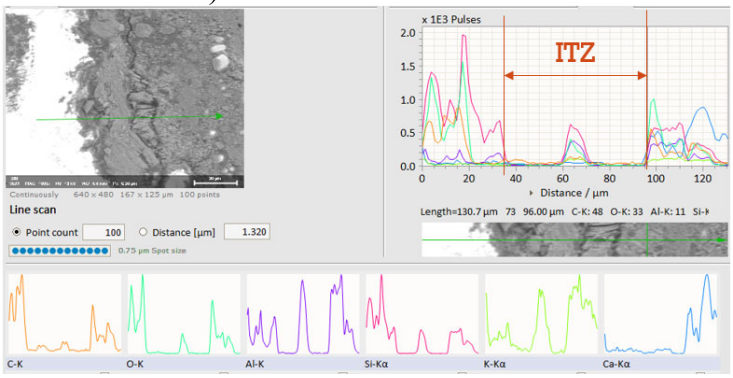

f) EDS line scan – location 3

Figure 82. SEM and EDS analysis of DO_WY_A (as received).

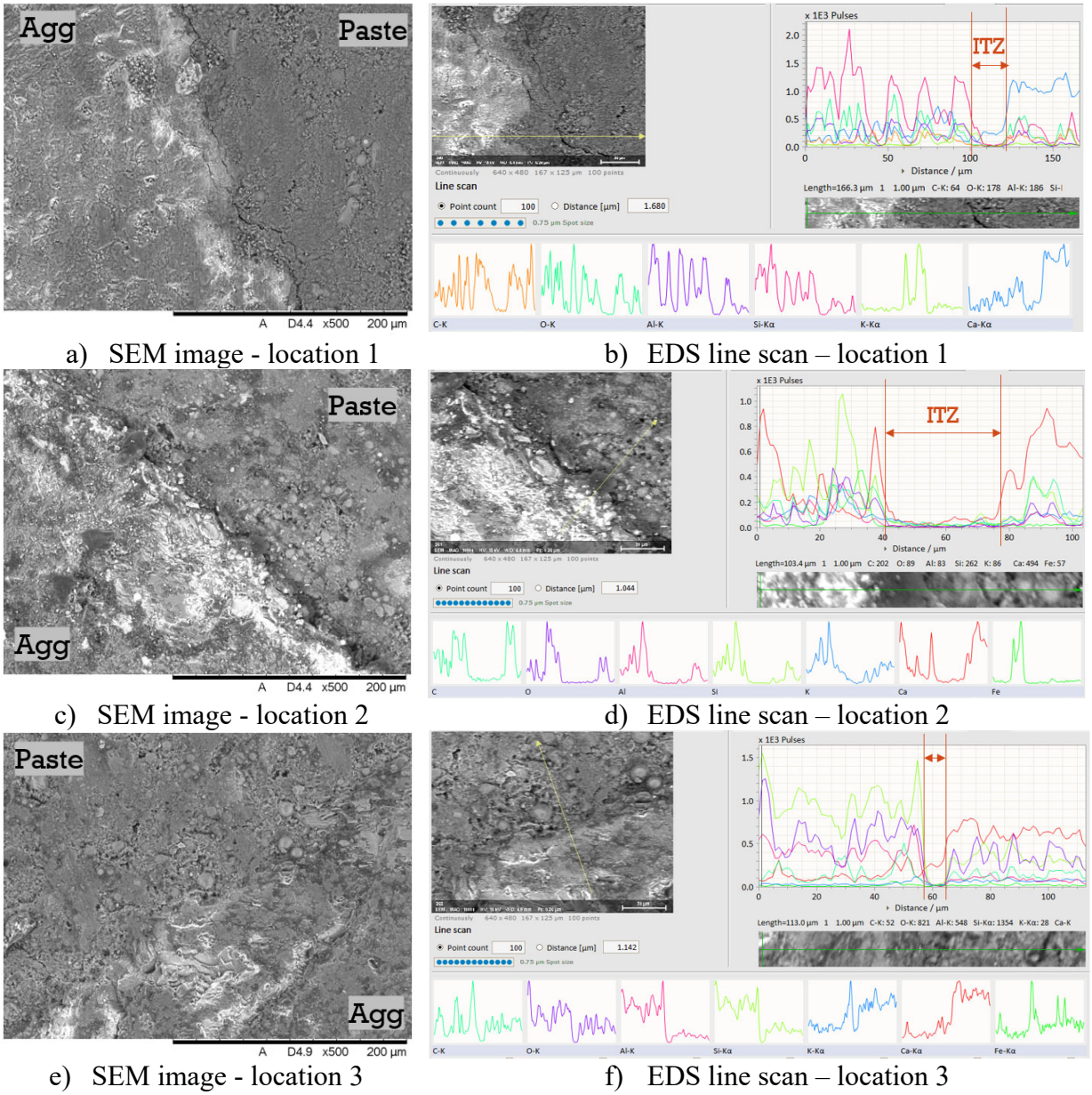

a) SEM image - location 1 b) EDS line scan – location 1

c) SEM image - location 2 d) EDS line scan – location 2

e) SEM image - location 3 f) EDS line scan – location 3

Figure 83. SEM and EDS analysis of DO_WY_C (washed).

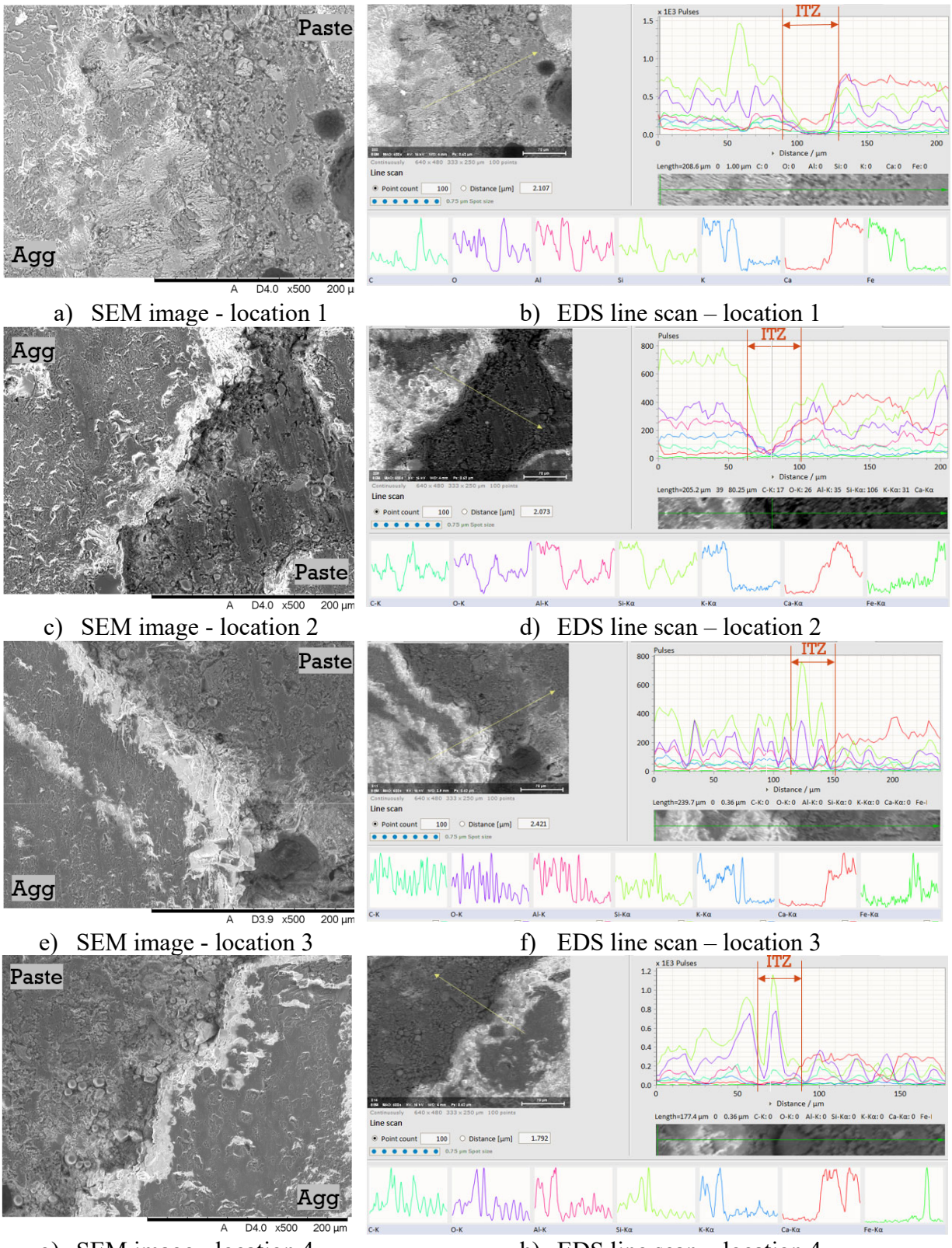

a) SEM image - location 1 b) EDS line scan – location 1

c) SEM image - location 2 d) EDS line scan – location 2

e) SEM image - location 3 f) EDS line scan – location 3

g) SEM image - location 4 h) EDS line scan – location 4

Figure 84. SEM and EDS analysis of DOWY.

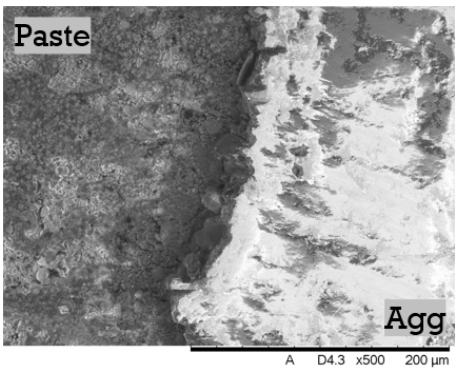

a) SEM image - location 1

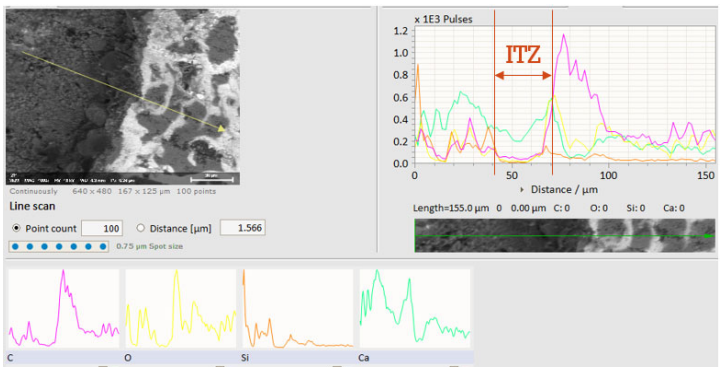

b) EDS line scan – location 1

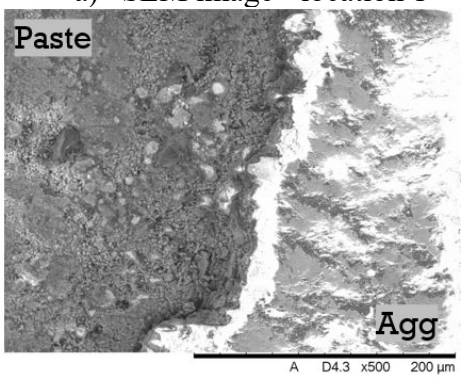

c) SEM image - location 2

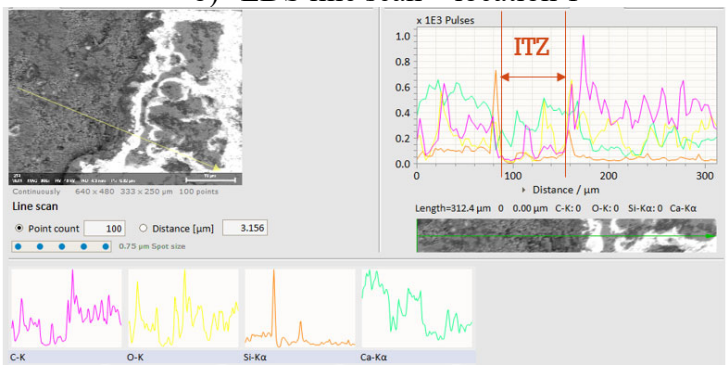

d) EDS line scan – location 2

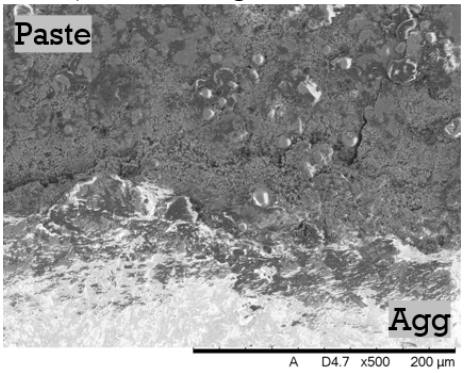

e) SEM image - location 3

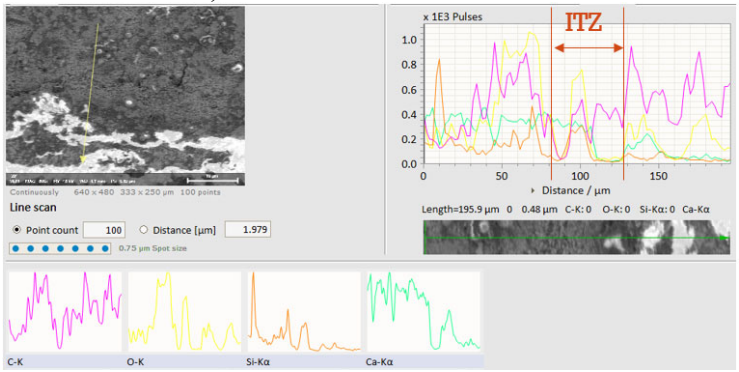

f) EDS line scan – location 3

Figure 85. SEM and EDS analysis of QZ_SD_A (as received).

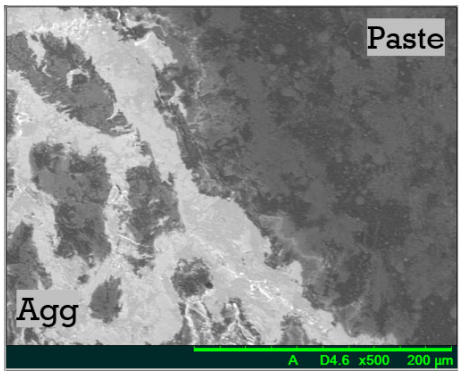

a) SEM image - location 1

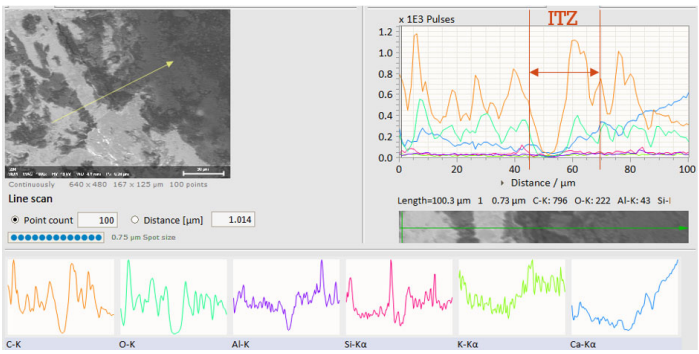

b) EDS line scan – location 1

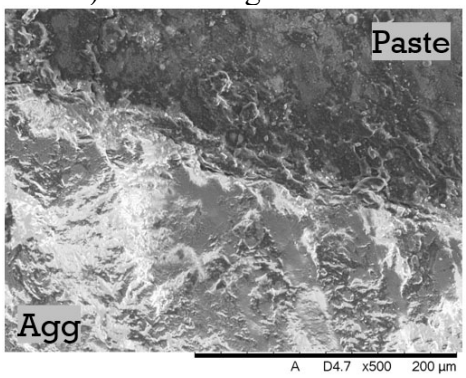

c) SEM image - location 2

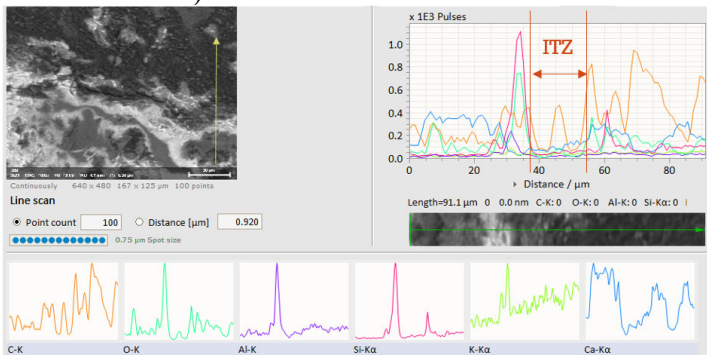

d) EDS line scan – location 2

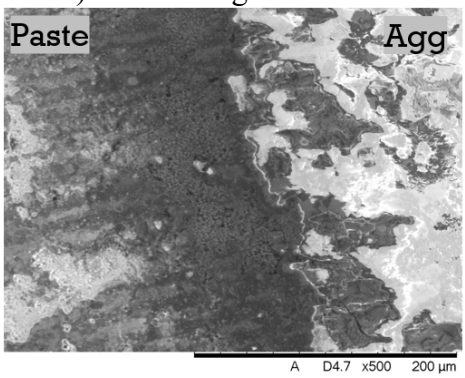

e) SEM image - location 3

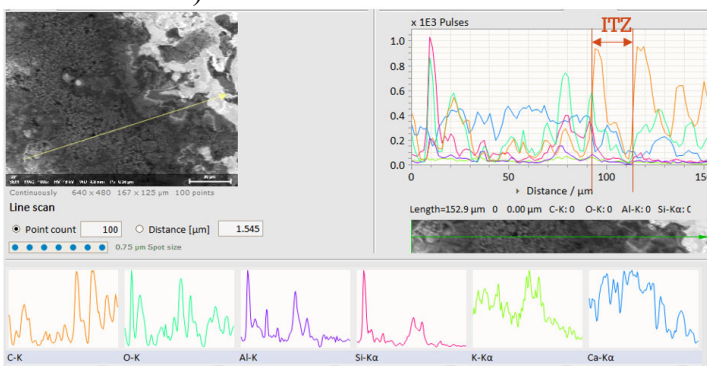

f) EDS line scan – location 3

Figure 86. SEM and EDS analysis of QZ_SD_C (washed).

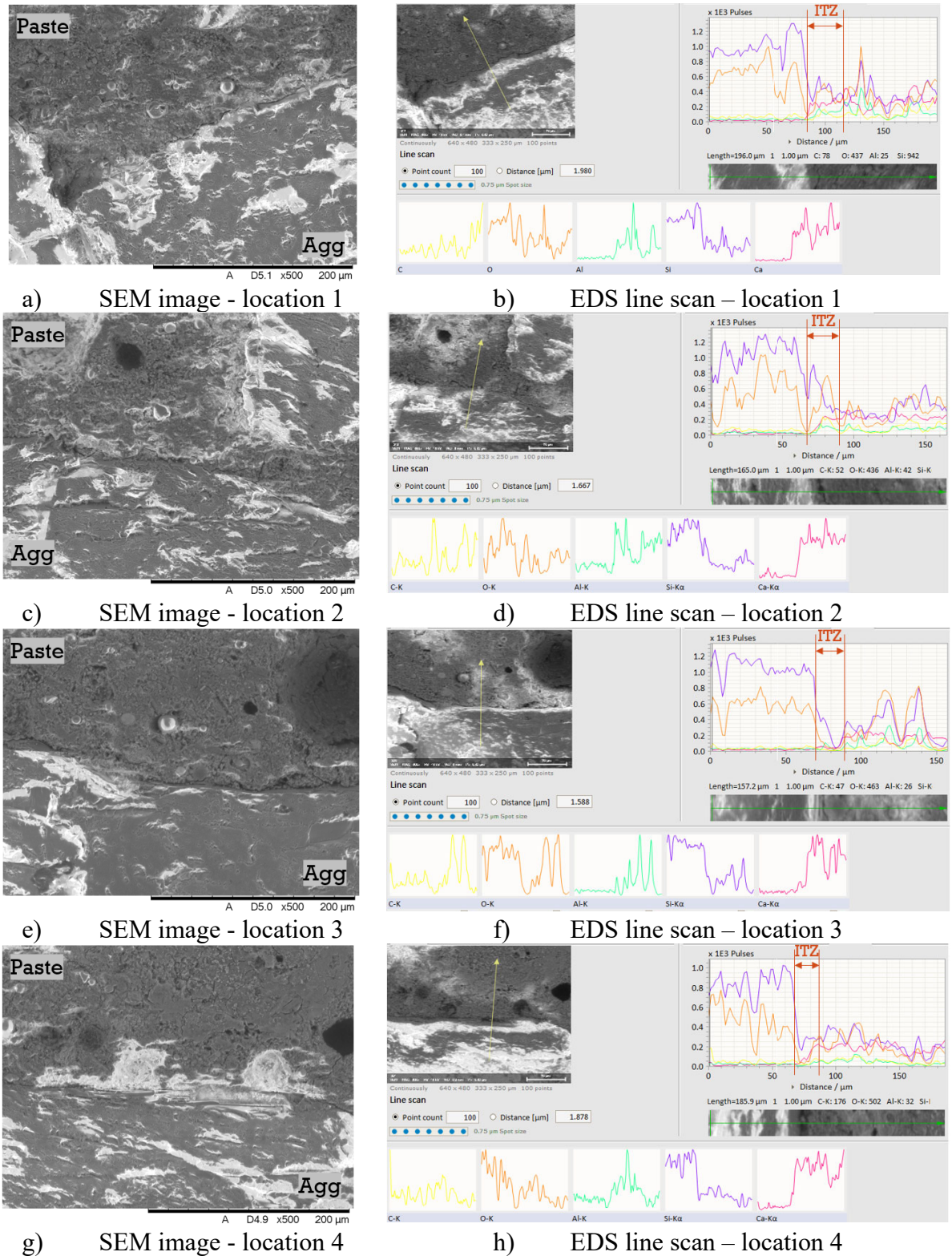

a) SEM image - location 1 b) EDS line scan – location 1

c) SEM image - location 2 d) EDS line scan – location 2

e) SEM image - location 3 f) EDS line scan – location 3

g) SEM image - location 4 h) EDS line scan – location 4

Figure 87. SEM and EDS analysis of QZ_SD.

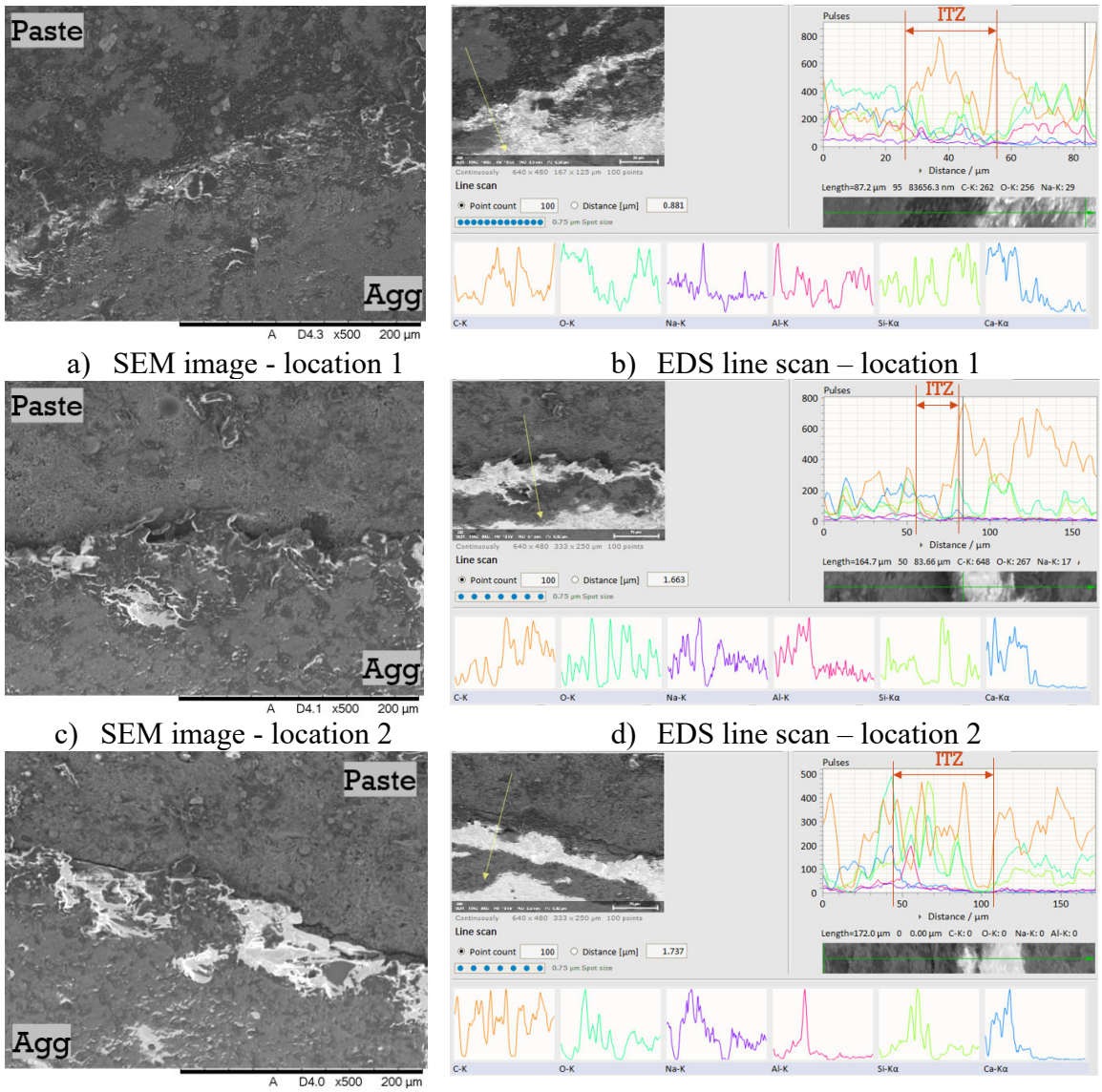

Figure 88. SEM and EDS analysis of GR_NEW_A (as received).

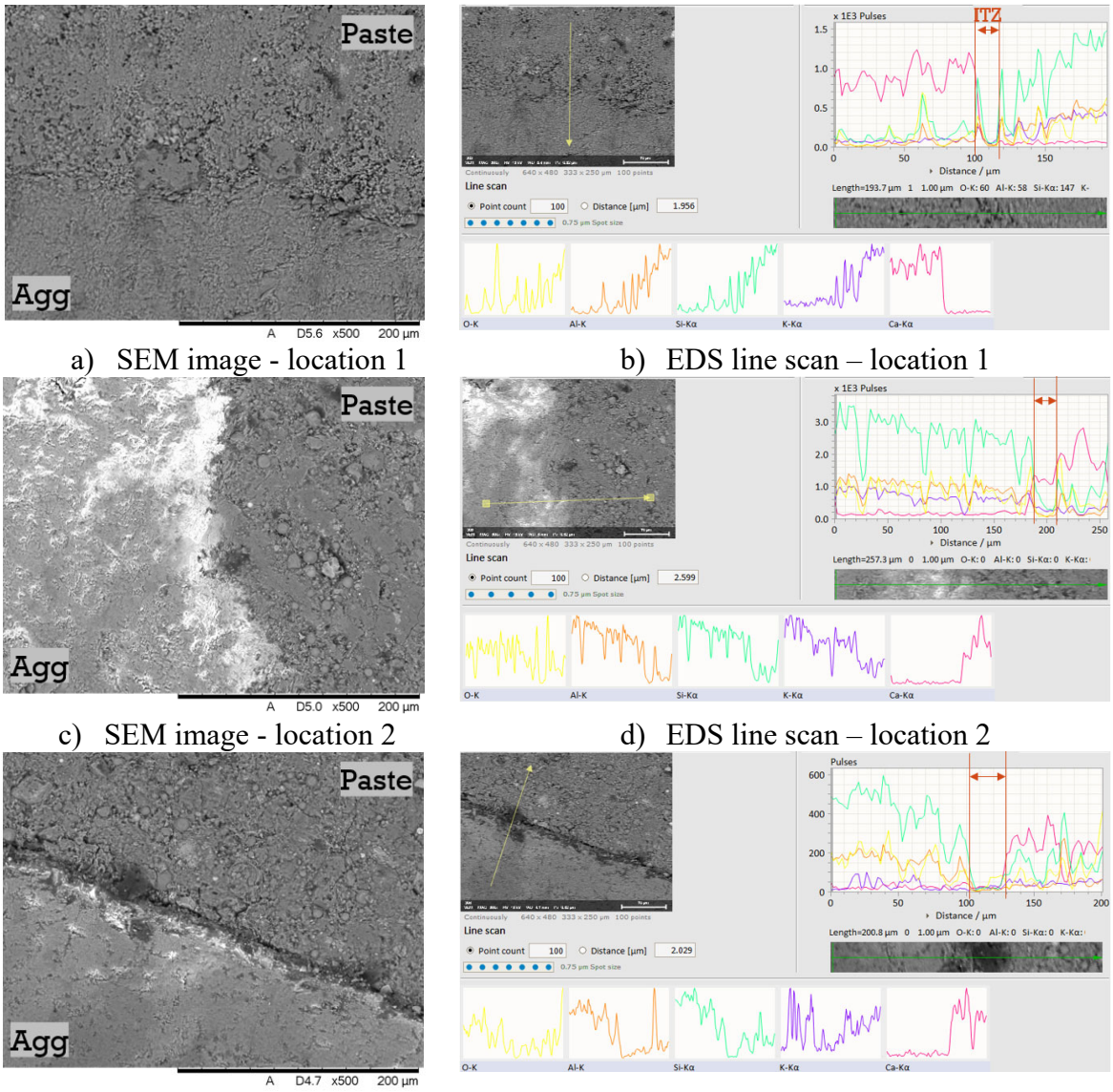

a) SEM image - location 1 b) EDS line scan – location 1

c) SEM image - location 2 d) EDS line scan – location 2

e) SEM image - location 3 f) EDS line scan – location 3

Figure 89. SEM and EDS analysis of GR_NEW_C (washed).

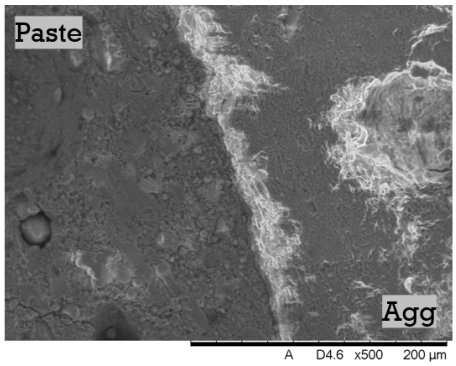

a) SEM image - location 1

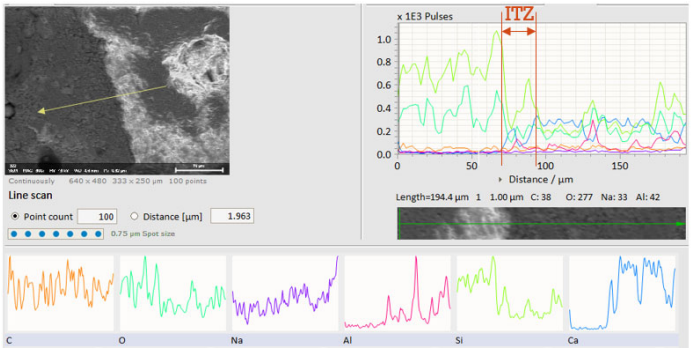

b) EDS line scan – location 1

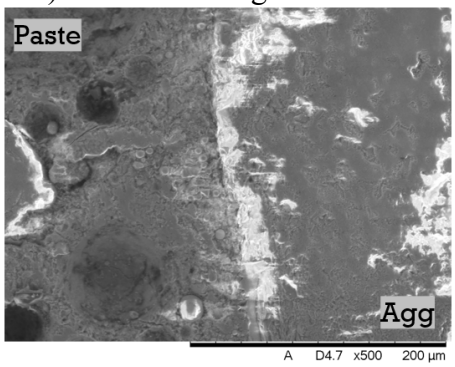

c) SEM image - location 2

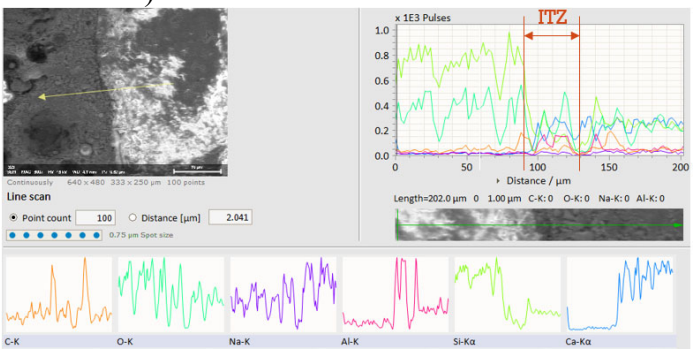

d) EDS line scan – location 2

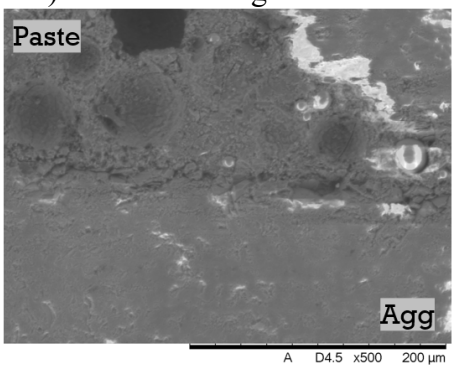

e) SEM image - location 3

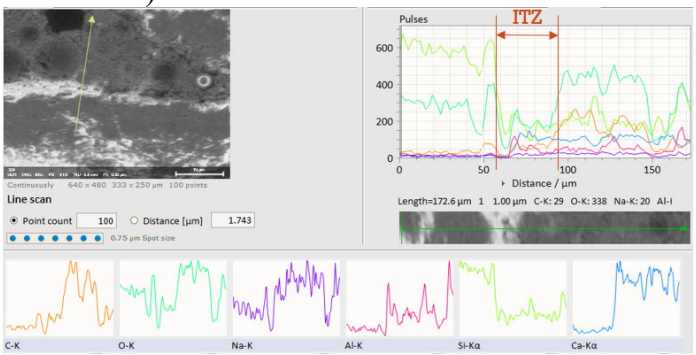

f) EDS line scan – location 3

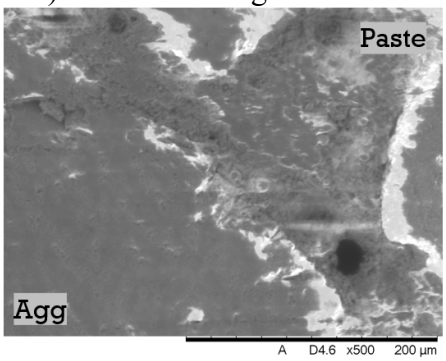

g) SEM image - location 4

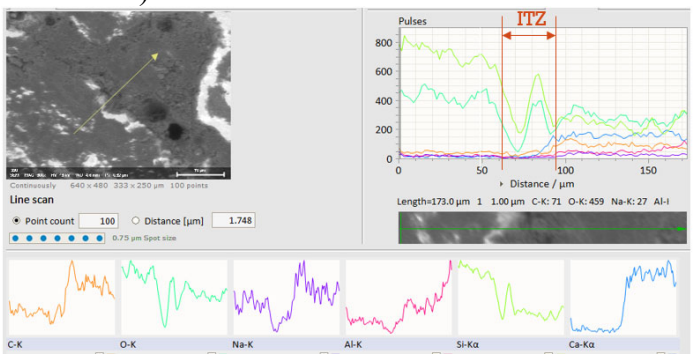

h) EDS line scan – location 4

Figure 90. SEM and EDS analysis of GRNEW.

A-6. Results from Micro-CT Scanning

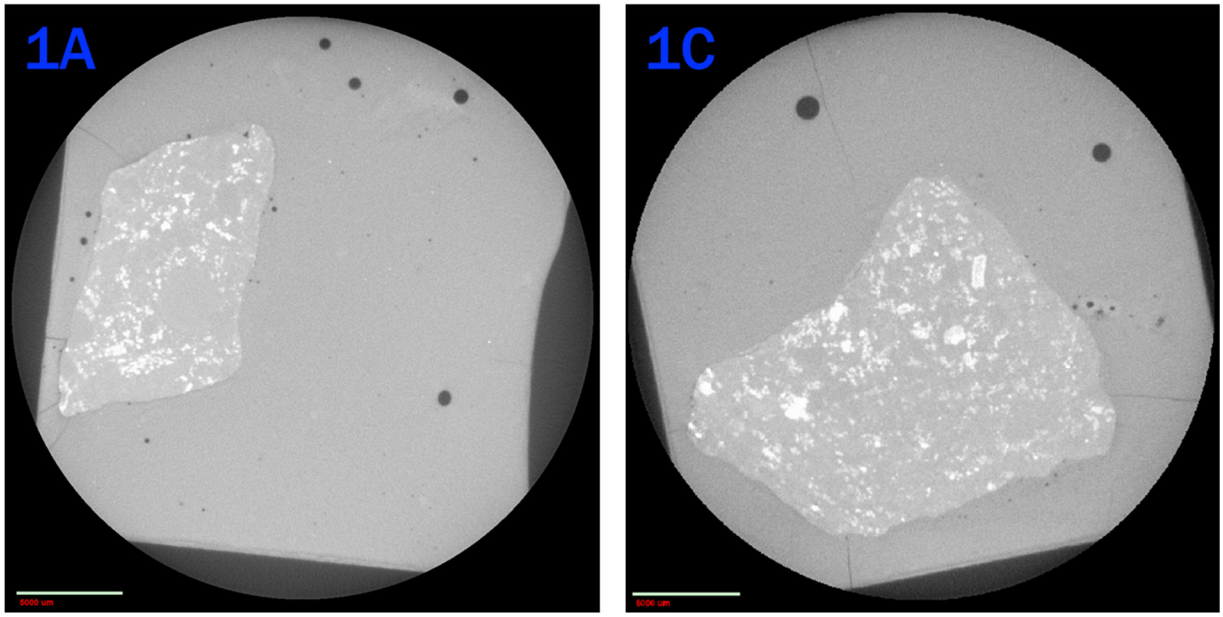

Figure 91. Dolomite-paste cross-section: as-received (left) and washed (right).

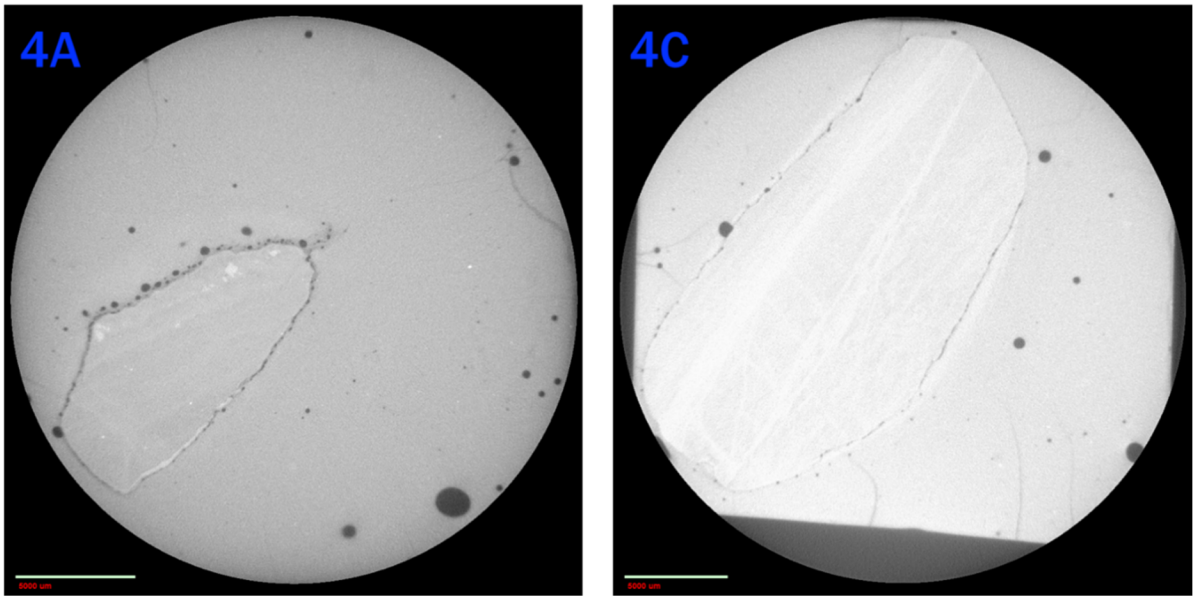

Figure 92. Quartzite-paste cross-section: as-received (left) and washed (right).

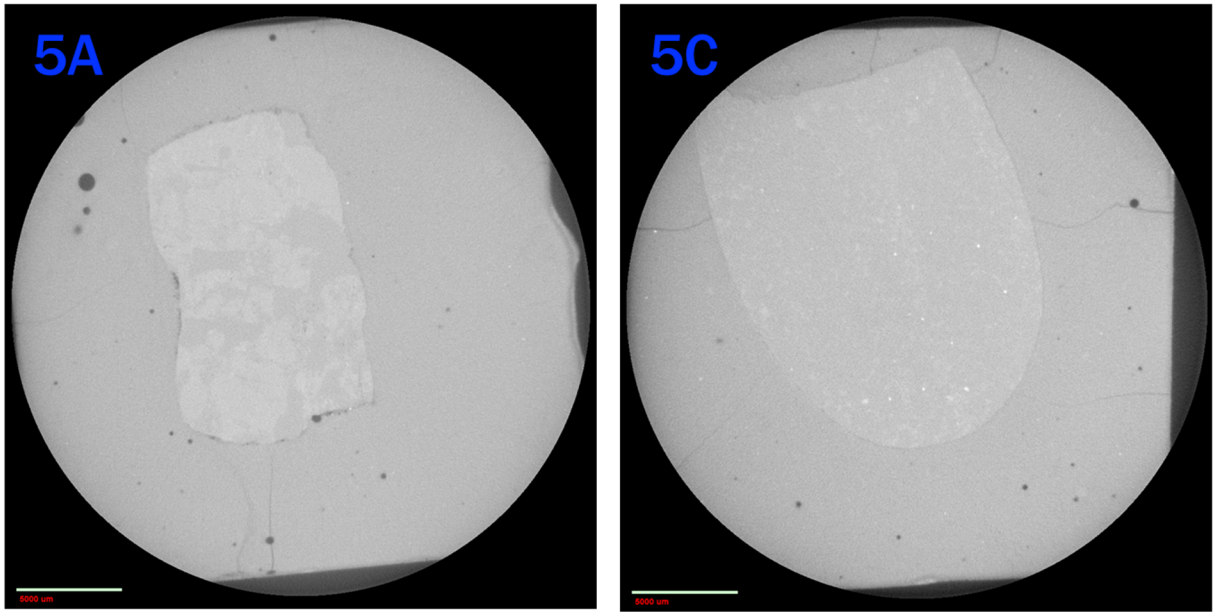

Figure 93. Crushed Gravel-paste cross-section: as-received (left) and washed (right).

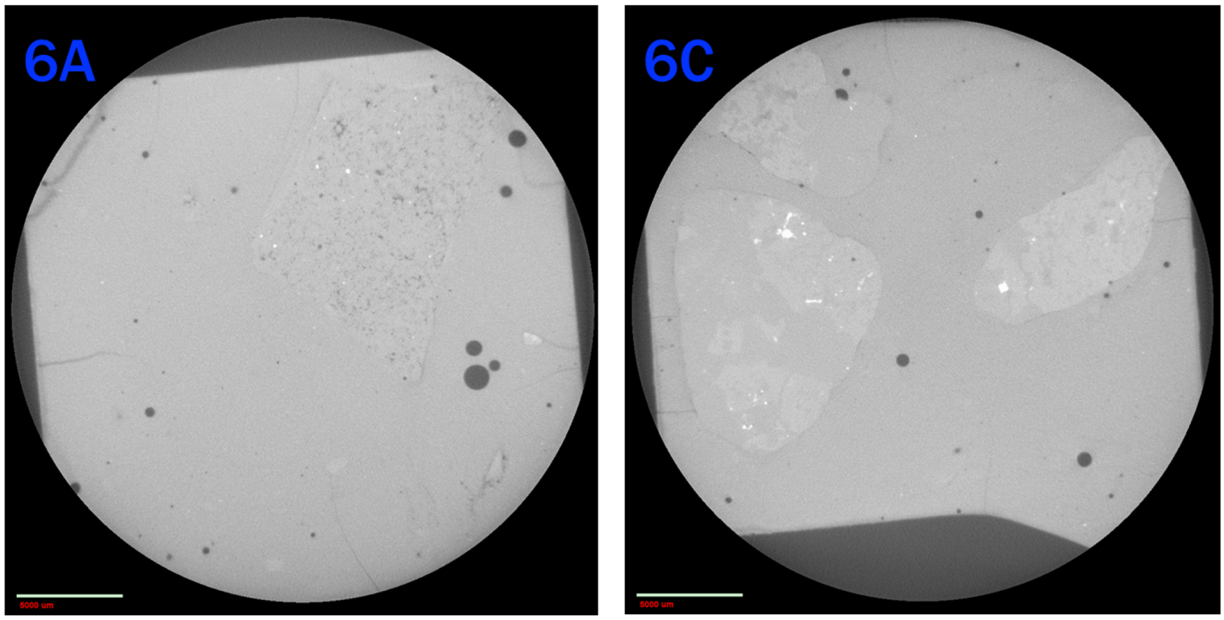

Figure 94. Sand and Gravel-paste cross-section: as-received (left) and washed (right).

A-7. Results from 3D Interphase Topography

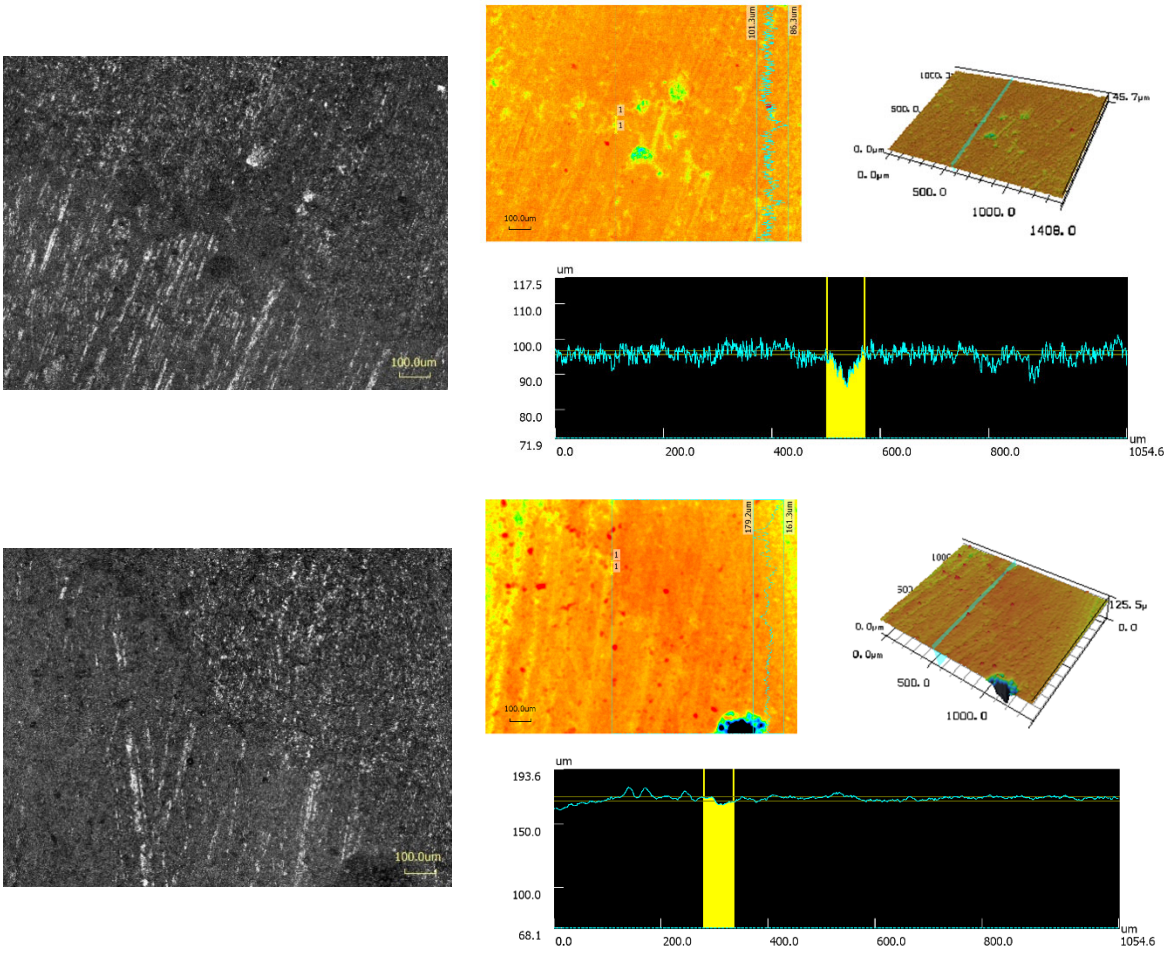

Figure 95. Specimen 1A: LSCM image, 3D topography, and 2D profile line.

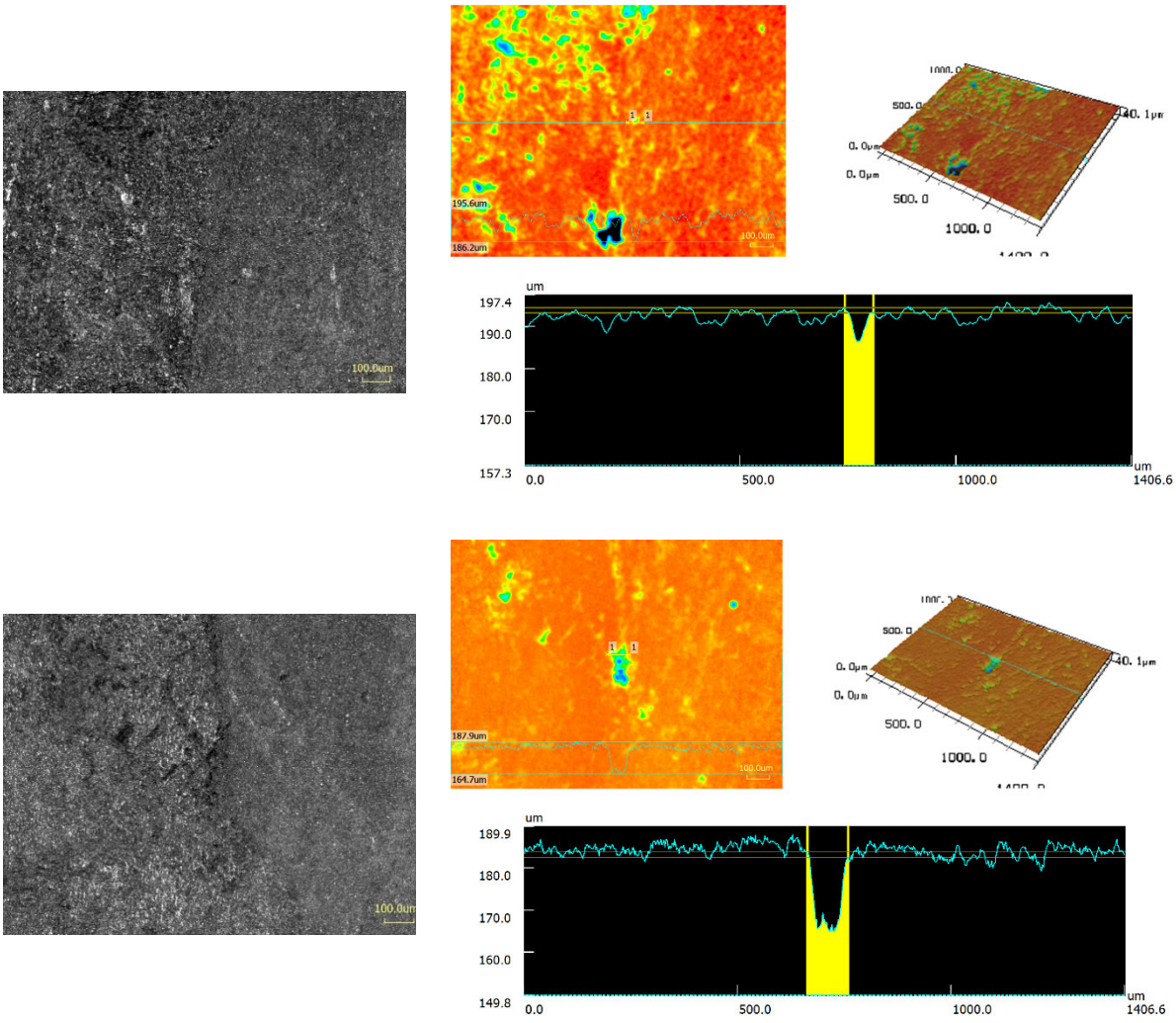

Figure 96. Specimen 1C: LSCM image, 3D topography, and 2D profile line.

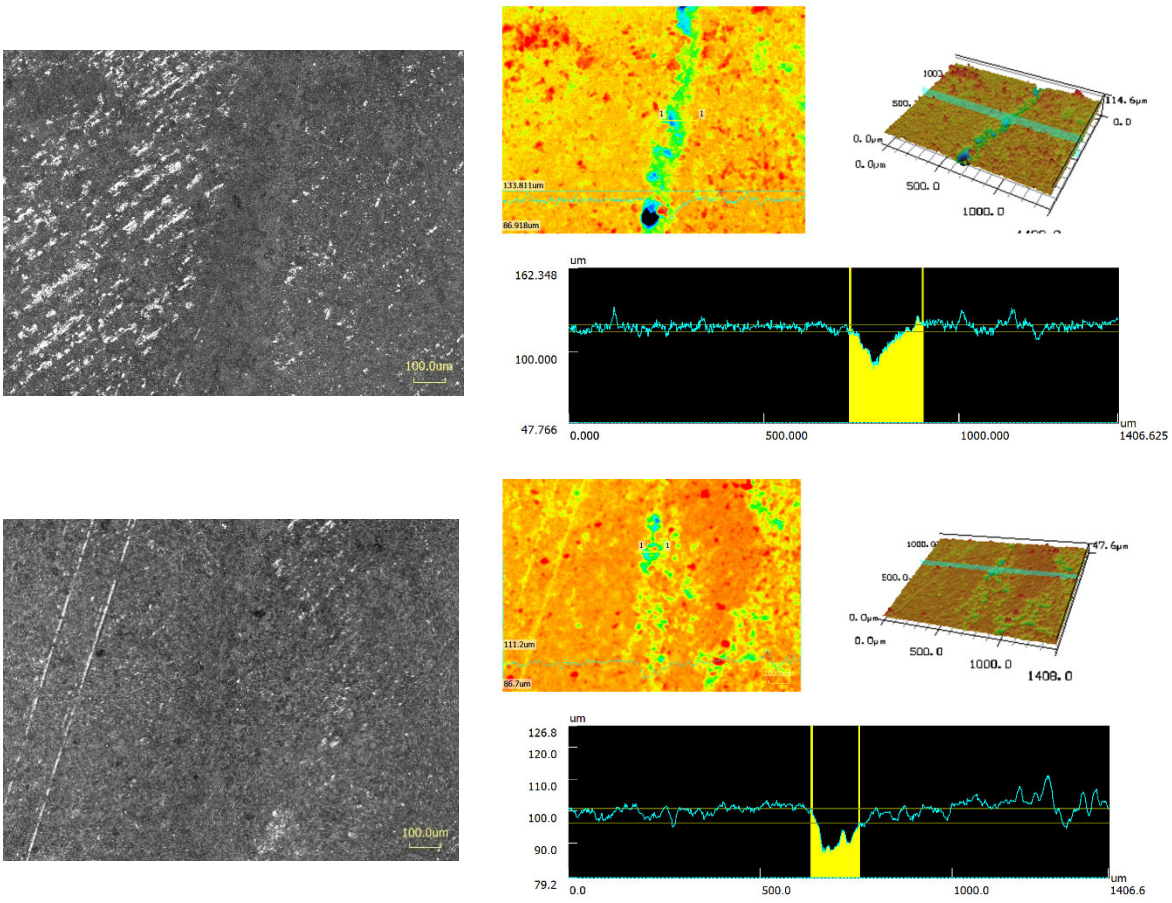

Figure 97. Specimen 4A: LSCM image, 3D topography, and 2D profile line.

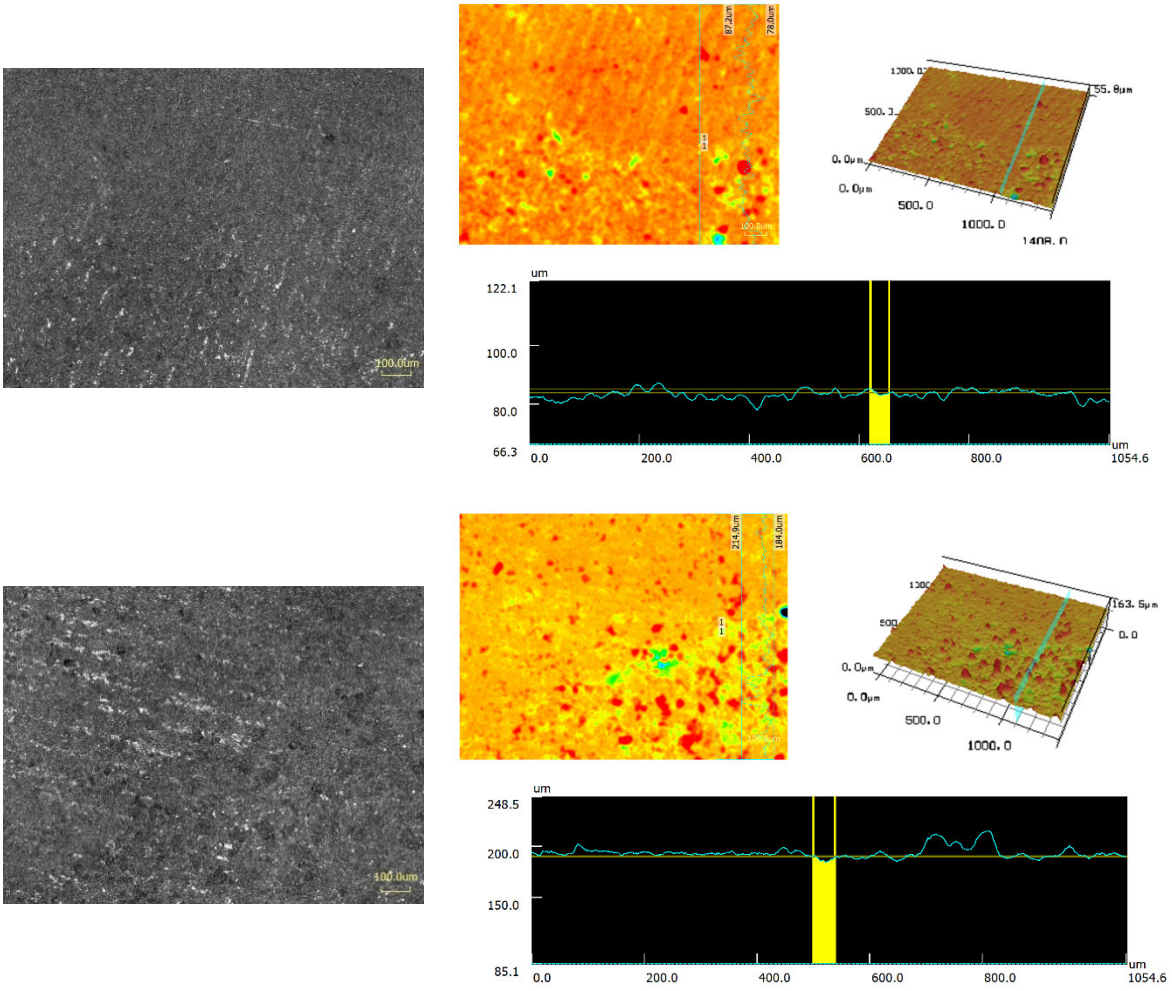

Figure 98. Specimen 4C: LSCM image, 3D topography, and 2D profile line.

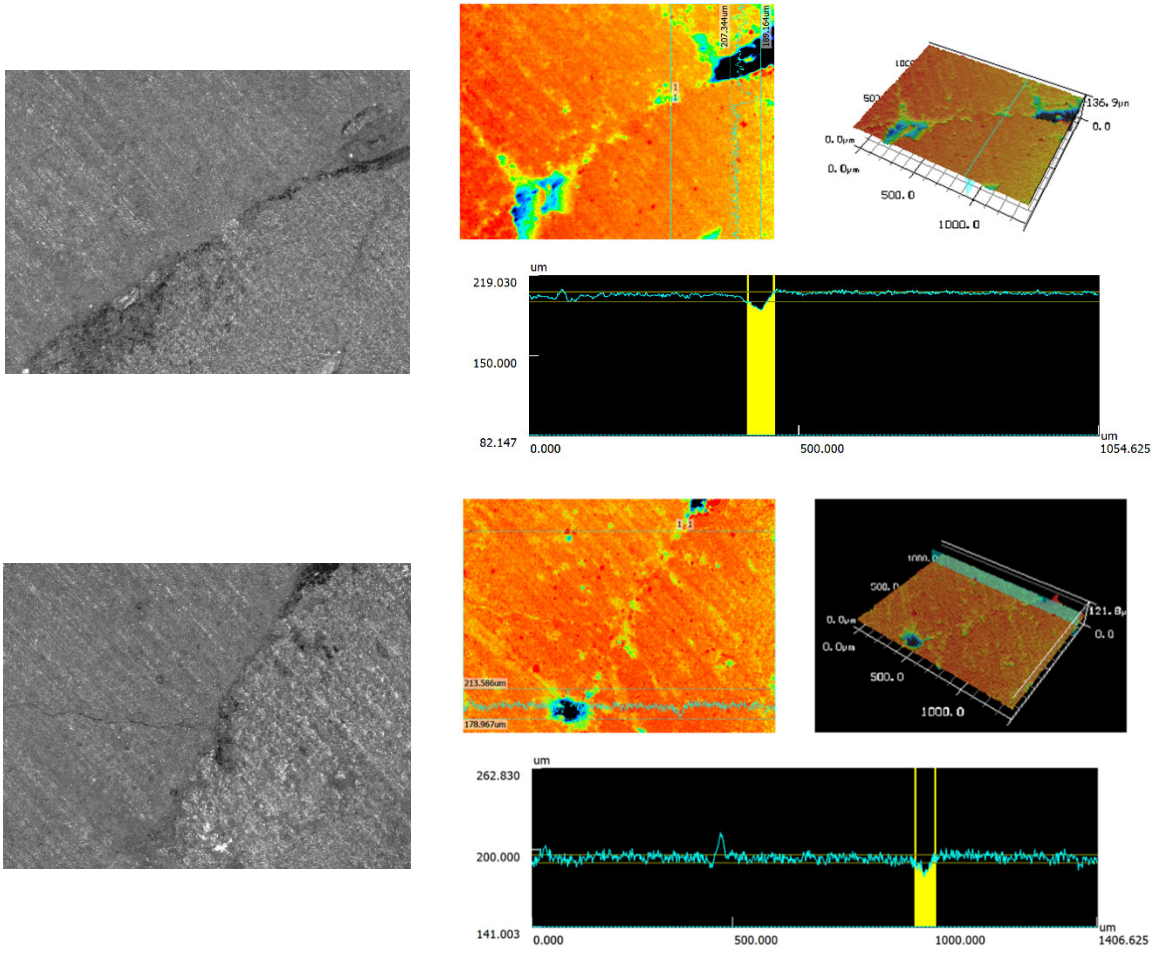

Figure 99. Specimen 5A: LSCM image, 3D topography, and 2D profile line.

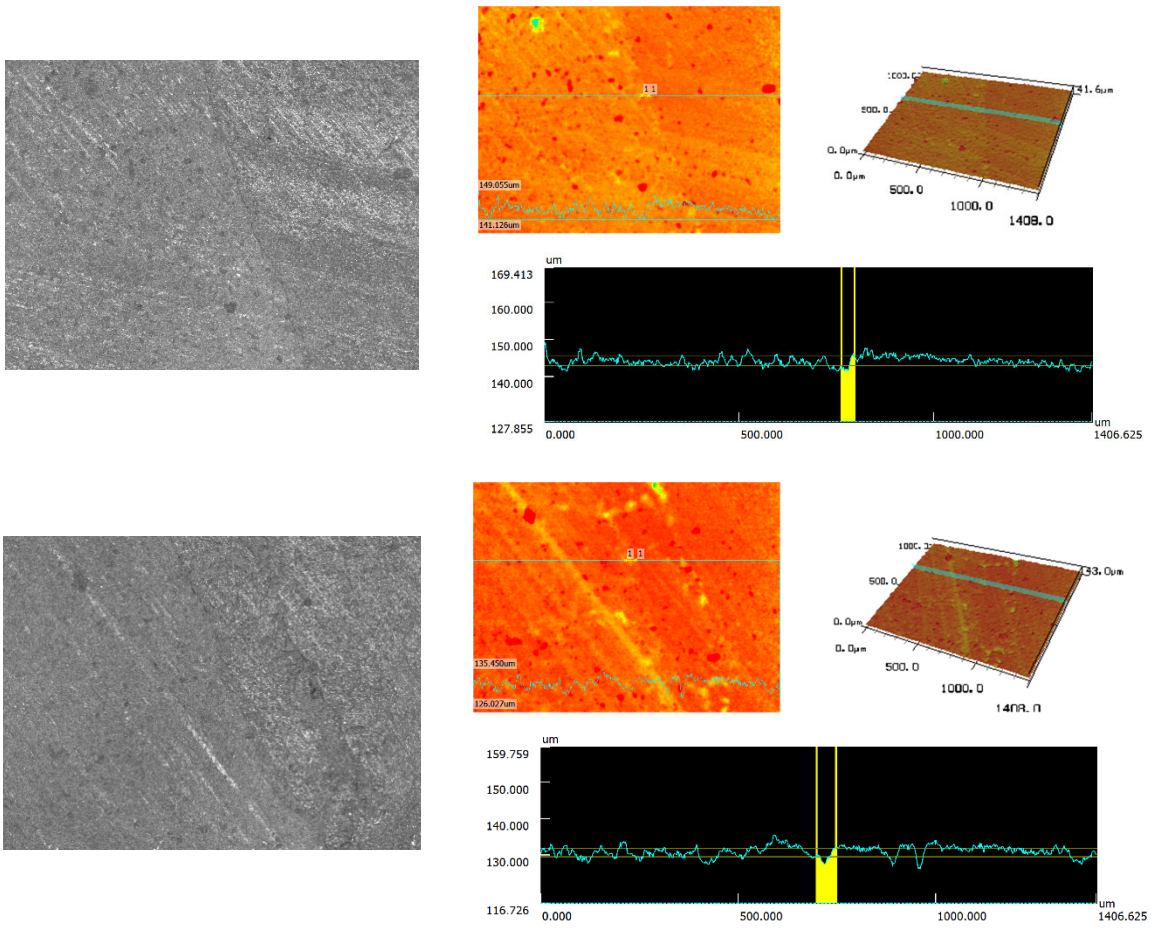

Figure 100. Specimen 5C: LSCM image, 3D topography, and 2D profile line.

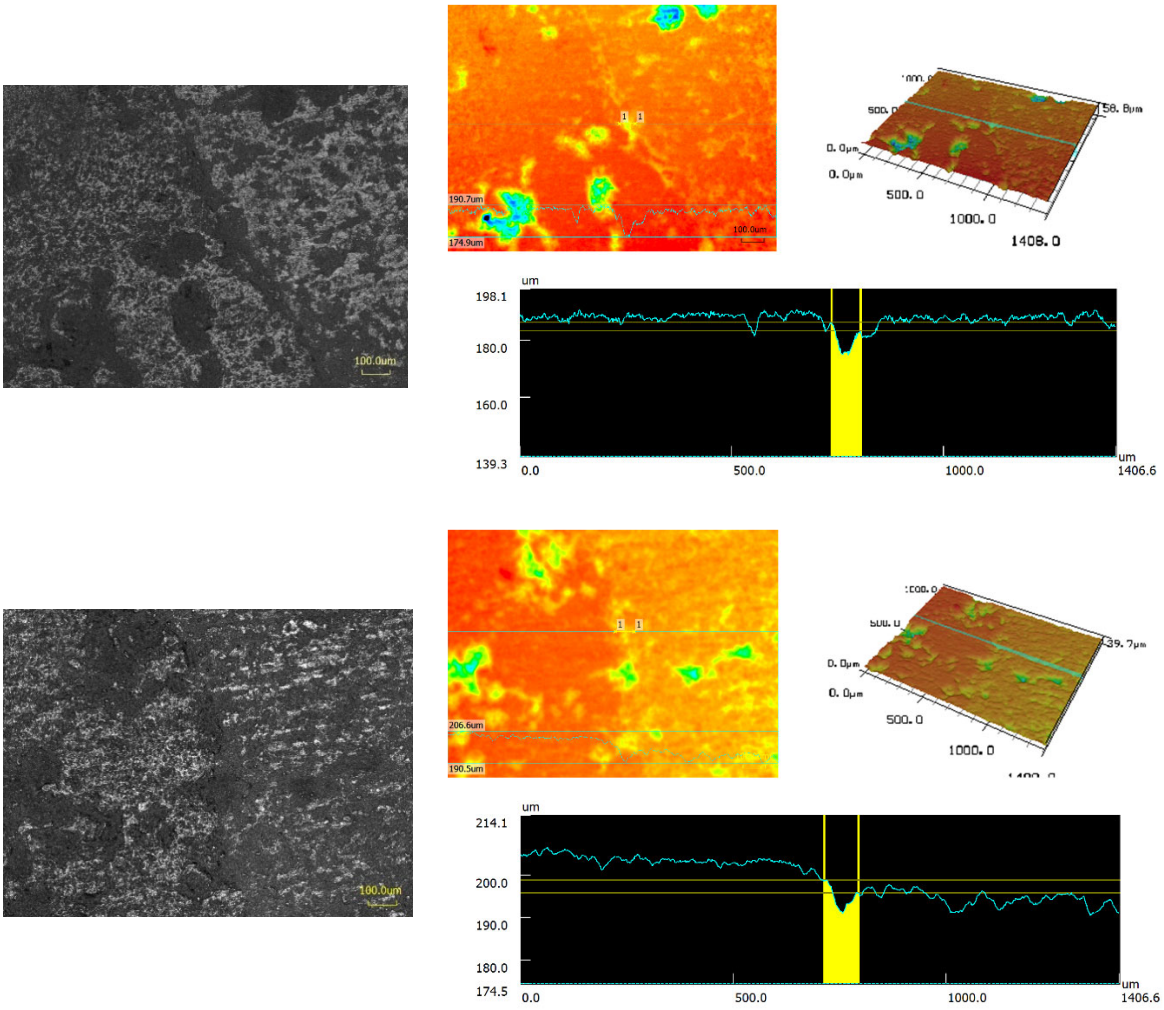

Figure 101. Specimen 6A: LSCM image, 3D topography, and 2D profile line.

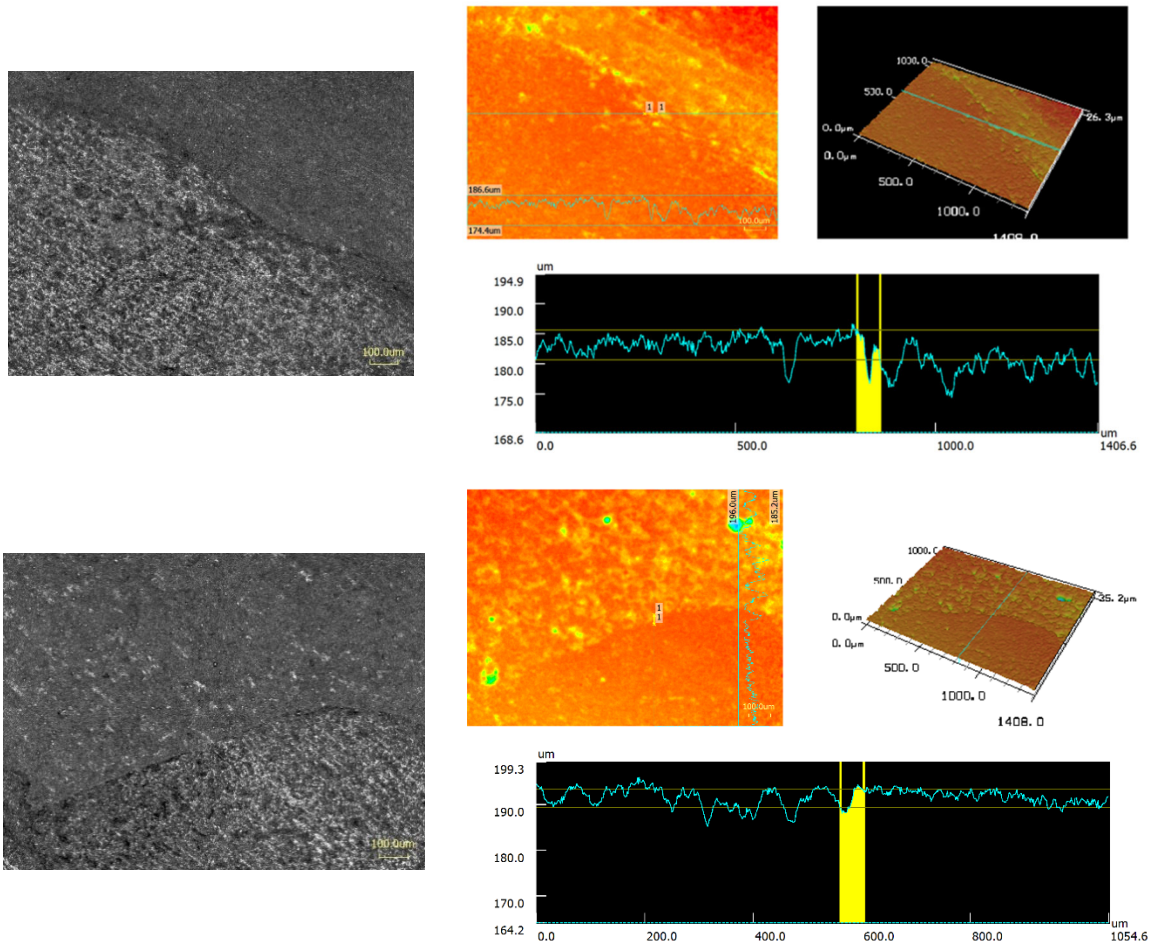

Figure 102. Specimen 6C: LSCM image, 3D topography, and 2D profile line.

A-8. Results from Nanoindentation

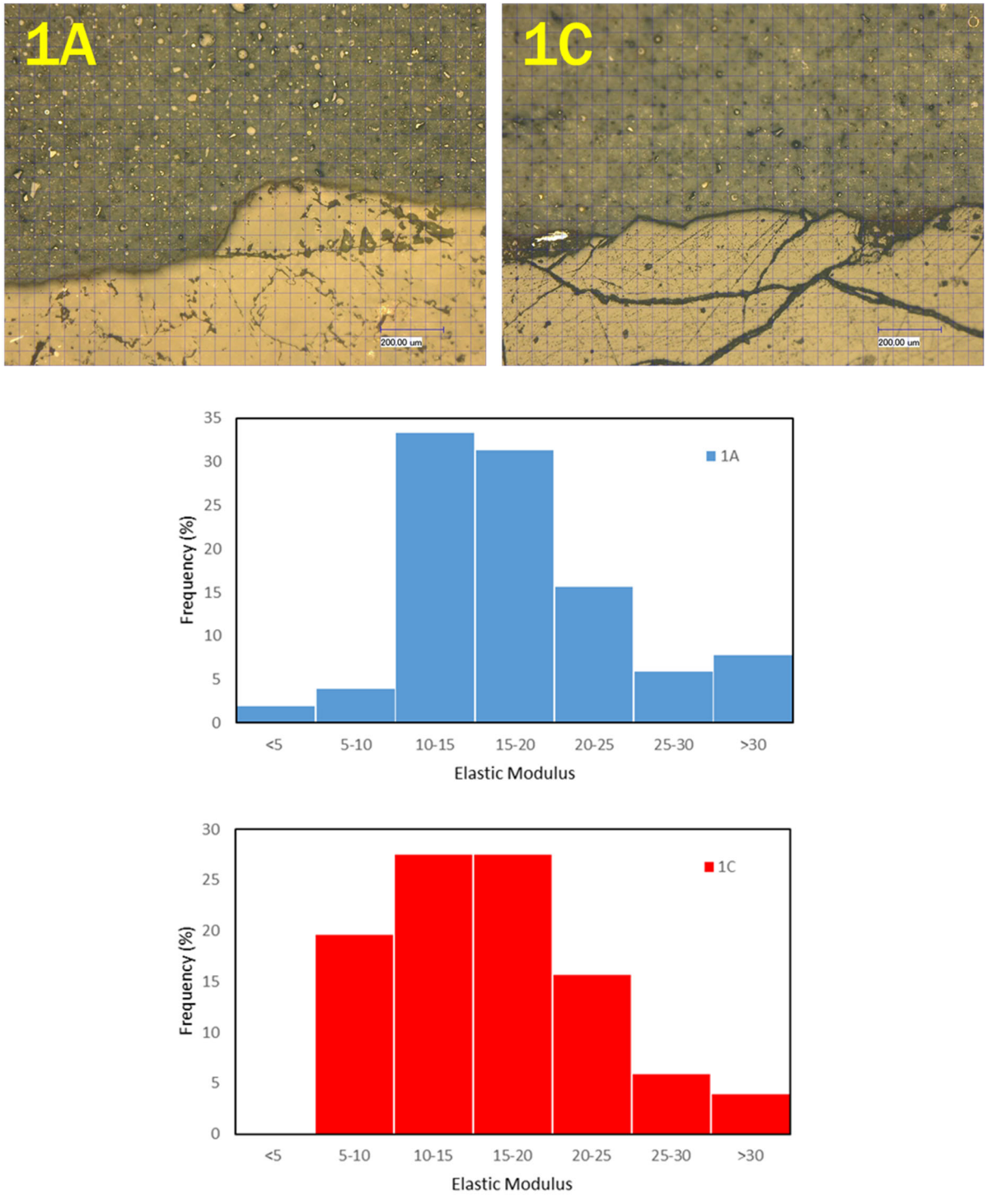

Figure 103. Dolomite: The indented region locations and correlated elastic modulus histograms.

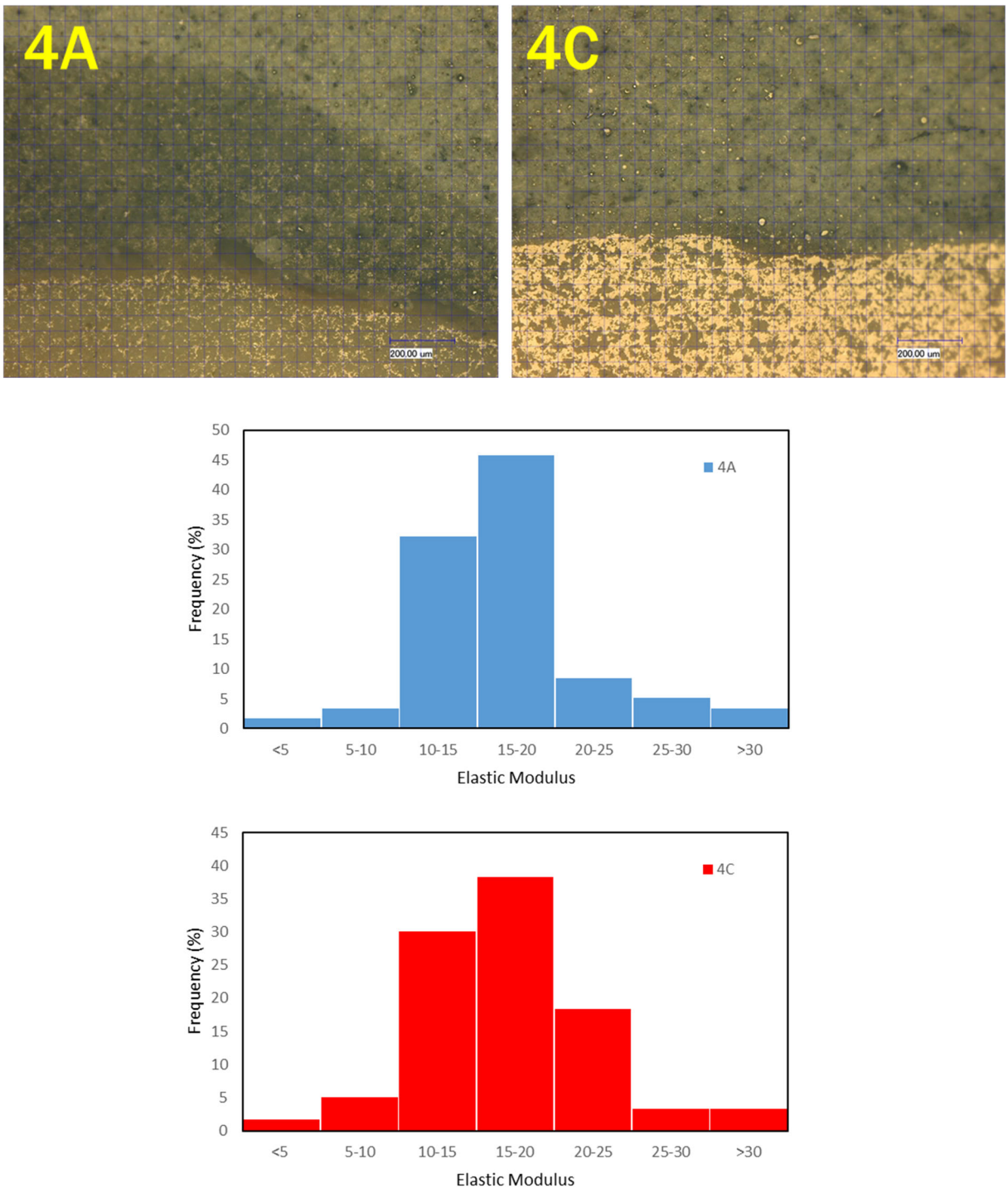

Figure 104. Quartzite: The indented region locations and correlated elastic modulus histograms.

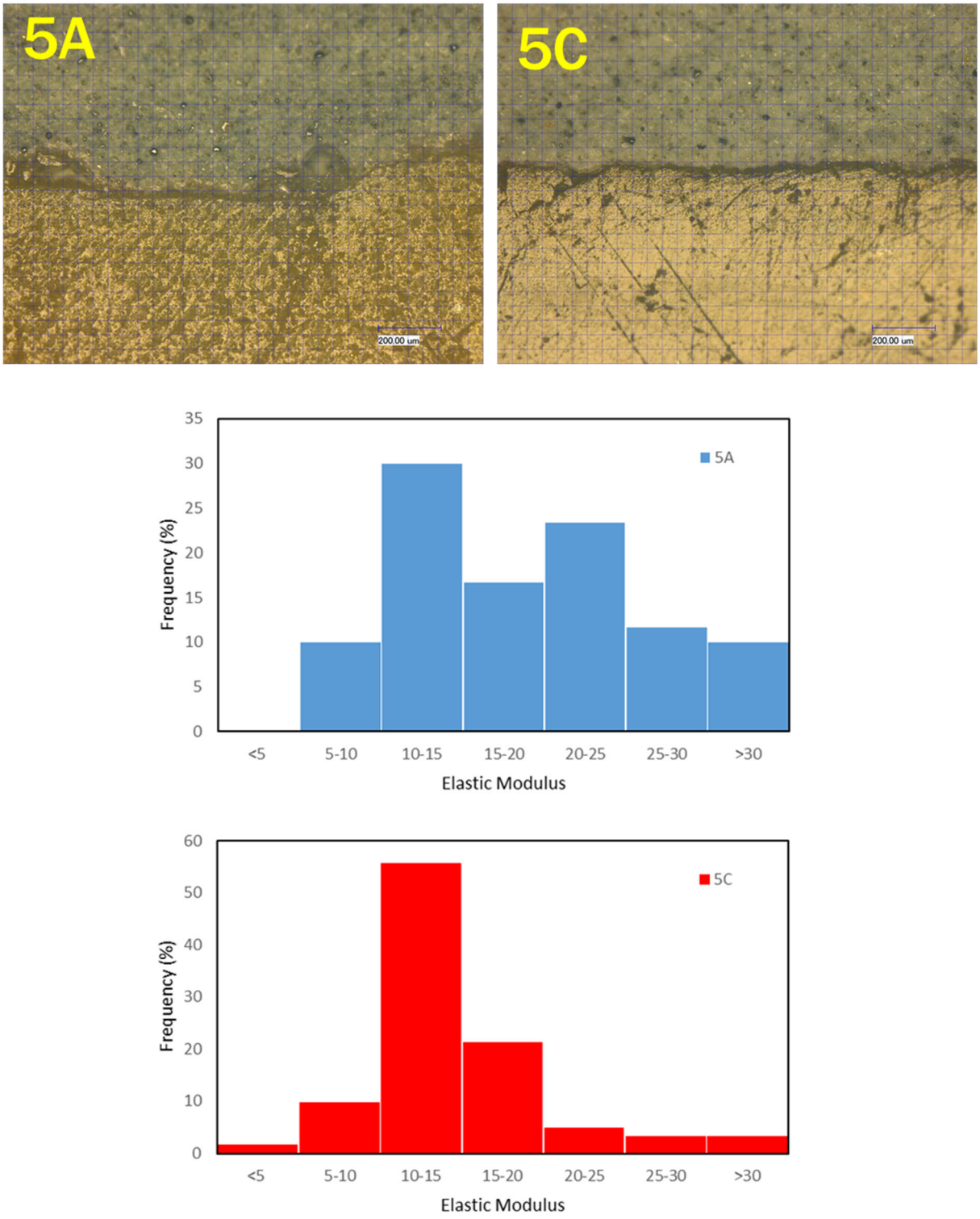

Figure 105. Crushed Gravel: The indented region locations and correlated elastic modulus histograms.

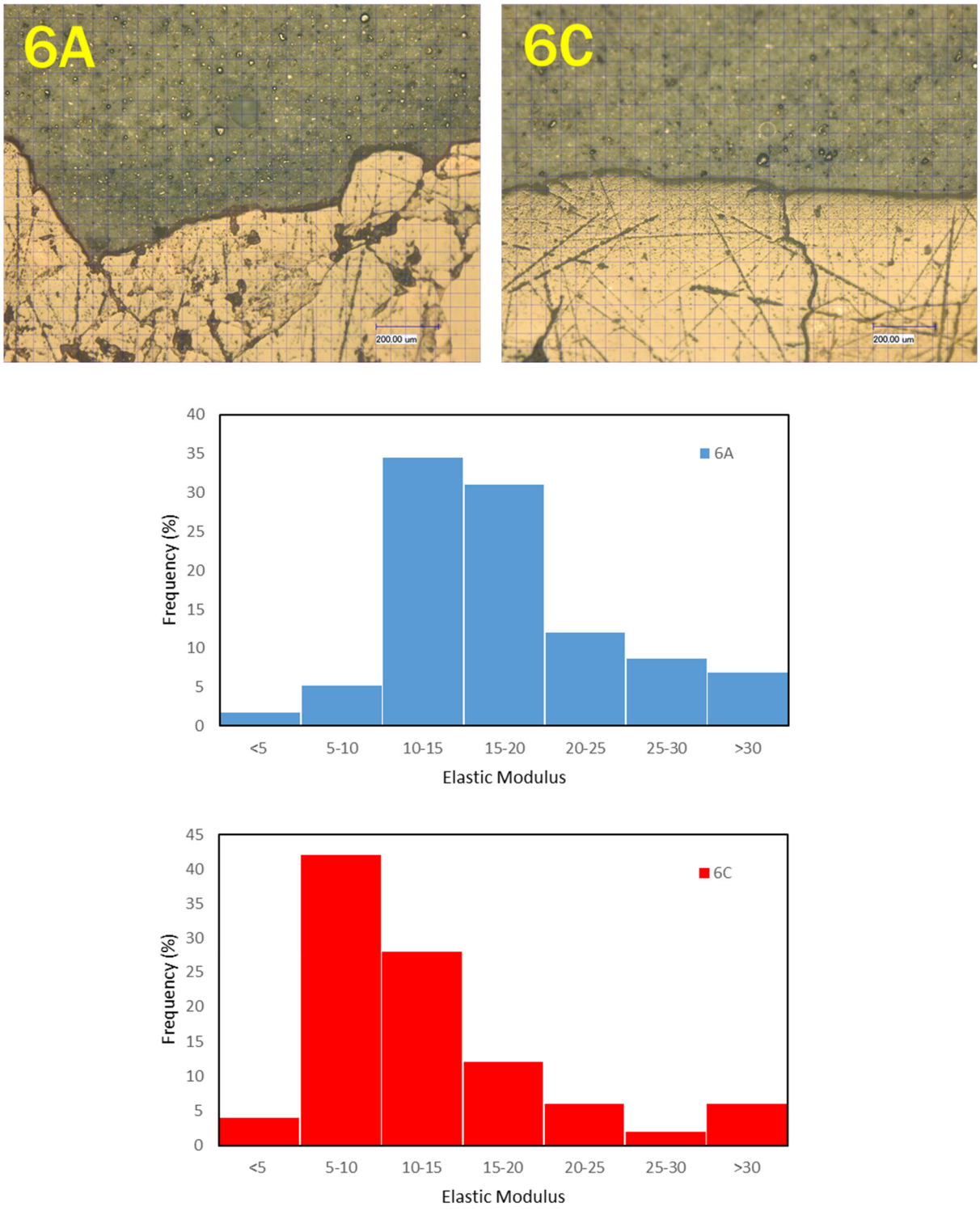

Figure 106. Sand & Gravel: The indented region locations and correlated elastic modulus histograms.

APPENDIX B - CONCRETE PERFORMANCE EVALUATION

B-1. Lab-Casted Concrete Evaluation

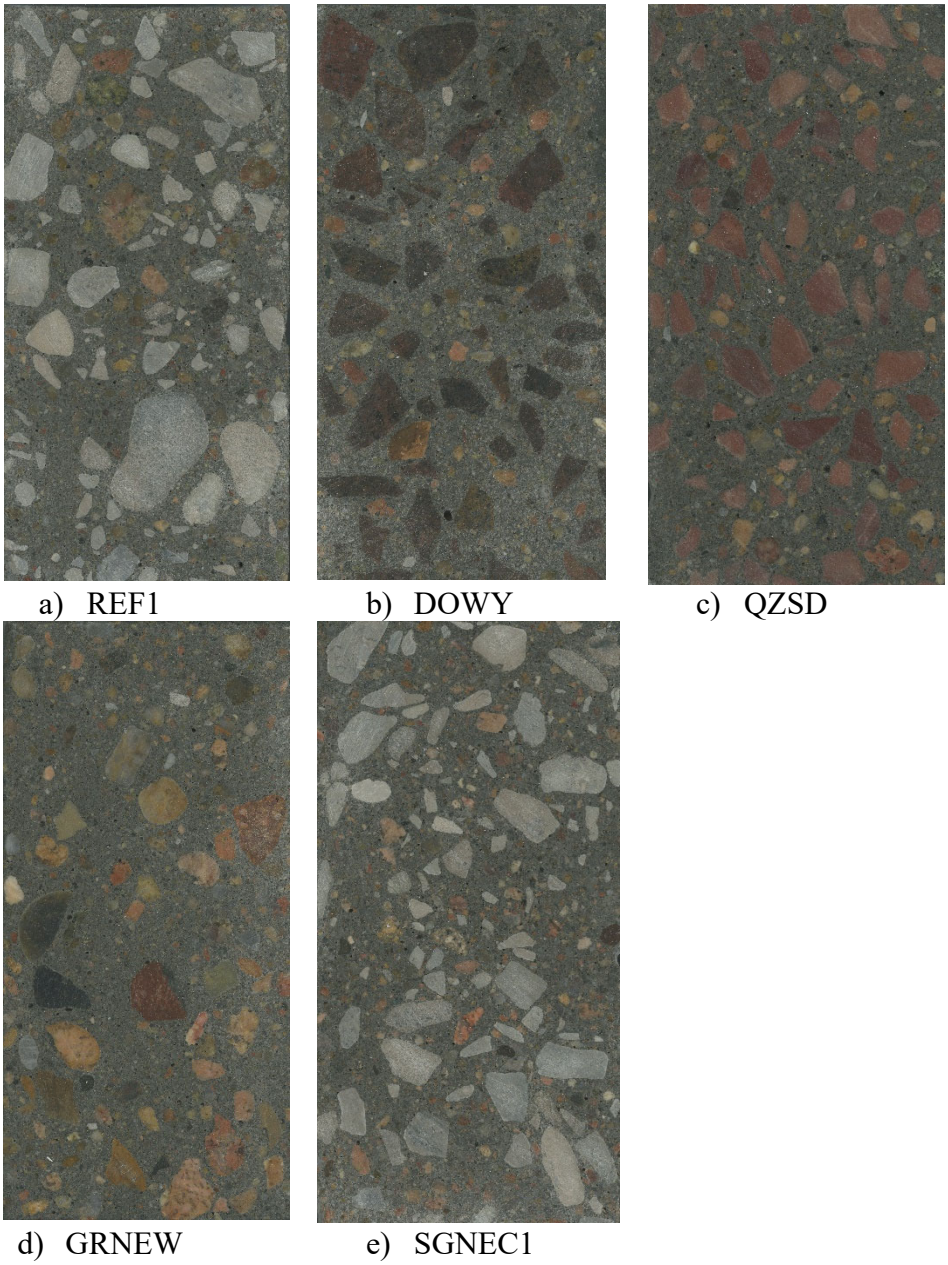

a) REF1 b) DOWY c) QZSD

d) GRNEW e) SGNEC1

Figure 107. Cross-section of lab-casted cylindrical samples.

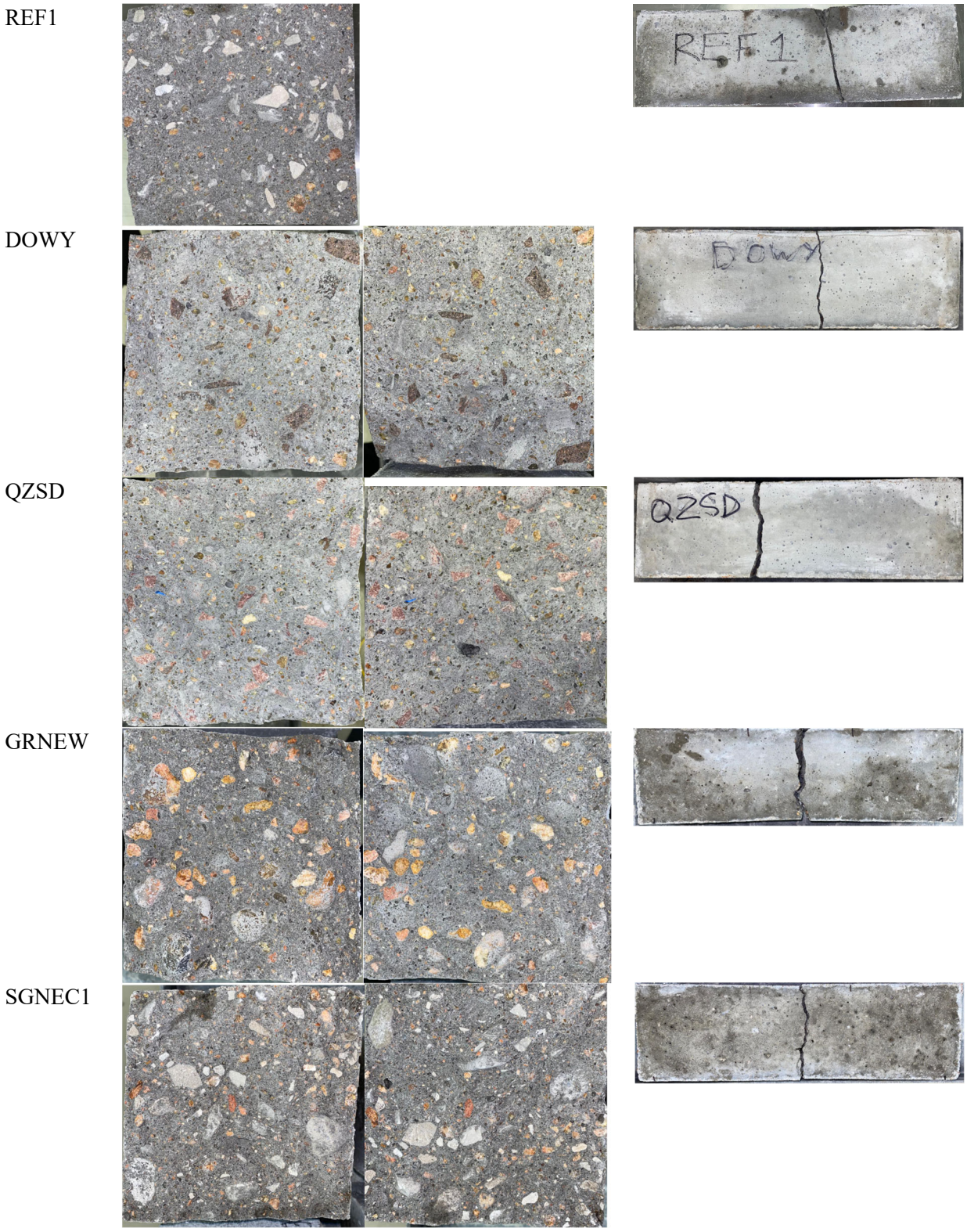

Figure 108. Cross-section of fracture path after MOR test.

Table 26. Appearance of concrete specimens before F/T and after 300 F/T cycles.

MIX ID	Prior to F/T cycle	After 300 F/T cycles
REF1	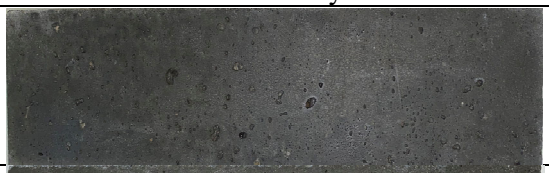	
DO_WY		
QZ_SD		
GR_NEW	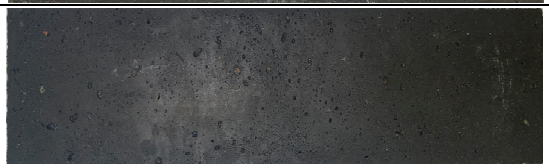	
SG_NEC1	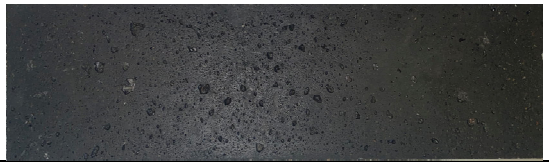	

B-2. Field Concrete Core Specimen Evaluation

Table 27. Summary of visual inspection.

	
R1 sample: Diameter: 4” Depth: 11” No apparent deterioration/soft substances	R2 sample: Diameter: 4” Depth: 11” No apparent deterioration/soft substances
	
R3 sample: Diameter: 4” Depth: 11” No apparent deterioration/soft substances	R4 sample: Diameter: 4” Depth: 13” No apparent deterioration/soft substances

	
R5 sample: Diameter: 4” Depth: 9” No apparent deterioration/soft substances A slight amount of voids/small cavities on the side surface	R6 sample: Diameter: 4” Depth: 9” No apparent deterioration/soft substances A slight amount of voids/small cavities on the side surface
	
R7 sample: Diameter: 4” Depth: 9” No apparent deterioration/soft substances A slight amount of voids/small cavities on the side surface	R8 sample: Diameter: 4” Depth: 9” No apparent deterioration/soft substances A slight amount of voids/small cavities on the side surface

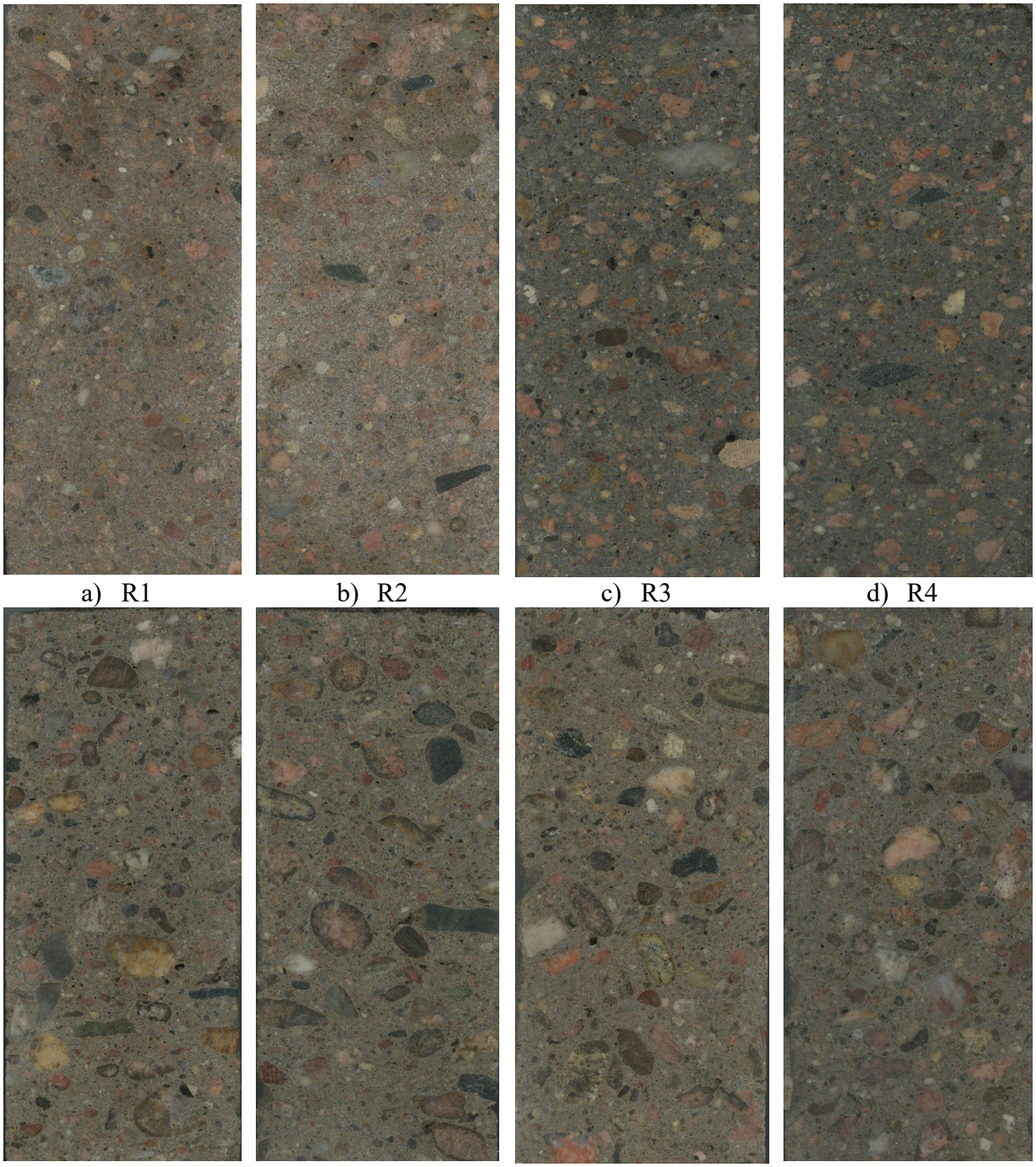

a) R1 b) R2 c) R3 d) R4

e) R5 f) R6 g) R7 h) R8

Figure 109. Vertical cross-section of each of the obtained core samples.